Diatoms and their response to phosphate limitation

Dissertation

zur Erlangung des Grades eines

Doktor der Naturwissenschaften

(Dr. rer.nat.)

des Fachbereichs Biologie der Philipps-Universität Marburg

Vorgelegt von

Gianluca Dell´Aquila

Aus Neapel, Italien

Marburg, 2020

Die vorliegende Dissertation wurde von September/2016 bis September/2020 am Fachbereich Biologie, Zellbiologie unter Leitung von Prof. Dr. Uwe Maier angefertigt.

Vom Fachbereich Biologie der Philipps-Universität Marburg
(Hochschulkennziffer 1180) als Dissertation angenommen am _____

Erstgutachter: Prof. Dr. Uwe Maier

Zweitgutachter: Prof. Dr. Alfred Batschauer

Prof. Dr. Andreas Brune

Prof. Dr. Lars Voll

Tag der Disputation: _____

Publications

Parts of this work were published in:

Stukenberg, D., Zauner, S., **Dell'Aquila, G.**, & Maier, U. G. (2018). Optimizing CRISPR/Cas9 for the diatom *Phaeodactylum tricornutum*. *Frontiers in plant science*, *9*, 740.

Dell'Aquila, G., Zauner, S., Heimerl, T., Kahnt, J., Samel-Gondesen, V., Runge, S., Hempel, F., & Maier, U. G. (2020). Mobilization and Cellular Distribution of Phosphate in the Diatom *Phaeodactylum tricornutum*. *Frontiers in Plant Science*, *11*, 579.

Review article:

Dell'Aquila, G. & Maier, U. G. Specific acclimations to phosphorus limitation in the marine diatom *Phaeodactylum tricornutum* (2020)*. Biological Chemistry (in print)*

Ignorance affirms or denies roundly. Science doubts.

(Voltaire)

Content

Figure legend

Table legend

Summary

Phosphorus is an essential element for all living forms. It is an integral part of several biomolecules that play a crucial role in the cellular structures and processes. Phosphate, which is the most common form of phosphorus in the biological systems, is present in a plethora of important biomolecules (e.g. DNA, phospholipids) and it is involved in fundamental cellular activities such as the modulation of proteins activity via phospho/dephosphorylation. Cellular activity is often influenced by environmental P availability and in the case of marine protists such as microalgae, this can potentially impact on the global primary production.

Diatoms, which are believed to largely contribute to the global carbon fixation, are able to adapt to fluctuations in nutrient concentrations such as phosphorus. Recent transcriptomic and proteomic studies indicated possible strategies that diatoms adopt to cope with P scarcity showing a significant impact on cell metabolism and physiology. In the model diatom *Phaeodactylum tricornutum* specific traits of P-stress response can be recognized in the induction of genes encoding for alkaline phosphatases and P transporters. Several important players that might be essential for the cellular acclimation to P deficiency were identified by the "omics" studies, providing a first general overall. However, the understanding of P-homeostasis requires more detailed knowledge on P-responsive specific proteins. Further studies on these proteins (e.g. on function and/or subcellular localization) are needed to clarify and characterize more aspects of the response.

The work presented here aims to integrate the existing omics data with subcellular localization, transcriptional, and posttranslational regulation studies on several P-regulated/non-regulated proteins that are supposed to play major roles in maintaining P-homeostasis in *P. tricornutum*. The *in vivo* localization and expression studies showed that *P. tricornutum* in response to P-starvation expresses extracellular alkaline phosphatases, one phytase-like, and 5´ nucleotidase and one intracellular alkaline phosphatase in the endomembrane system. P_i- transporters are localized at cell borders, endomembrane systems and vacuolar membranes. These results highlight the ability of the diatom to mobilize P_i from alternative intra/extracellular P source, uptake and distribute it intracellularly. An early investigation on candidates related to a possible polyP metabolism and P-storage was also conducted. Some of the investigated proteins were studied also with respect to their transcriptional regulation, showing interesting regulation patterns under diverse extracellular

P-conditions. The results shown here integrate the knowledge about P-starvation response in diatoms, providing additional informations that are necessary to sketch a P-homeostasis atlas in *P. tricornutum*. As a side aspect of this part, strongly P_i-dependent promoter/terminator modules were identified, providing new molecular tools for the expression of transgenes in the *P. tricornutum* model organism.

Zusammenfassung

Phosphor ist ein wesentliches Element für alle Lebensformen. Es ist ein wesentlicher Bestandteil mehrerer Biomoleküle, die eine entscheidende Rolle in den zellulären Strukturen und Prozessen spielen. Phosphat, die häufigste Form von Phosphor in den biologischen Systemen, kommt in einer Vielzahl wichtiger Biomoleküle (z.B. DNA, Phospholipide) vor und ist an grundlegenden zellulären Aktivitäten wie der post-translationale Modifikation von Proteinen durch Phospho/Dephosphorylierung beteiligt. Die zelluläre Aktivität wird oft von der P-Verfügbarkeit in der Umwelt beeinflusst, und im Falle von marinen Protisten wie Mikroalgen kann sich dies potenziell auf die globale Primärproduktion auswirken.

Kieselalgen tragen weitgehend zur globalen Kohlenstofffixierung bei und können sich an Schwankungen der Nährstoffkonzentrationen, wie z.B. Phosphor, anpassen. Neuere transkriptomische und proteomische Studien zeigen einen signifikanten Einfluss auf den Zellstoffwechsel und die Physiologie der Kieselalgen unter Pi-Mangel auf. In dem Modellorganismus *Phaeodactylum tricornutum* werden während der P-Stress-Reaktion spezifische Gene induziert, die für alkalische Phosphatasen und P-Transporter kodieren. Die ersten omics Studien liefern einen allgemeinen Überblick über die wichtigen Akteure, welche für die zelluläre Anpassung an den P-Mangel essentiell sein könnten. Für das Verständnis der P-Homöostase ist jedoch eine detailliertere Kenntnis der P-reaktiven spezifischen Proteine erforderlich. Weitere Studien über diese Proteine (z.B. über Funktion und/oder subzelluläre Lokalisation) sind erforderlich, um weitere Aspekte der Reaktion zu klären und zu charakterisieren.

Anhad der vorhandenen omics Daten wurden Kandidatengene bestimmt, die eine wichtige Rolle bei der Aufrechterhaltung der P-Homöostase bei *P. tricornutum* spielen könnten. Diese Kandidatengene wurden mittels subzellulären Lokalisierungsstudien und Expressionsstudien untersucht. Die *in vivo*-Lokalisierungs- und Expressionsstudien zeigten, dass *P. tricornutum* als Reaktion auf P-Starvation extrazelluläre alkalische Phosphatasen, ein Phytase-ähnliches Protein, eine 5'-Nukleotidase sowie eine intrazelluläre alkalische Phosphatase im Endomembransystem exprimiert. Pi- Transporter sind an den Zellgrenzen, dem Endomembransystem und der Vakuolarmembran lokalisiert. Diese Ergebnisse unterstreichen die Fähigkeit der Kieselalge *P. tricornutum*, P_i aus einer alternativen intra-/extrazellulären P-Quelle zu mobilisieren, aufzunehmen und intrazellulär zu verteilen. Es wurde auch eine erste

Untersuchung zu Kandidaten im Zusammenhang mit einem möglichen PolyP-Metabolismus und der P-Speicherung durchgeführt. Einige der untersuchten Proteine wurden auch im Hinblick auf ihre transkriptionelle Regulation untersucht und zeigten interessante Regulationsmuster unter verschiedenen extrazellulären P-Bedingungen. Die hier gezeigten Ergebnisse tragen zum Wissen über die P-Speicherungsreaktion in Kieselalgen bei und liefern zusätzliche Informationen, die zur Skizzierung eines P-Homöostase-Atlas bei *P. tricornutum* erforderlich sind. Als ein Nebenaspekt dieses Teils wurden stark Pi-abhängige Promotor/Terminator-Module identifiziert, die neue molekulare Werkzeuge für die Expression von Transgenen im Modellorganismus von *P. tricornutum* liefern.

Abbreviations

α	anti
µl	Microliter
µg	Microgram
° C	Grad Celsius
AA	Amino acid
AP	Alkaline phosphatase
ATP	Adenosine triphosphate
bp	Base pairs
BLAST	Basic Local Alignment Search tool
cDNA	*complementary* DNA
cER	*chloroplast* ER
ddH_2O	Double distilled water
DMSO	Dimethylsulfoxid
DNA	*Deoxyribonucleic acid*
dNTP	*Deoxynucleotide triphosphate*
EDTA	*Ethylenediaminetetraacetic acid*
eGFP	*enhanced green fluorescent protein*
ELF	Enzyme labeled fluorescence
et al.	et allii
ER	Endoplasmic Reticulum
EST	*expressed sequence tag*
gDNA	Genomic DNA
GDP	*Guanosindiphosphate*
GEF	*guanosine exchange factor*
GET	Guided entry of tailor proteins
GTP	*Guanosintriphosphate*
h	*hours*
HP_i	Inorganic phosphate transporter
HRP	*horseradish peroxidase*
kDa	Kilodalton
KO	Knockout
CLSM	Confocal Laser Scanning Microscope
M	Molar
mA	Milliampere
MFS	Major Facilitator superfamily
mg	Milligram
min	Minute
ml	Milliliter
nm	Nanometer
mM	Millimolar
NR	Nitrate reductase
NH_4	Ammonia
NO_3	Nitrate
Ntase	5´ nucleotidase
OD	Optical density
PAF	Plastid autofluorescence
PAGE	Polyacrylamide gel electrophoresis
PBS	Phosphate buffered saline
PMTs	Post translational modifications
psi	*pound-force per square inch*
RNA	*Ribonucleic acid*
RT	Room temperature
s	Second
sgRNA	Single guide RNA
SRP	Soluble reactive phosphorus
SP	Signal peptide
SPX	SYG1/Pho81/XPR1
TBS	*Tris buffered saline*
TCA	*trichloroacetic acid*
TDN	Total dissolved nitrogen
TDP	Total dissolved phosphorus
TEMED	*Tetramethylethylenediamine*
TL	*transmitted light*
U	Unit
V	volts
Vol	Volume
Vpt	Vacuolar phosphate transporter
Vtc	Vacuolar transport chaperon
v/v	*volume per volume*
W	Watt
WB	Western blot
WT	Wildtype

1. Introduction

1.1. The phosphorus in nature

1.1.1. Why nature choose phosphate?

“Phosphate esters and anhydrides dominate the living world”: F.H. Westheimer started his thought about phosphate importance in biology with this sentence (Westheimer, 1987). The answer to the question “why nature chose Phosphate” is probably to be found in its advantageous biochemical properties. The genetic material represents the striking evidence in which the phosphate plays a crucial role: nucleotides are held together by phospho-esteric bonds forming either DNA or RNA single filaments. This resulting arrangement confers an important feature of biological relevance, that according to Davis, created the right conditions for the evolution of life: the ionization of the molecule (Davis, 1958). In this publication, Davis underlined “the importance of being ionized” and recalling the example of the nucleic acids, the resulting negative charge serves both to stabilize the diesters against hydrolysis and to retain it within a lipid membrane. It is reasonable that retaining and protecting such molecules or metabolites within the cell membrane was one of the first steps of evolutionarily primitive organisms (Davis, 1958). Why is phosphate the predestinated? By definition, phosphate is a salt with an anionic entity, built of a single PO_4 tetrahedron for example or by condensation of multiple PO_4 anions. There are several compounds where one or more oxygen atoms can be exchanged by other atoms like Hydrogen (H), Sulfur (S) and Fluorine (F). The most common form of phosphate are compounds based on an anionic phosphorus (V) entity ($[PO_4]^{3-}$). Four oxygens surround a central phosphorus atom and this structure is usually referred to as “monophosphate” or “orthophosphate”, the most stable and the only one to be found in the natural world (Kamerlin et al., 2013). The protonated form of the monophosphate represents phosphoric acid (H_3PO_4). The latter can be esterified in any of one or three positions forming mono-, di- or triesters. DNA and RNA are for example diesters of phosphoric acid. Several suitable alternatives to phosphate to be considered as a basis for a possible genetic material were discussed. In many cases as examples of citric, arsenic and silicic acid, the negative charge is conserved but at the expense of the resistance to hydrolysis (Westheimer, 1987). Furthermore, the case of Arsenic (As) as a possible alternative in the life chemistry was more

intensely discussed after the discovery of a bacterial strain that can grow in the presence of arsenate and possibly in the absence of phosphate (Wolfe-Simon et al., 2011).

1.1.2. **Biological importance of phosphate**

In the previous paragraph, the biological importance of the phosphate is contained in the example of the nucleic acids. Anyway, in living cells, besides structural roles as in DNA/RNA as well as in phospholipids, phosphate groups are embedded in many cellular processes especially at protein level. After the genetic code was fixed, a second role for phosphate esters emerged in biology: reversible proteins phosphorylation became one of the most prominent types of post-translational modifications (PMTs) (Hunter, 2012). More in detail, phosphorylation involves exchanging of the hydrogen atom for a phosphoryl group (PO_3) of an –OH or –NH of a side chain of a protein. This reaction introduces a conformational change in the structure caused by interactions with other hydrophobic and hydrophilic residues (Todd, 1959). Phosphorylation or dephosphorylation processes can affect the biological activity of a protein modulating it on several levels: adding or removing phosphate can mark a protein for breakdown or stabilize its whole structure, facilitate or inhibit movement between cellular compartments and initiating or disrupting protein-protein interaction. This because a phospho-amino acid in a protein acts as a completely new chemical entity that impacts tremendously on the whole protein structure and therefore its functionality (Cohen, 2002; Kamerlin et al., 2013). For example, the phosphorylation state of some transcription factors (TFs) can influence the ability of the latter to bind regulatory region regions of target genes or even prevent/stimulate their import into the nucleus (Whitmarsh and Davis, 2000). However, not only proteins are subjected to phospho/dephosphorylation processes. Nucleotides exist in phosphorylated form and they are essential players in the metabolism of the cells. For example, the adenosine triphosphate (ATP) molecule accumulates chemical energy in the bonds between phosphate groups and this energy is later released *via* hydrolysis supporting diverse fundamental ana/catabolic reactions within the cells. Still, ATP can serve as a substrate to create specific molecules involved in cellular signaling pathways like cAMP (cyclic adenosine monophosphate). Furthermore, the phosphorylation state of a nucleotide such as guanosine di/triphosphate (GDP/GTP) is one of the factors that influence the ability of some important GTPases (e.g. G-, Ras proteins) to interact with other partners. The α-subunit

of some G-proteins, for example, is activated when bounded to GTP and inactivated when GDP-bounded, determining the association state of the remaining subunits β and γ. GTP hydrolysis is accelerated by the GTPase accelerating proteins (GAPs). The association state of these subunits is crucial for signal transduction determining their interaction with target proteins (Lodish et al., 2008). The above-mentioned examples give only a small overall view of a very large landscape of cellular processes in which phosphate groups are directly or indirectly involved.

1.1.3. **Phosphorus in the aquatic environment**

Phosphorus (P) has been discovered by the German alchemist, Henning Brand in 1669 and it is the eleventh most abundant element in the Earth´s crust (0.10%-0.12% on a weight basis). It occurs in inorganic and organic forms distributed in rocks, soils, and sediments (Benitez-Nelson, 2000; Paytan and McLaughlin, 2007; Mackey et al., 2019b). The P inventory in the Oceans consists of about ~3×10^{15} mol of P of which ~2.9×10^{15} mol are in the deep-water and ~0.1×10^{15} mol are in surface waters (Broecker and Peng, 1982). Several debates on the oceanic phosphorus composition have been raised in the last decades. Many classifications are based on the methods of how the compounds are measured analytically. For this reason, it is generally accepted to separate dissolved inorganic phosphorus (DIP) from the dissolved organic phosphorus fraction (DOP). In general, the soluble fraction is commonly delineated as material that typically passes through a 0.2-0.7 µm pore size filter. The material retained in the filter is generally named “particulate” (PIP, particulate inorganic phosphate). In solutions, soluble inorganic phosphorus is analytically characterized as the fraction that can react with molybdic acid and upon ascorbic acid reduction, forming a colored complex (Osmond, 1887) that can be subsequently measurable spectrophotometrically. It mainly consists of HPO_4^- (~87%) and PO_4^{3-} (~12%). Other additional components are represented by easily hydrolysable compounds (Benitez-Nelson, 2000). Several reviews discussed the limits of the colorimetric approach and their implications in the overestimation and classification of the phosphorus compounds in the Oceans (Benitez-Nelson, 2000; Paytan and McLaughlin, 2007; Lin et al., 2016). For that, the SRP (soluble reactive phosphorus) term is more accepted as the phosphorus fraction detectable using the phosphomolybdate technique. The counterpart that does not react with phosphomolybdate is then represented by the SNP (soluble non-reactive

phosphorus) primarily represented by the DOP which is recognized as a class of chemical compounds that comprises those existing or derived from living organisms. However, this fraction can contain compounds in which P does not bind C such as polyphosphates that are usually associated with living organisms (Benitez-Nelson, 2000). The difference between TDP (total dissolved phosphorus) and the SRP is recognized as DOP fraction. TDP can be analytically determined using strong oxidizing agents that convert the total P to inorganic P, measurable *via* the molybdate method. DOP is classified according to the molecular weight where the low molecular weight (LMW, <10 kDa) fraction is the most abundant (50-80%). The high molecular weight (HMW, > 50 kDa) represents typically a smaller fraction (15-30%). Despite the composition of the organic fraction remain not fully characterized, it is possible to divide it into two major groups: phosphoesters (C-O-P bond) and phosphonates (C-P bond) where the phosphoesters fraction is the most abundant (~75%) present in constant proportions throughout the Oceans (Clark et al., 1998; Kolowith et al., 2001). In figure 1, important examples of P compounds are shown.

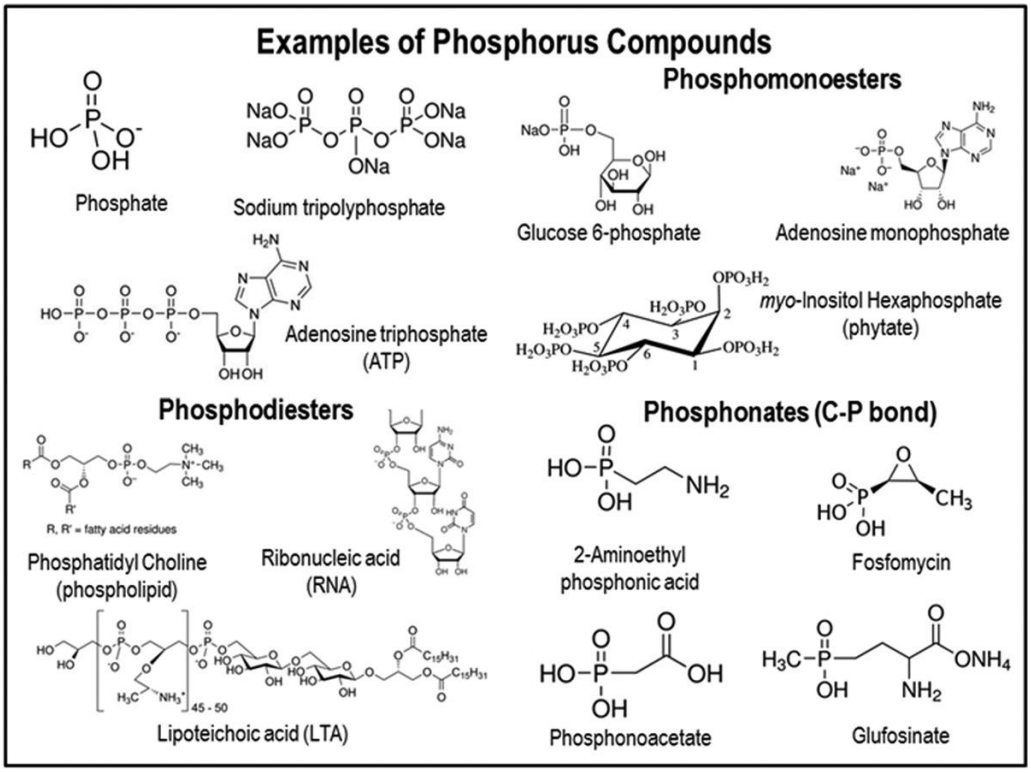

Figure 1. Examples of P molecules of P-compounds associate with living organisms. Modified from (Mackey et al., 2019a).

1.1.4. **The oceanic cycle of phosphorus**

Phosphorus concentrations in the Oceans can largely vary in relation to several factors. Considerable variations are registered when the phosphorus levels are measured according to the depth. In the open Ocean, this is due to biological activity within the euphotic zone where phosphorus is rapidly utilized by the phytoplanktonic and bacterial organisms. Indeed, in surface waters (typically within 80-200 meters), phosphorus concentration ranges from 0.2 nM (Sargasso Sea) to 1-3 µM (eastern margins of the Atlantic and Pacific Oceans, figure 2). The SRP concentration values increase and stay constant with the depth where biological activity drops down due to the reduction of the light. This condition disadvantages the primary production in favor of P remineralization/regeneration activities (Figure 2a). DOP trends show an opposite pattern (Figure 2b): these compounds are not readily utilized by phytoplankton and therefore are present in higher concentrations in surface water where the zooplankton grazing and excretion, cell, plankton cell lysis generate and release nucleic acids, free nucleotides, phospholipids and phosphorylated proteins (Young and Ingall, 2010).

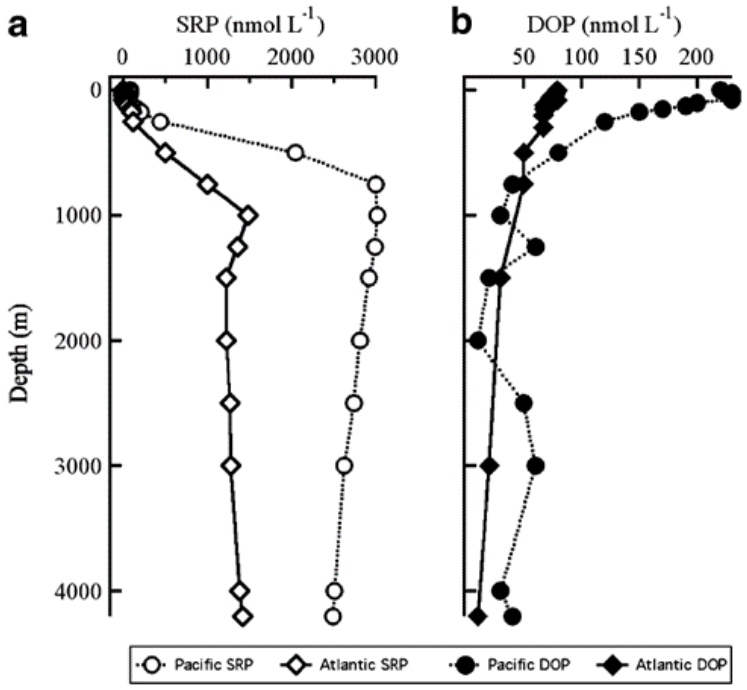

Figure 2. Soluble reactive phosphorus concentration and dissolved organic phosphorus concentration profiles for the Atlantic and the Pacific eastern margins. Soluble reactive phosphorus concentration and dissolved organic phosphorus concentration profiles for the Atlantic and the Pacific eastern margins. Soluble reactive phosphorus (SRP) is depleted in surface waters due to intense biological uptake. Dissolved organic phosphorus (DOP) is generated in surface waters and is remineralized to SRP at depth. Modified from (Paytan and McLaughlin, 2007).

Since P availability has a great influence on the phytoplankton physiology and ecology, it has thus a big impact on the carbon cycle and hence to the global climate. To understand how and why P becomes limiting, it is necessary to explore the P oceanic biogeochemical cycle. This cycle is considered an important link between earth's living and non-living entities and it is governed both by the biotic and abiotic factors (Mackey et al., 2019a). Starting from the non-living part, a significative fraction of phosphorus is delivered in the oceans through continental weathering. It generally consists of particulate and dissolved phases that are transported via riverine influxes. Regarding the particulate fraction, it exists as inorganic particulate (PIP) which is associated with inorganic matter occurring in grains of Apatite or being adsorbed by iron-manganese oxide/oxyhydroxides. However, the described fraction does not contribute directly to the bioavailable pool, instead is quickly deposited in estuarine and coastal shelf environments. Otherwise, clay particles can contain iron and aluminum oxyhydroxides that adsorb P in freshwater. Once the salinity increases in the proximity of the sea outlet, P is released giving a P-input that is 2-5 times higher of the one provided by PIP fraction (Paytan and McLaughlin, 2007). The 10-30% of the P coming from riverine inputs is "bioavailable/reactive" and one-quarter of that may be trapped in the estuaries and never reach open water. The remaining part is deposited on continental shelves and therefore removed from the cycle. Another source of P-influxes comes from the atmosphere. Differently from the N-cycle that has a large atmospheric pool in the N_2, the P-cycle lacks such a significant gaseous component but it still comprises 5% of the total pre-anthropogenic P input in the oceans. Aerosols are the vectors that can transport P and they are associated with eolian dust particles, existing both in organic and inorganic fractions. The inorganic P in mineral aerosols resemble the crustal material composition being bounded to Fe oxides or associated with Ca, Al, and Mg (Chen et al., 2006; Anderson et al., 2010; Nenes et al., 2011; Wu et al., 2020). The organic fraction is still not extensively characterized but recent research showed that land plants could play a role in the input of volatile P compounds such as triethyl-phosphate (Li et al., 2020).

The inorganic fraction is weakly soluble but has been demonstrated that atmospheric P deposition increased the primary production on oligotrophic P-limited regions (Duce, 1986; Migon and Sandroni, 1999; Mackey et al., 2007). Both riverine and continental weathering has undergone a major change as a result of increased anthropogenic activity. Phosphorus-based fertilizer usage and many human activities like sewage, soil erosion, livestock are washed into

rivers, groundwaters, and estuaries. Other types of anthropogenic activity such as soil erosion of cleared land and biomass burning, have instead increased the amount of phosphorus in aerosols. Anthropogenic activity increases considerably the amount of the P input in the Oceans in causing some cases algal overgrowth, phenomena known as eutrophication. The phosphorus of volcanic origin can derive both from gases and lava. Although not extensively studied, it seems that the P-contribution that comes from volcanoes is restricted to a temporary and local but still significant effect. Volcanic gases possess significative amounts of P_i that is converted into polyphosphates upon rapid cooling (Yamagata et al., 1991). Even the entry points of lava can produce gases with a considerable amount of reactive phosphate (Resing and Sansone, 2002).

The oceanic phosphorus cycle is largely shaped by the biotic components of the marine systems. In the open ocean euphotic zones, DIP is rapidly immobilized by microbes that incorporate its organic molecules. Grazing activity as well as phytoplankton cells lysis, release P organic molecules in the form of dissolved and particulate. A large part of it is readily remineralized in the microbial loop (both by phytoplankton and marine bacteria) and re-transformed into inorganic P forms in the spot. Other fractions sink or are moved by downwelling to the aphotic zone, where can be remineralized and utilized in situ and/or returned to the euphotic zone as a result of upwelling phenomena, making it again available for primary producers. Part of this fraction is also deposited and sequestrated into the sediments by sinking (Figure 3).

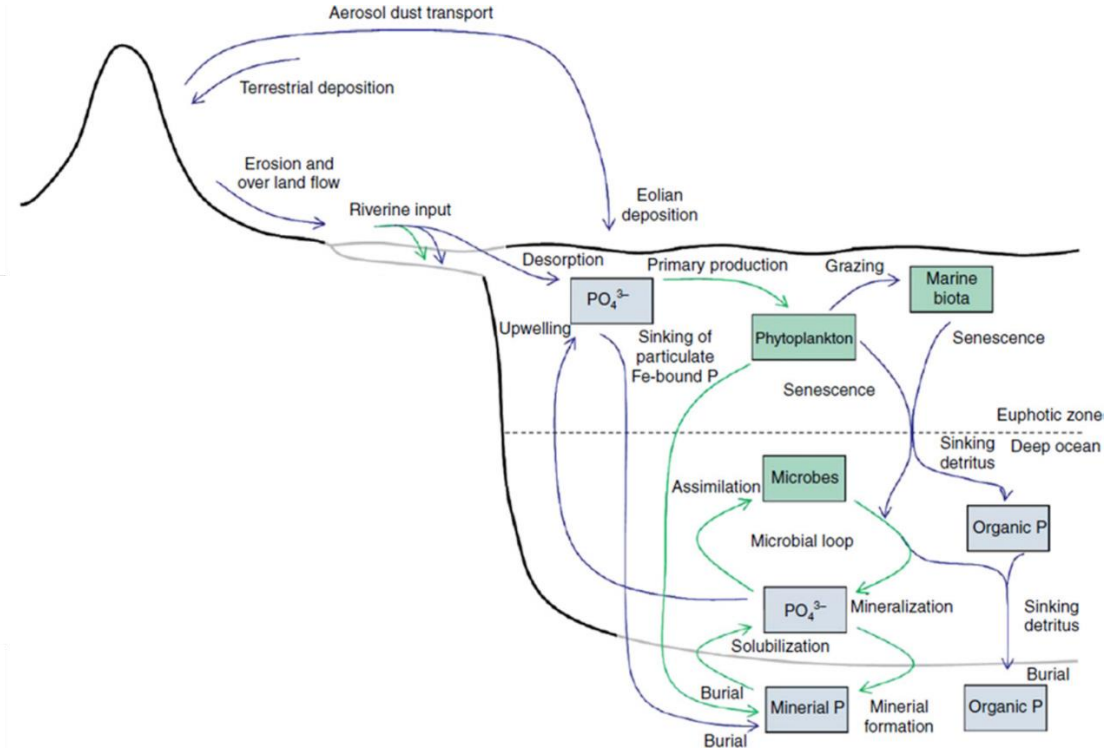

Figure 3. The marine phosphorus cycles. P is mainly delivered in inorganic forms to the Oceans via riverine inputs, aerosol dust transport and continental weathering. The primary sink for phosphorus in the marine environment is the loss to the sediments. In the open waters, P undergoes several transformations mainly due to biological activity. P-reservoirs are shown as living as green boxes and in non-living as blue boxes). The physical transport pathways are represented with blue arrows and microbially-mediated transformations with green. Modified from (Mackey et al., 2019).

1.1.5. **P-limitation in marine waters**

For almost one century, P has been often regarded as the "ultimate" limiting nutrient over long time scales. Marine primary productivity has traditionally been characterized as being mainly N- or Fe-limited. One reason for that was the discovery of the so-called "Redfield ratio". The researchers noticed a striking similarity between the C/N/P elemental composition of bulk marine organic matter and dissolved nutrient concentrations in the deep waters. This finding led to hypothesize that plankton organisms have a constrained C/N/P elemental ratio which is commonly fixed to an average proportion of 106:16:1 representing one of the fundamental tenets of oceanographic biogeochemistry. Redfield hypothesized that the deep ocean nutrient concentrations were controlled by the elemental requirements of the surface plankton (Redfield, 1934). According to this theory, P-limitation should have less impact than N and C in the physiology of primary producers. However, this relationship is not globally consistent

as recently reported where a recalculation of the C, N, and P have different individual ratios of 163, 22, and 6.6 (C:P, N:P, and C:N respectively) (Martiny et al., 2014). Concerning the N:P ratio, several global oceanic surveys on dissolved inorganic nutrients levels (GEOSECS, TTO), have been performed. Often the recorded measurements that spoke for N running out before P (Karl et al., 2001), leading to think that primary production in the Oceans was mainly influenced by the availability of N more than P (Benitez-Nelson 2000). This presumption of a single limiting nutrient like N was based on measurements that did not consider the possible role of organic nutrients in plankton production. Jason and Williams (Jackson and Williams, 1985), implemented the measuring studying the TDP versus TDN. They discovered that TDP is exhausted just prior TDN, contrarily to what generally believed until then. It has been further demonstrated that P availability limits the primary productions at different latitudes: (Krom et al., 1991; Tyrrell, 1999; Litchman et al., 2006; Dyhrman et al., 2007; Elser et al., 2007; Moore et al., 2013; Ly et al., 2014; Andersen et al., 2019; Song et al., 2019). Recently, a global assessment of surface ocean DIP concentrations based on high-sensitivity methods measurements have been conducted revealing previously un-recognized new low-P areas (Martiny et al., 2019).

1.2. Phosphate starvation in Diatoms

1.2.1. **Diatoms: living in a glass cage**

As described in the previous paragraphs, phytoplankton activity has a great influence on global P-cycle. Diatoms represent one of the most successful components of marine plankton communities. Responsible for the 40% of the marine primary productivity (Falkowski et al., 1998), diatoms are believed to carry out one-fifth of the global photosynthesis and the generated organic carbon is rapidly used to sustain many marine ecosystems (Falkowski et al., 1998; Field et al., 1998; Armbrust, 2009). Besides Carbon, diatoms primary production largely impacts on the biogeochemical cycles of other important elements such as Nitrogen (N) and Silicon (Si) (Bowler et al., 2010). It is deemed that diatoms arose on earth in the Triassic period, 250 Myr ago even if the first good-preserved diatom fossil dates back to early Jurassic. They probably became dominant on the planet about 135 million years ago (Armbrust, 2009; Falciatore et al., 2020). They are unicellular photosynthetic organisms evolved as a result of

endosymbiosis events, in which a eukaryotic cell engulfed an organism belonging to the Rhodophyta lineage, previously evolved in primary endosymbiosis event (Cavalier-Smith, 2000). Nowadays, there are several discussions concerning the monophyletic origin of "Chromalveolata" (Cavalier-Smith, 1999) where "Chromalveolata" is intended as a group of organisms descended from a single secondary endosymbiosis involving a red alga and a bikont (Keeling, 2009). Later comparative genomic analyses, revealed the possibility that a green-like alga has been involved in a further endosymbiosis event, as suggested by the presence of more than 1000 genes of green alga origin (Moustafa et al., 2009). Although the debate is still alive with even more theories, these evolutionary steps were crucial not only to acquire the photosynthesis capability. During the reduction of the endosymbiont, a lateral gene transfer occurred from the host and the endosymbiont as revealed by several diatom species genome sequencings (Armbrust et al., 2004; Bowler et al., 2008; Tanaka et al., 2015; Mock et al., 2017; Ogura et al., 2018; Osuna-Cruz et al., 2020). The diatom "chimeric" genomes are probably one of the key factors that contributed to their ecological success. The general classification is based on their morphology, in particular on their symmetry: the first diatoms were "centric", having radial symmetry. About 120 Myr ago, "araphid pennates" diatoms evolved, characterized by bilateral symmetry (Armbrust, 2009). Later arose "raphid pennates", characterized by the presence of a longitudinal slit called "raphe", from which the cells can secrete mucilage to enable a limited active movement. There are more than 250 different genera of diatoms and more than 12000 species (Guiry, 2012) with potentially more cryptic species are known (Mann, 1999). They are able to populate terrestrial and aquatic environments at all latitudes with a greater predilection for marine environments colonizing any available surface such as rocky and sandy substrates, aquatic plants and other algae living as epiphytic flora or adhering to polar ice (Norton et al., 1996). Most of the diatom cells, present a special cell wall named frustule, predominantly composed of hydrated glass ($SiO_2.nH_2O$) (Drum and Gordon, 2003). It is organized in two halves that enclose the cell, arranged together like a Petri dish.

Given their ecological relevance, a lot of knowledge about the physiology of these organisms has been generated. Among several addressed topics, many studies have focused on understanding the adaptations to environmental changes that characterize the aquatic environment, both as a response to stimuli to abiotic (Falciatore et al., 2000; Depauw et al., 2012; Amato et al., 2017) or biotic factors (Amato et al., 2018). The continuous evidence

supporting the limitation of productivity in the oceans, due to fluctuations in concentrations of essential macro- and micronutrients (see paragraph 1.1.5), has directed researches towards the understanding the adaptations of important players in primary production such as diatoms. A lot has been understood concerning physiologic and molecular adaptations to Iron (Fe), Silica (Si) and Nitrogen (N) deficiency (Allen et al., 2008; Shrestha et al., 2012; Alipanah et al., 2015), previously considered as the most important limiting nutrients for diatoms growth. However, when phosphorus limitation was becoming an important topic with respect to microalgae productivity, much effort has been putting in the last decade to understand the cellular response to phosphorus deficiency in diatoms.

1.2.2. **Diatoms and P_i-limitation**

Diatoms response to phosphate limitation has been studied using several approaches. "Omics" is a good starting point to study cellular response to a precise stimulus. As mentioned above, P deprivation in diatoms has been intensively studied profiling transcriptome and/or proteome (Dyhrman et al., 2012; Yang et al., 2014; Feng et al., 2015; Shih et al., 2015; Cruz de Carvalho et al., 2016; Zhang et al., 2016; Alipanah et al., 2018). The overall showed a huge impact on the general metabolism underlying molecular strategies that can be classified both as P-limitation-specific and secondary general stress response (Brembu et al., 2017). The secondary stress response slightly varies among the different diatom species. Field studies and meta-omics data also confirmed that the specific responses are conserved in diatoms and also in other microalgae classes (Alexander et al., 2015; Harke et al., 2017). Transcriptional responses are specifically characterized by the induction of alkaline phosphatases and P-transporters. These mechanisms reflect the common microalgae P-stress strategies that comprise, among the others, modulation of the P transport, P scavenging and degradation of alternative P sources such as DOP (Lin et al., 2016). In the next chapters, the specific and general response to P_i-starvation of the diatom *P. tricornutum* will be described in detail.

1.3. Phosphate starvation response in *Phaeodactylum tricornutum*

1.3.1. The model diatom *Phaeodactylum tricornutum*.

Phaeodactylum tricornutum is a marine pennate diatom firstly described by Bohlin in 1897 in samples collected in Plymouth and Baltic rock pools. It is poorly silicified and shows several morphotypes: fusiform, triradiate, cruciform, round, and oval which are observed in all the available strains (Martino et al., 2007). To date, 10 ecotypes have been characterized concerning their genotype and features (De Martino et al., 2007; Rastogi et al., 2018; Rastogi et al., 2020). The strain named "Pt1" has been used to sequence the genome (Bowler et al., 2008) that was recently re-annotated to update the gene models catalog (Rastogi et al., 2018). The relative ease of cultivation in the laboratory makes this species a suitable and well established experimental model (Bowler and Falciatore, 2019). Several genetic tools are available (Siaut et al., 2007) like genetic transformation (Apt et al., 1996; Zaslavskaia et al., 2000; Zhang and Hu, 2014; Karas et al., 2015) and routine genome editing techniques (De Riso et al., 2009; Daboussi et al., 2014; Nymark et al., 2016; Serif et al., 2017). Currently, it represents a good model to understand diatom biology but it is also used in a large range of science branches. Biotechnology applications find in *Phaeodactylum tricornutum* a good platform, ranging from the medical field (Hempel et al., 2011; Hempel and Maier, 2012; Vanier et al., 2015; Gille et al., 2019), omega-3 oil (Cui et al., 2019) and monoterpenoids production (Fabris et al., 2020) to plastic biodegradation (Moog et al., 2019), displaying potentially more promising and sustainable possibilities (Butler et al., 2020).

1.3.2. Phosphorus stress in *P. tricornutum*

In the last decade, many laboratories focused their research on P-limited *P. tricornutum* using multi-disciplinary approaches. Many studies were mainly carried out profiling the proteome and the transcriptome from cells cultivated under P-stress conditions (Yang et al., 2014; Feng et al., 2015; Cruz de Carvalho et al., 2016; Alipanah et al., 2018) providing the first step in the investigation on whole-cell response. Although the "omics" experiments under P-limiting conditions differ from each other in respect to used strains, cell concentrations, experimental settings and methods (Table 1), the overall view of the generated data sets does not strongly qualitatively differ among each other. In the work of Yang et al., (2014), the transcriptome

(RNA seq.) of *P. tricornutum* cells was studied after 48 hours of P-starvation. An analog experiment was used to profile the proteome (Feng et al., 2015). An important aspect of these two experiments is that the incubation in P_i-depleted condition was applied to cells that were precultured until the early stationary growth phase. The transcriptome (DNA microarray) was studied after 48 and 72 hours in P_i-starved cells cultured in the exponential growth phase (Alipanah et al., 2018). Still, a transcriptome study after 4 and 8 days of P-starvation gave an overview of the long-term P-stress response (Cruz de Carvalho et al., 2016). In the same experiment, the response was additionally studied after 4 days P-resupplementation. The set of genes found as differentially expressed was homogeneous in the described datasets and in line with what was already described in diatoms and microalgae in general.

Table 1. Overview of the "omics" studies on P-stress in *P. tricornutum*.

Omics	Experimental setting	Cell concentration (sampling point)	reference	notes
Proteomics	2 days P-starvation	8.3×10^6 (-P) 7.7×10^6 (+P)	(Feng et al., 2015)	Experiment conducted in early stationary phase
Transcriptomics (RNA seq.)	2 days P-starvation	8.3×10^6 (-P) 7.7×10^6 (+P)	(Yang et al., 2014)	Experiment conducted in early stationary phase
Transcriptomics (RNA seq.)	4- and 8 days P-starvation, 4 days P-resupplementation	Day 4: 1.2×10^6 (-P); 3×10^6 (+P). Day 8: 1.2×10^6 (-P); 4.8×10^6 (+P)	(Cruz de Carvalho et al., 2016)	Experiment conducted in the exponential phase
Transcriptomics (DNA microarray)	2- and 3 days P-starvation	Day 2: 0.5×10^6 (-P, +P) Day 3: 0.8×10^6 (-P) 1.8×10^6 (+P)	(Alipanah et al., 2018)	Experiment conducted in the exponential phase

1.3.3. **General stress response and physiologic changes**

The "omics" studies were integrated with investigations on the physiology of the P-starved cultures. A slowdown of the cell growth and the decrease of the photosystem efficiency (PSII) was observed during P-stress (Yang et al., 2014; Cruz de Carvalho et al., 2016; Alipanah et al., 2018). Cellular density values are at comparable levels after two days of P-starvation where cell division eventually halts and then diverges after 3 days, showing halved growth rates in case of P-starved cultures (Cruz de Carvalho et al., 2016; Alipanah et al., 2018). Similarly, the

Fv/Fm values start to decrease after 1 day of starvation, in line with the changes in pigment concentrations: light-harvesting pigments as chlorophyll *a* (Chl*a*) and fucoxanthin showed significant reduction after 3 days of P-starvation (Alipanah et al., 2018). According to the authors, reduced levels of photoprotective pigments as diadinoxanthin and diatoxanthin play a minor role in the decrease of photosynthetic energy conversion efficiency (Alipanah et al., 2018).

As mentioned in paragraph 1.2.2, the P-stress transcriptome reprogramming is also characterized by a general stress response. Several metabolic pathways are affected by P-limitation. The central carbon metabolism Calvin cycle-related genes showed reduced expression whereas transcripts for glycolysis or gluconeogenesis and pentose phosphate pathway (OPPP) enzymes were more abundant (Yang et al., 2014; Cruz de Carvalho et al., 2016; Brembu et al., 2017; Alipanah et al., 2018). Amino acid and nucleic acid metabolisms are also downregulated (Feng et al., 2015). Interestingly, several traits of this general response are shared with a N-stress general response. Alipanah and coworkers (2018) compared the transcriptome and metabolome of P- to N-deprived *P. tricornutum* cells: similar regulation patterns were observed indeed in genes involved in central carbon metabolism, porphyrin and chlorophyll metabolism, purine/pyrimidine biosynthesis, transcription, amino acid biosynthesis, and translation (Levitan et al., 2015).

1.3.4. **Specific P-stress response**

According to the differentially expressed genes and available physiology studies, the P_i-specific response can be articulated in several levels: P scavenging, transport, lipid metabolism, and storage, and P-regulatory network.

1.3.4.1. Phosphate scavenging

P-limitation primarily triggers the upregulation of transcripts encoding for alkaline phosphatases/phosphodiesterases. When the availability of inorganic P_i is scarce, these classes of enzymes are able to hydrolyze phosphate groups from DOP molecules (dissolved organic phosphate) (Lin et al., 2016) which include for example several intra- and extracellular esters of phosphorus (Paytan and McLaughlin, 2007). In the above-mentioned data sets, genes

encoding for alkaline phosphatases, phytases and 5´-nucleotidases were found to be upregulated in P-starvation independently from the duration of the experiment (Yang et al., 2014; Feng et al., 2015; Cruz de Carvalho et al., 2016; Alipanah et al., 2018). Some of these proteins like Phatrdraft_49678 and 47612 were found to be secreted into the surrounding medium (Lin et al., 2013; Buhmann et al., 2016; Erdene-Ochir et al., 2019). Other putative phosphatases (Phatrdraft_39432, 49678, 47869, and 47174) and 5´nucleotidases (Phatrdraft_43694) were still not characterized in detail, but the research by Flynn and colleagues (1986) suggests an extracellular localization as proteins anchored to the cell surface/plasma membrane. In line with the upregulation of APs, extracellular and cellular phosphatase activity significantly increases during P-stress (Cañavate et al., 2017a; Cañavate et al., 2017b). Phosphatase activity assays are also used as a biomarker for P limitation in the marine environment and single cultures (Dyhrman and Palenik, 1999; Cañavate et al., 2017a). Furthermore, the experiment with P-resupplementation revealed interesting aspects concerning the sensitivity to the external P concertation of some genes. For example, alkaline phosphatase genes expression (Phatrdraft_39432, 49678, 47869) showed a reverse tendency in respect of early/late P-starvation when the P-starved cells were moved in fresh P-replete f/2 (Cruz de Carvalho et al., 2016).

1.3.4.2. Phosphate transport

Alkaline phosphatase induction reflects a common strategy to scavenge phosphorus in the surrounding environment. The most readily bio-accessible form of P is represented by inorganic phosphate (PO_4^{3-}, P_i) that can be easily taken up by the cell. During P-starvation induction of putative P_i-transporters was observed in *P. tricornutum* (Yang et al., 2014; Feng et al., 2015; Cruz de Carvalho et al., 2016; Alipanah et al., 2018). Several genes encoding for putative sodium-dependent P_i, inorganic P_i transporters, and permeases were found to be significantly upregulated: Phatrdratf_40433, 47667, 49842, 47666, 47239, 23830, 39515, 22315, 33266. This strategy is coherent with the increased P demand and the presence of the P_i provided by phosphatase activity. For that, the cells increase the number of P_i-transporter possibly at the cell surface to maximize the uptake efficiency. Recently, a paper described the dynamics of response of *P. tricornutum* P_i-uptake machinery in different temporal P_i gradients combining nutrient-uptake bioassays, transcriptomic analyses and mathematical modeling (Cáceres et al., 2019). They showed that the transcriptional upregulation of three putative

transporters (Phatrdraft_47666, 47667, 39515) was coupled with an increase of maximum nutrient-uptake (V_{max}) when the cells are P-starved and P-resupplied with low P amount (3 µM). Bot Vmax and gene expression decreased using a stronger P pulse supplementation (15 µM).

1.3.4.3. Lipid dynamics

Nutrient or more in general environmental stress causes lipid accumulation as an adaptation response in many phytoplankton species. Besides the increase of number and size of lipid droplets, *P. tricornutum* P-starved cells showed lipidome profiles characterized by a significative increase of total lipids levels (e.g. triacylglycerol (TAG), diacylglycerol (DAG) and a decrease of phospholipids (PL) content (Gong et al., 2013; Yang et al., 2014; Abida et al., 2015; Cruz de Carvalho et al., 2016; Alipanah et al., 2018; Huang et al., 2019). Transcriptional data also support these physiologic changes. According to Yang et al., (2014) TAG accumulation was proposed to be partially attributed to *de novo* synthesis since genes encoding for ACCases (Acetyl-CoA carboxylase), pyruvate-dehydrogenase precursors and, ketoacyl-CoA synthase were upregulated during P-starvation. Contrarily, in the work of Alipanah et al., (2018) such genes were not differentially expressed and, in some cases, even downregulated, supporting the idea that P-stress induced lipid accumulation could be related to diverse aspects. Indeed, a different scenario is suggested by the lipid remodeling under P-deprivation. It has been shown in several experiments that PL content dramatically and specifically decreases for the effect of P starvation being substituted by betaine class lipids like diaglyceryl-hydroxymethyl-N,N,N-trimethyl-β-alanine (DGTA), sulfoquinonevosyldiaglycerol (SQDG), or galactolipids as monogalactosyldilgycerol (MGDG) and digalactosyldilacyl-glycerol (DGDG) (Gong et al., 2013; Abida et al., 2015; Cañavate et al., 2017a; Cañavate et al., 2017b; Huang et al., 2019). Upregulation of specific genes encoding for phospholipase type-C and D and sulfo- and betaine lipid biosynthesis enzymes during P-starvation supports these physiologic changes. As a result of this process, some intracellular membranes resulted in poorly organized and disrupted (Yang et al., 2014).

1.3.4.4. Phosphate storage

Many unicellular organisms are able to store di excess of phosphate, mostly in the form of polyphosphate (polyP). These molecules are often accumulated in the vacuole in a process called “luxury uptake” and allow these organisms to tap into a readily accessible pool of P_i in case of non-optimal P-conditions (Harold, 1966; Lin et al., 2016; Sforza et al., 2018; Solovchenko et al., 2019a; Solovchenko et al., 2019b). So far, no studies have been performed in *P. tricornutum* in this direction. Organisms that store polyP in their vacuoles, usually express a set of proteins named vacuolar transporter chaperone subunits (Vtcs), that form the so-called Vtc complex. This machinery mediates the polymerization and transport of polyP into the vacuole in many eukaryotes (Yang et al., 2017). At least 4 genes encoding for putative Vtcs proteins were found to be differentially expressed in P-starvation datasets: Phatrdraft_48811, 35739, 48538, and 50019. Phatrdraft_35439, encoding for a putative Vtc subunit, was found to be localized in the vacuolar membrane (Schreiber et al., 2017) supporting the idea of the vacuole as P storage compartment. However, expression data among the different omics data sets are not homogenous. In Yang et al., (2014), Phatrdraft_50019 which is supposed to be the polymerization core of the putative Vtc complex (Vtc4), is downregulated during P-starvation. This in line with the hypothesis that this complex might be involved in polyP accumulation in P-replete conditions. Contrarily, the upregulation of this gene was observed in Alipanah et al., (2018) and Cruz de Carvalho et al., (2016). In the latter, this gene was strongly upregulated with a downregulation after P-resupplementation which is not coherent with the luxury uptake hypothesis.

1.3.4.5. P-Regulatory network

The specific P-starvation response is tightly controlled to coordinate the expression of essential proteins. Cruz de Carvalho and coworkers (Cruz de Carvalho et al., 2016) found that 62.5% of the annotated TFs were differentially expressed under P-limiting conditions, and 32% of the upregulated ones are members of the heat shock factor family (HSF). Two putative HSF TFs were predicted to interact with upstream/downstream regions of several protein-coding genes, including such for signaling/sensing and TFs functions. In higher plants and green algae, this response is mainly orchestrated by the activity of a Myb (myeloblastosis) transcription factors (PSR1, *C. reinhardii*; PHR1, *A. thaliana*) that regulates the expression of most of the phosphate responsive genes (Rubio et al., 2001). The transcriptomic study by Cruz de Carvalho

et al., (2016), and Alipanah et al., (2018) revealed the presence of several Myb-like transcription factors among the upregulated genes in P-starvation. One of these, Phatrdraft_47256 (PtPSR) protein was discovered to be one of the master regulators of P-stress response, controlling the expression of P-responsive alkaline phosphatases, P-transporter genes and PL recycling processes (Sharma et al., 2019). This transcription factor is supposed to bind specific regulatory regions (5´-YGAATCTH-3´) present in the upstream region of P-responsive genes that are present in promoter regions of at least 84 P-responsive genes (Sharma et al., 2019).

However, other regulatory mechanisms might play a role in the P-stress response. Cruz de Carvalho and colleagues (2018) suggested a possible role of long intergenic non-coding RNAs (lincRNAs) and micro-RNAs (miRNAs) being specifically induced in P-starvation. The natural antisense transcripts (NATs) were further investigated and 121 P-stress responsive NAT-mRNA pairs predominantly involved in positive regulation of the expression of their cognate sense genes were identified (Cruz de Carvalho and Bowler, 2020). Furthermore, another possible regulator in the P-stress response was discovered: Phatrdraft_47434 is an SPX-containing protein most likely acting upstream to PtPSR as a negative regulator (Zhang et al., 2020). Concerning the sensing of the extra/intracellular sensing of P_i levels, Ca^{2+}-dependent signaling pathways might play an essential role in P-homeostasis: such pathways were shown to be active when the cells were resupplied with 36 µM P, after 4 days in P-limitation (1.8 µM), indicating possible sensing of external P concentrations (Helliwell et al., 2020).

2. Aim of the project

The purpose of this work is to characterize different aspects of P-stress response in the *Phaeodactylum tricornutum* model diatom. The analysis of available transcriptomes has provided several proteins that are potentially important in the acclimatization mechanisms under low-P environmental conditions. To obtain more information on specific cell dynamics and processes related to P-stress response, these proteins need to be investigated in more detail. For example, understanding the cellular compartment in which these proteins are located can provide new information about their function and role under unfavorable phosphorus conditions. To do this, the proteins of interest will be expressed by fusing them with a reporter/tag in order to study the extracellular/subcellular localization. As described in the other organisms, P-stress cellular response is tightly controlled. Besides transcriptional control, many proteins can be regulated at the posttranslational level. With this respect, a possible posttranslational control on the secretion of an important P-responsive protein will be investigated.

In addition, the gene regulation of P-responsive candidates also needs more information. In previous studies, the response was studied only under two environmental P-conditions, i.e. under P-depletion or under standard P-condition in the cultivating medium. For example, studying the behavior of responsive genes under environmental conditions of high phosphorus concentration may help to understand whether these genes are expressed only in the absence of phosphorus or if they are upregulated by a basal level of expression. In this case, an approach will be used that involves the analysis of the expression of a reporter led by upstream and downstream regions of the genes of interest. With this approach, the impact and importance of these regulatory regions will first be evaluated and more accurate expression profiles will be obtained under diverse extracellular P-conditions.

The storage of phosphorus is still an unexplored topic in this organism. In order to identify and characterize possible storage compartments, studies of protein localization potentially involved in such processes will be combined with morphology inspections and functional studies by knockout of specific genes. The latter is carried out with an improved CRISPR/Cas9 technology developed in the hosting laboratory.

The obtained results should add a further level of knowledge of the topic, and integrating them with the available transcriptomic data is possible to map the first atlas of P-homeostasis in *P. tricornutum*.

3. Results

3.1. Identification of P-stress related proteins

The *in-silico* investigations, analyzing P-regulated proteins from published datasets (Yang et al. 2014; Feng et al., 2015; Cruz de Carvalho et al., 2016; Alipanah et al., 2018) and BLAST-searches, identified several putative players involved in P_i-stress response in respect to alkaline phosphatase/nucleotidase activity, P_i-transport, and vacuolar transporter chaperone complex functions. Eight putative alkaline phosphatases were identified in the genome of *P. tricornutum* and named PtPhos1 to 8 (Table 2). One alkaline phosphatase, PtPhos1 (Phatrdraft_49678) is a protein harboring a PhoA domain. PtPhos2 (Phatrdraft_47612) has a predicted phytase-like domain. PtPhos3 to 7 (Phatrdraft_45959, 39432, 48970, 45757, 45174) are proteins with a conserved PhoD-metallophosphatase domain while PtPhos8 (Phatrdraf_47986) is a protein belonging to Aty-PhoA (Atypical PhoA) superfamily. A putative 5´ nucleotidase was found, Phatrdraft_43694, named PtNtase. Putative P_i-transporters were identified as well: PtPho4 is a permease/high-affinity transporter (Phatrdraft_23830) and PtHp$_i$1-2 (Phatrdraft_17265, bd642) are two putative H^+/P_i symporters. Five putative Na^+/P_i cotransporters were found: PtNaP$_i$1 to 5 (Phatrdraft_33266, 40433, 47239, 47667, 49842). The SPX (SYG1/Pho81/XPR1) domain was shown to be present in P-transporters in *S. cerevisiae* and involved in their activity regulation (Broecker and Peng, 1982; Hürlimann et al., 2009). Only one putative P_i-transporter with SPX domain was found in the genome of *P. tricornutum* and it is a close homolog of a vacuolar phosphate transporter in *A. thaliana* (Liu et al., 2015): Phatrdraft_19586, named PtVpt1 that is a putative P_i-transporter with SPX and MFS (Major facilitator superfamily) domain. Searches for putative proteins involved in P-storage, identified Phatrdraft_48811, 35739, 48538 (PtVtc1, to 3) were identified as potential Vtc (vacuolar transporter complex) subunits. PtVtc1 and -2 have a predicted unknown function domain (DUF202). PtVtc3 possesses CYTH-like_Pase sup. Fam. predicted Domain in addition to DUF202 and Phatdraft_50019 (PtVtc4) is a protein with SPX and CYTH-like_Pase sup. Fam. predicted domains.

Table 2. Identified P_i-regulated/non-regulated candidate proteins. Protein IDs refer to Phatr2 database (https://mycocosm.jgi.doe.gov/Phatr2/Phatr2.home.html). Notice that the ID of PtVtc1 is present only in the "all models" of Phatr2 database. (+) signal peptide predictions with the significant score; (-): no signal peptide predicted; (C-term. /N-term.): indicates the position of the predicted transmembrane helix; reported transcriptomic data are from Alipanah et al., (2018) (log2 fold change), determined after P*i*-starvation for 48 hours in exponential phase, equivalent to the experiments of this work. (/): not determined.

	Running name	ID	SP	THMs	Conserved domain	Transcriptional Regulation
						Alipanah et al. 2018 (2 days -P_i). Log_2 fold change
Alkaline phosphatases/esterase	**PtPhos1**	49678	+	-	PhoA	8,4
	PtPhos2	47612	+	-	Phytase-like	7,4
	PtPhos3	45959	-	1 (N-term.)	MPP-PhoD	1,3
	PtPhos4	39432	/	-	MPP-PhoD	9,2
	PtPhos5	48970	+	1 (C-term.)	MPP-PhoD	/
	PtPhos6	45757	-	1 (C-term.)	MPP-PhoD	7,9
	PtPhos7	45174	-	1 (C-term.)	MPP-PhoD	/
	PtPhos8	47869	+	1 (C-term.)	Aty-PhoA	9,1
	PtNtase	43694	+	1 (C-term)	5'-nucleotidase	7,8
Phosphate transporters	**PtPho4**	23830	+	8	P_i permease	4,3
	PtHp$_i$1	17265	-	12	H^+/P_i transporter	0,4
	PtHp$_i$2	Bd462	-	10	H^+/P_i transporter	/
	PtNap$_i$1	33266	-	10	Na/P_i transporter	/
	PtNap$_i$2	40433	-	10	Na/P_i transporter	5,8
	PtNap$_i$3	47239	-	10	Na/P_i transporter	5,9
	PtNap$_i$4	47667	-	10	Na/P_i transporter	3,7
	PtNap$_i$5	49842	-	10	Na/P_i transporter	0,3
	PtVpt1	19586	-	11	MFS_1 Sup. Fam.+ SPX	4,3
Vtc subunits	**PtVtc1**	48811	-	3	DUF202	/
	PtVtc2	35739	-	3	DUF202	1,8
	PtVtc3	48538	-	3	CYTH-likePase sup. fam.+ DUF202	/
	PtVtc4	50019	-	3	SPX+CYTH-like_Pase sup. fam.	-0,9

In table 2 are listed all the candidate proteins that are subsequently investigated in this work. All the protein sequences were selected according to the availability of the gene models and screened for putative signal peptides, transmembrane domains (TMHs). Transcriptional regulation according to Alipanah et al., (2018) is also reported. PtPhos1 and 2 showed predicted signal peptide and no transmembrane helices. PtPhos5, 6, 7 and 8, and PtNase, showed single TMH at C-terminus while in PtPhos3 the TMH is predicted to be located at N-terminus. Of these proteins, only PtPhos5-8 and PtNtase possess a predicted signal peptide. For PtPhos4 no significant score for THMs and signal peptide was predicted. Among all the identified putative P-transporters only PtPho4 encodes for a predicted signal peptide. As expected all the transporters show several multiple predicted TMHs (Table 2). Topology predictions on the subunits of the putative vacuolar transporter chaperone complex show three TMHs for all the candidates and no signal peptide.

Based on the *in-silico* predictions, several scenarios on the topology of these proteins can be deducted. For all the proteins having a signal peptide and a single TMH at C-terminus (PtPhos5, 8 and PtNtase) is plausible that they might be targeted in the final compartment *via* a classical secretory pathway, exposing the catalytic domain in a "non-cytoplasmic" space that could be extracellular space or a lumen of the interested compartment. Proteins with predicted signal peptide only might be secreted into the extracellular space. PtPhos3, 6 and 7 might be a type II/III membrane proteins with its catalytic domain exposed either to the cytosol or a compartment lumen/extracellular space. Topology predictions for PtPhos6 and 7 revealed the possibility that these two proteins might be integrated into a membrane *via* guided entry being putative tail-anchored proteins (GET pathway).

3.2. Alkaline phosphatases

3.2.1. **Transcriptional Regulation**

To characterize the transcriptional regulation of P-responsive proteins, the expression of selected candidates was investigated via a transgenic approach. For each gene of interest, approximately 1000 bp upstream and 500 bp downstream regions were used to drive the expression of eGFP reporter. Independent eGFP-expressing strains were incubated for 48h in f/2 with different P_i concentrations (0, 36, 72, 90 and 108 µM) and eGFP analyzed *via* confocal

laser scanning microscopy and western blot. Notably, the culture conditions for this experiment and for those that will be described below were the same adopted in Alipanah et al., (2018), where P-starvation treatment was applied to cells in the exponential growth phase. Analysis of *in vivo* eGFP expression revealed diverse patterns of the promoter/terminator cassettes driven-expression. A significant expression level was detected under P_i-starvation for all the genes investigated except *ptPhos5* (Figure 4) were eGFP was constitutively expressed in respect to P_i availability. To better characterize levels of expression, eGFP was additionally studied at protein level *via* western blot.

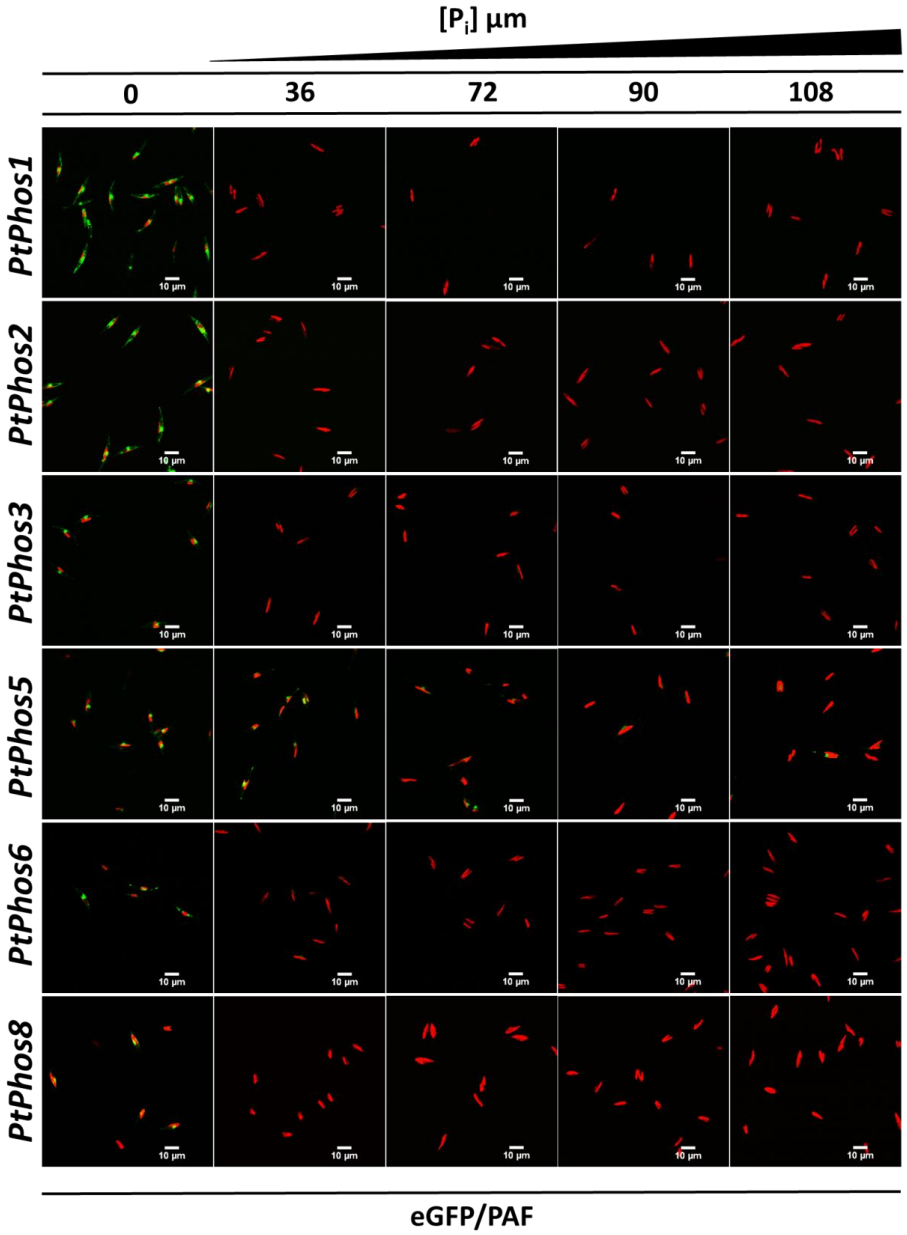

Figure 4. Confocal scanner laser microscopy analysis of *in vivo* eGFP expression of different promoter/terminator cassette strains (denoted in the left side), incubated under different P_i concentrations for

48h. Figures are shown as merged pictures with eGFP (green) and autofluorescence (red). For each cell line, pictures were acquired using the same setting.

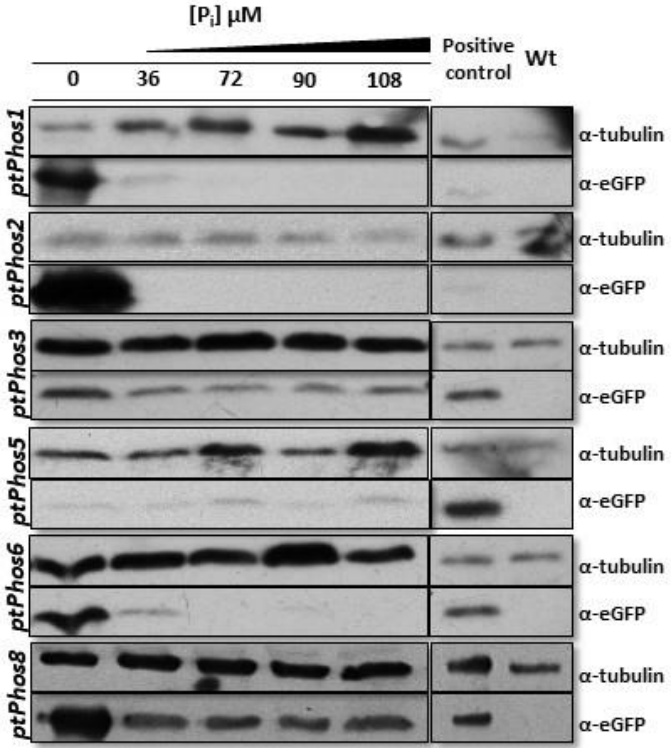

Figure 5. Western blot detection of eGFP protein fused with promoter/terminator cassettes from different phosphatases. Strains expressing eGFP driven by different promoter/terminator cassettes (denoted on the left) were incubated under different P_i concentrations for 48 h. An anti-alpha-tubulin antibody was used as loading control. An eGFP-expressing strain (BTS/EGFP) was used to isolate eGFP and served as positive control. Wild-type protein extract was used as negative control for the eGFP antibody. PtPhos3 and -6 were blotted together and shared the positive and negative controls.

The eGFP protein analysis integrated the results from microscopy *in vivo*: *ptPhos1* and *ptPhos6* showed a significantly increased expression in P-deplete exhibited a basal level when cells were incubated in 36 µM P_i f/2. At higher P_i concentrations, expression was repressed (Figure 5). *ptPhos2* showed expression only under P_i-deplete conditions. *ptPhos3* showed a slight increase of expression under P_i-deplete conditions and a lower level at all the P_i conditions. Similarly, *ptPhos8* showed a lower expression level under P_i-replete conditions but displaying a stronger eGFP expression in P_i-deplete medium. The P_i-constitutive expression of *ptPhos5* was confirmed with no significant variations among the P_i-conditions (Figure 5).

3.2.2. **Secretion of alkaline phosphatase.**

Alkaline phosphatases are generally secreted in the extracellular environment in response to P-deprivation. *P. tricornutum* releases two phosphatases into the medium as already described (Lin et al., 2013; Buhmann et al., 2016; Erdene-Ochir et al., 2019). The secretion of these two proteins was also previously reported in a research conducted in the hosting lab. During the investigation on the secretion of antibodies artificially produced by a transgenic *P. tricornutum* strain, PtPhos1 and 2 were detected into the medium and their relative bands in SDS-page analyzed *via* mass spectrometry. To search for additional secreted proteins in response to P-availability, culture supernatant was further inspected after 2 days of experimental treatment. The analysis was performed testing the secretion under different P_i concentrations. The two bands relative to PtPhos1 and 2 were only detected when the cells were cultivated in P_i-free f/2 (Figure 6). The bands were excised from the Coomassie-stained SDS gel and analyzed again via Mass Spectrometry whose results confirmed the identity of the two proteins (Table 3).

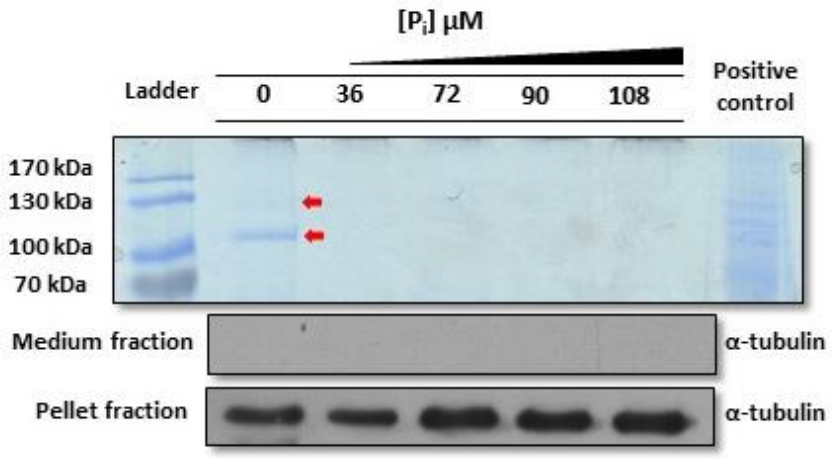

Figure 6. Analysis of *Phaeodactylum tricornutum* proteins secreted in F/2 medium under different P_i concentrations. Coomassie blue staining revealed that two signals at approximately 130 and 100 kDa (red arrows, PtPhos2, and PtPhos1, respectively) are present only under P_i-depleted conditions. A P. tricornutum cell lysate was used as positive control for the Coomassie staining. To verify that the protein extracts of the medium were not contaminated with lysed cells or cell debris, an aliquot of each sample was tested via western blot for the detection of α-tubulin. The same approach was performed with the protein extracts from the cell pellet (same blot) that served as loading control as well as an α-tubulin positive control. A cropped section of the blots is shown.

Table 3. Summary of the Mass Spectrometry analyses performed on the bands showed in figure 7. These results are relative to the experiment ran using the Orbitrap Velos Pro mass spectrometer (Thermo Fisher Scientific) and analyzed using Proteome Discoverer 2.2 (Thermo Fisher Scientific).

Gel slice	Description	Coverage [%]	Peptides	PSMs	Unique Peptides
~100 kDA	Predicted protein OS=*Phaeodactylum tricornutum* (strain CCAP 1055/1) OX=556484 GN=PHATRDRAFT_49678 PE=4 SV=1	24	15	50	15
~130 kDA	Predicted protein OS=*Phaeodactylum tricornutum* (strain CCAP 1055/1) OX=556484 GN=PHATRDRAFT_47612 PE=4 SV=1	12	7	22	7

Interestingly, the molecular masses indicated by Coomassie staining of SDS gels (PtPhos1: ~100 kDa; PtPhos2: ~130 kDa) differed significantly from those calculated based on their amino acid composition (PtPhos1: 77.2 kDa; PtPhos2: 83.8 kDa). In the case of PtPhos1, the protein was expressed from cDNA in the phospho-mimicry experiment obtaining again the same molecular mass band when analyzed *via* western blot (Figures 22 and 23). Despite the Coomassie staining is a reliable method to visualize protein bands within an SDS-page, weakly-expressed proteins might eventually elude their detection. For this reason, extracts of concentrated supernatant were submitted to mass spectrometry analysis whose results revealed no additional secreted phosphatases or P-stress related proteins. A possible target of this approach was the identification of PtPhos4 whose topology predictions indicated that this protein might be secreted into the medium. Thus, this candidate was no further investigated.

3.2.3. *In vivo* localization of membrane-associated phosphatases.

Sub-cellular localization of the additional phosphatases identified *in silico* was determined by expressing them as eGFP-fusion proteins *via* NR promoter/terminator to avoid P_i-regulatory mechanisms. As shown in figure 8, PtPhos3 and PtPhos8 were integrated into the plasma membrane when expressed as eGFP-fusion proteins. The localization was not limited to the

plasma membrane, as endomembrane localization was also detected under the conditions used. PtPhos5- and 7-eGFP fusion proteins were not integrated into the plasma membrane but instead inserted into an internal cell membrane. The eGFP signals were observed in the nuclear envelope and outermost plastid-surrounding membrane suggesting a cER (chloroplast endoplasmic reticulum) localization (Figure 8). PtPhos6 showed the same pattern that was extended to the ER. For all the predicted candidates, *eGFP* was cloned at the 3´ end of the phosphatase genes so that eGFP would be located at the C-terminus when expressed as a fusion protein. For PtPhos6, we additionally designed an expression vector in which eGFP was fused at the N-terminus to avoid putative masking of the ultimate C-terminal membrane domain which might be important in case this protein is integrated via GET pathway. In the case of PtPhos6, relocation of eGFP to N-termini did not alter the localization pattern as an ER/cER pattern was observed again (Figure 7).

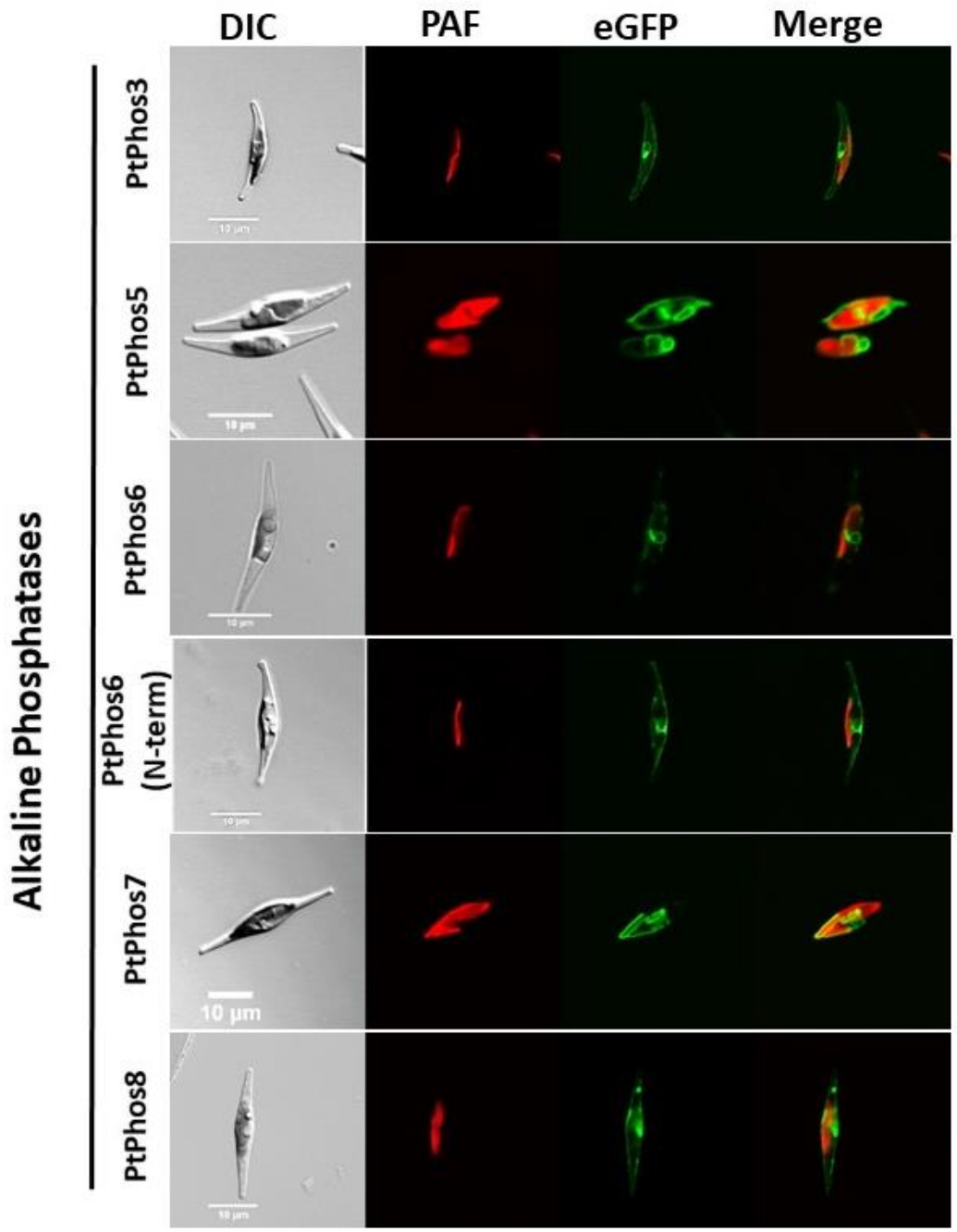

Figure 7. *In vivo* localization of eGFP fusion phosphatases. DIC: transmission light; PAF: plastid autofluorescence; eGFP: eGFP fluorescence. The expression of eGFP-fusion proteins was performed incubating cells in f/2 containing 0.9 nM $NaNO_3$ instead of 1.5 nM NH_4Cl for 24 h in sterile reaction tubes in the conditions described in the material and methods section. Localization studies were performed using confocal laser scanning microscopy using a Leica TCS SP2 with an HCXPL APO40/1.25-0.75 Oil CS objective.

3.2.4. **Phosphatase activity**

A classical approach to identify and localize phosphatase activity is the use of ELF97™ phosphatase substrate. This substrate can be hydrolyzed by phosphatases, forming an alcoholic compound visualized as a yellow-green fluorescent precipitate in the site of the reaction (e.g., Dyhrman and Palenik, 1999). *P. tricornutum* cultures grown in different P_i conditions were tested with this substrate and it was observed that a fluorescent precipitate is formed by *P. tricornutum* wildtype cells, grown both in P_i-limiting f/2 medium and P_i-supplemented medium (Figure 8). As the signals were observed via optical microscopy, it was not possible to determine the exact localization of phosphatase activity.

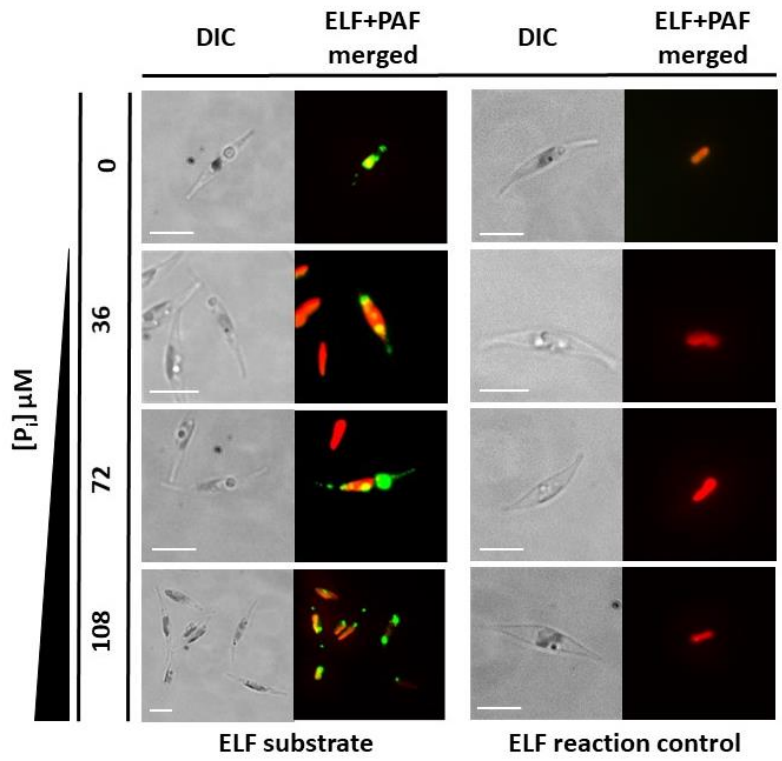

Figure 8. In vivo enzyme-labeled fluorescence (ELF) assays. Wild-type cells grown under different inorganic P_i concentrations for 48 h showed fluorescence (green) emitted through the reaction of phosphatases with ELF substrate. Chloroplast autofluorescence is shown in red. The ELF reaction does not occur without the substrate (ELF reaction control). Scale bar: 10 µm.

3.3. P_i-Transporters

3.3.1. Transcriptional regulation

Transcriptional studies for three selected putative P_i-transporters was carried out using the same strategy adopted for the phosphatases. Among the significantly differentially expressed genes, five candidates were selected for transcriptional regulation studies: PtPho4, PtNaP_i2, and 4, PtVpt1, and PtHp$_i$1. According to confocal scanning microscopy analysis, regulatory regions of *ptNaP$_i$2*, and *4*, *ptVpt1* and *ptPho4* led to an increase of eGFP expression under P_i-limitation (Figure 9). Differently, *in vivo* eGFP expression analysis tested with regulatory regions of *ptHpi1*, showed that P_i availability had not a strong influence driving a constitutive expression.

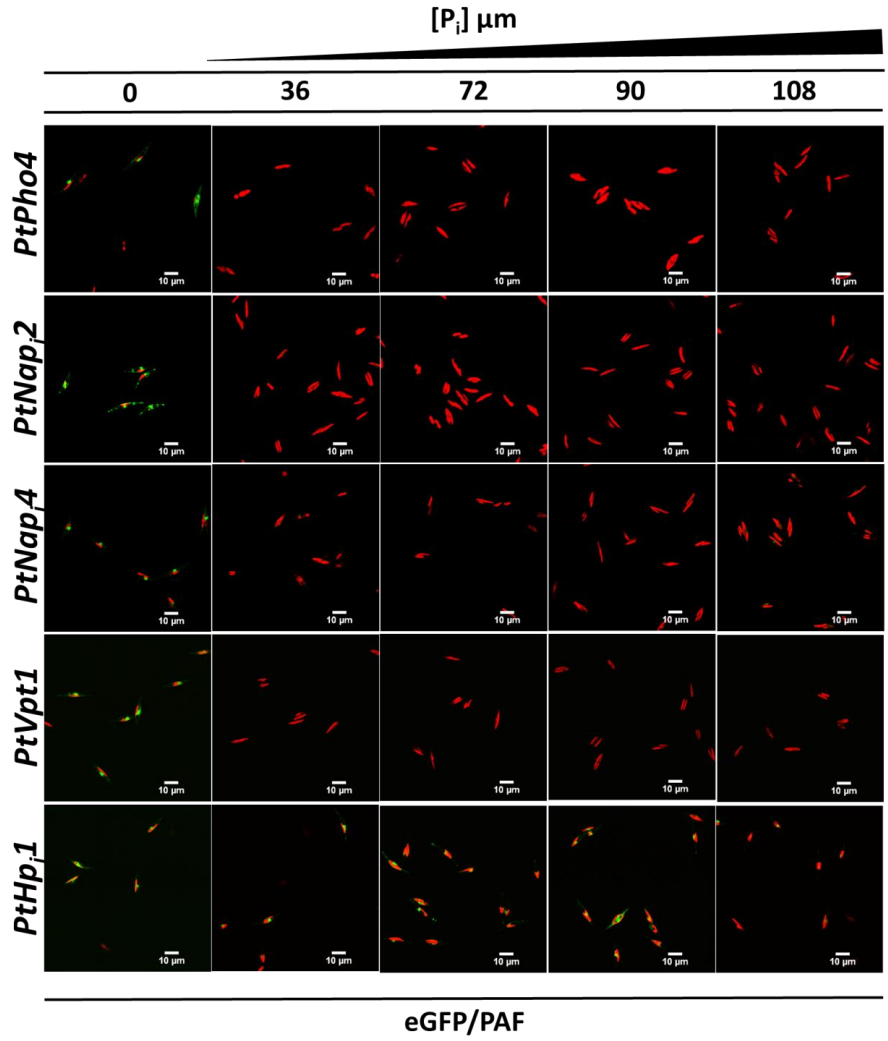

Figure 9. confocal scanner laser microscopy analysis of the *in vivo* eGFP expression of different promoter/terminator cassette strains (denoted in the left side), incubated under different P_i concentrations for

48h. Figures are shown as merged pictures with eGFP (green) and autofluorescence (red). For each cell line, pictures were acquired using the same setting.

To better characterize the expression patterns as it was done for the phosphatases, eGFP expression was evaluated *via* protein analysis. *ptPho4* expression was confirmed to be strongly P_i-stress specific being expressed only under P_i deprivation, whereas the two NaP_i and *ptVpt1* showed a basal level of expression under P_i-replete conditions with an increase of expression under P_i -deprivation. In the case of *ptHpi1*, protein analysis revealed that eGFP expression was lower under P_i-deprivation showing a possible decrease of expression (Figure 10)

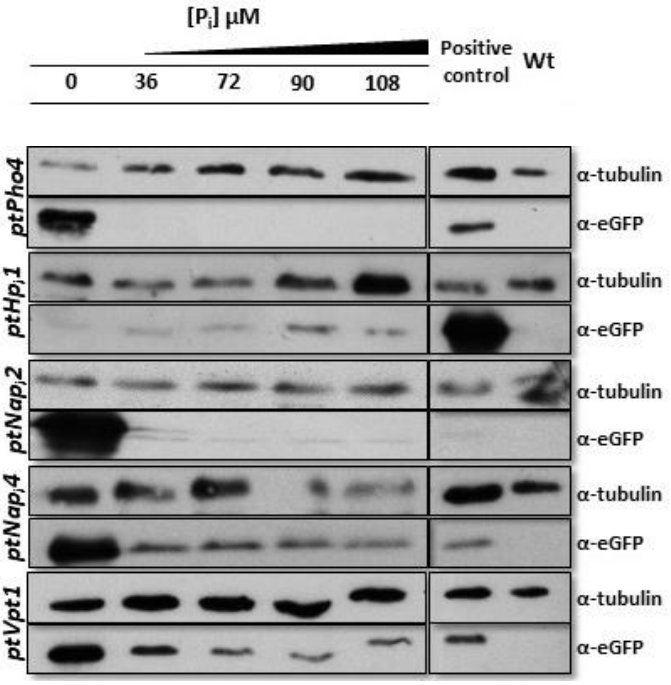

Figure 10. Western blot detection of eGFP protein fused with promoter/terminator cassettes from different P_i-transporters. Strains expressing eGFP driven by different promoter/terminator cassettes (denoted on the left) were incubated under different P_i concentrations for 48 h. An anti-alpha-tubulin antibody was used as loading control. An eGFP-expressing strain (BTS/EGFP) was used to isolate eGFP and served as positive control. Wild-type protein extract was used as negative control for the eGFP antibody. $PtNapi2$ share the positive and negative control with PtPhos2 (Figure 6) being blotted on the same membrane.

3.3.2. *In vivo* Localization of putative P_i-transporters.

Localization studies of putative P_i-transporters were performed as described for the phosphatases. According to the *in vivo* eGFP localization patterns, PtNaP_i2 to -5, PtHp_i2 localized to the plasma membrane. In addition to the plasma membrane, PtNaP_i3 and PtHp_i2 were shown to be localized also in a prominent spot-like structure. PtNaP_i1 and PtPho4 were integrated into the endomembrane system of the ER and cER as described for PtPhos6. PtVpt1-eGFP patterns resembled two lobes of the typical vacuolar membrane localization with as already reported in this specie (Schreiber et al., 2017) (Figure 11).

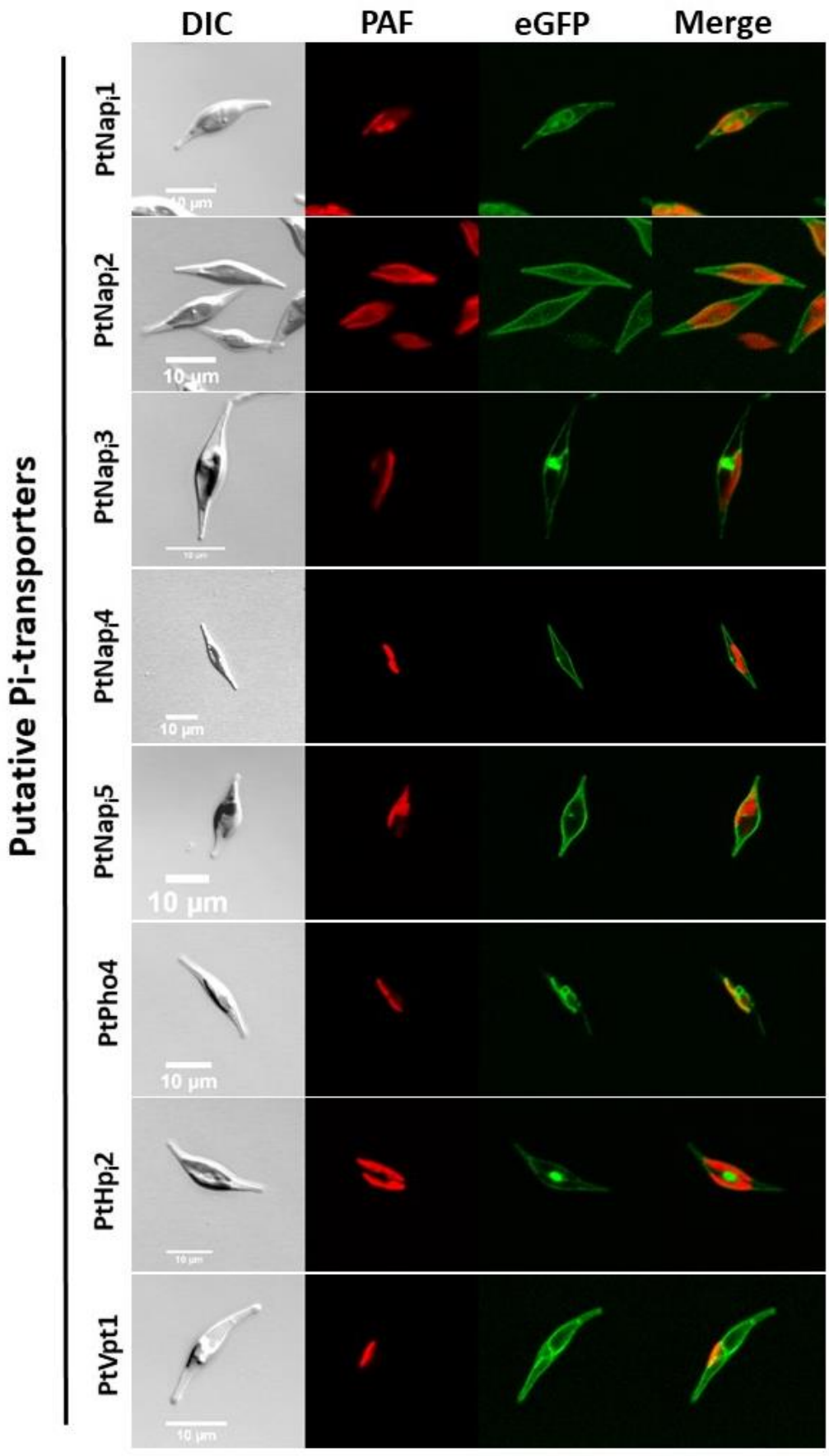
DIC
PAF
eGFP
Merge
Putative Pi-transporters
PtNapi1
PtNapi2
PtNapi3
PtNapi4
PtNapi5
PtPho4
PtHpi2
PtVpt1
10 µm

Figure 11. in vivo localization of eGFP-fusion Pi transporters. DIC: transmission light; PAF: plastid autofluorescence; eGFP: eGFP fluorescence. The expression of eGFP-fusion proteins was performed incubating cells in f/2 containing 0.9 nM $NaNO_3$ instead of 1.5 nM NH_4Cl for 24 h in sterile reaction tubes in the conditions described in the material and methods section. Localization studies were performed using confocal laser scanning microscopy using a Leica TCS SP2 with an HCXPL APO40/1.25-0.75 Oil CS objective.

3.4. 5´-Nucleotidase

Besides alkaline phosphatases, 5´-nucleotidase genes are upregulated under P_i-deprivation. The transcriptional regulation of a putative 5´-nucleotidase (PtNtase, Phatrdraft_43694) was investigated as already described. According to the eGFP analysis via western blot, this gene was expressed only in the case of P_i-deprivation (Figure 12), as already described for *ptPhos2* and *ptPho4* (Figures 5 and 10).

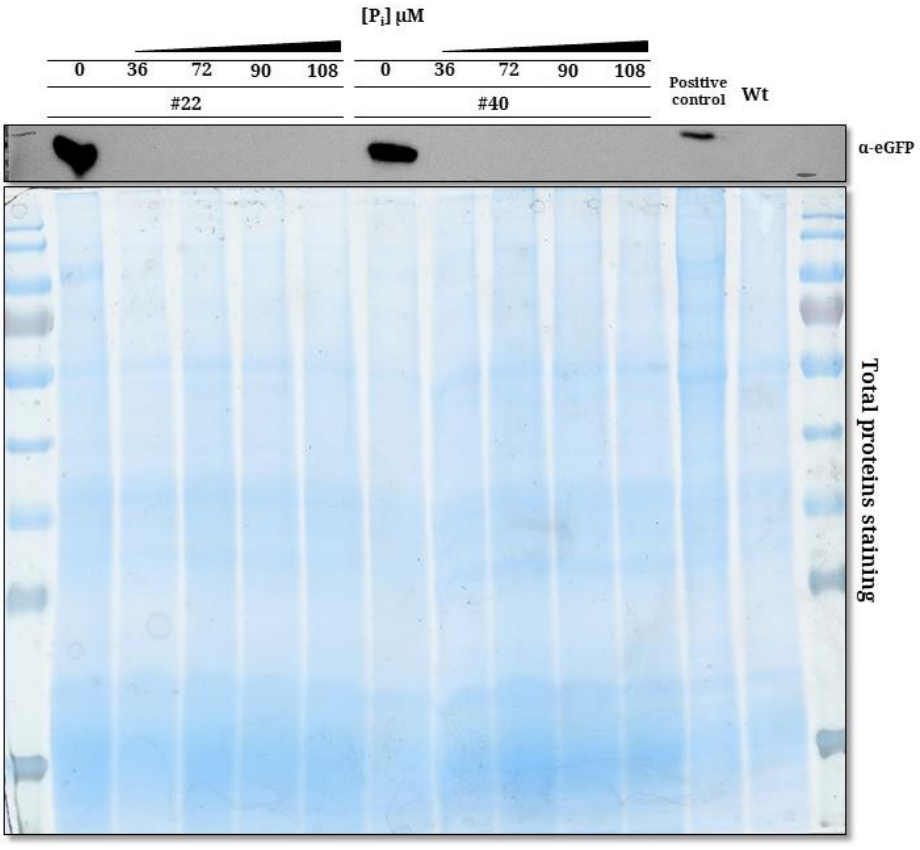

Figure 12. Western blot detection of eGFP protein fused with promoter/terminator cassette from PtNtase. Numbers denoted with #, represent individual analyzed clones. Total protein staining (Coomassie) was used as a loading control.

Next, subcellular localization was investigated. Using eGFP-fusion protein as described above it is showed that PtNtase was integrated into the plasma membrane and in undefined spots (Figure 13).

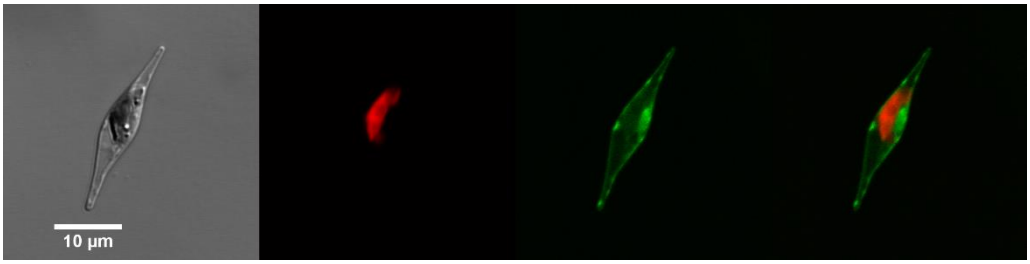

Figure 13. *In vivo* localization of PtNtase/eGFP.DIC: transmission light; PAF: plastid autofluorescence; eGFP: eGFP fluorescence. The expression of eGFP-fusion proteins was performed incubating cells in f/2 containing 0.9 nM $NaNO_3$ instead of 1.5 nM NH_4Cl for 24 h in sterile reaction tubes in the conditions described in the material and methods section. Localization studies were performed using confocal laser scanning microscopy using a Leica TCS SP2 with an HCXPL APO40/1.25-0.75 Oil CS objective.

However, it was not excluded that this protein is secreted to the extracellular environment as suggested by Alipanah et al., (2018). Furthermore, proteomic analysis on wildtype *P. tricornutum* supernatant revealed the presence of some peptides belonging to this protein with a not significant score and grade of confidence (PMSF, unique peptide, Dr. Daniel Moog, personal communication). To test if this protein is secreted into the medium, it was additionally expressed with FLAG and expressed to verify its presence in the medium and cell pellet fraction. Results showed that no signals for a FLAG-tagged PtNtase were found in the supernatant fraction (Figure 14).

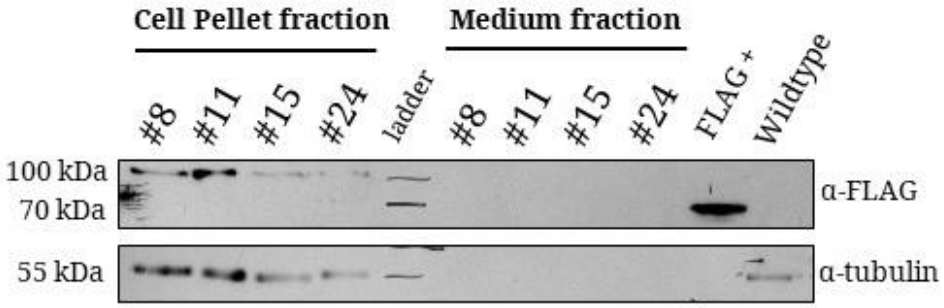

Figure 14. Detection of PtNtase-FLAG in the cellular and medium fraction. α-tubulin (~55 kDa) antibody was used for loading control and to verify the absence of cell debris in the medium fraction. A lysate containing

FLAG-tagged protein (Rockland) was used as a positive control (~60 kDa) and cell-fraction protein extract from wildtype was used both for FLAG negative and α-tubulin positive control. # indicates different used strains.

3.5. Vacuolar transporters chaperone characterization

3.5.1. *In vivo* localization studies

In the published transcriptomic datasets (Yang et al., 2014; Cruz de Carvalho et al., 2016; Alipanah et al., 2018) genes encoding for proteins involved in putative polyP metabolism were found to be differentially expressed. In table 2, four proteins were identified as possible players in such metabolism. PtVtc2 was already shown to be a tonoplast protein (Schreiber et al., 2017). The sub-cellular localization of the other three proteins was investigated: PtVtc1 and PtVtc4-eGFP fusion proteins localized in the endomembrane system (ER and cER) while PtVtc3 showed a similar localization pattern of PtVtc2, where eGFP signals were observed in undefined spots (Figure 15).

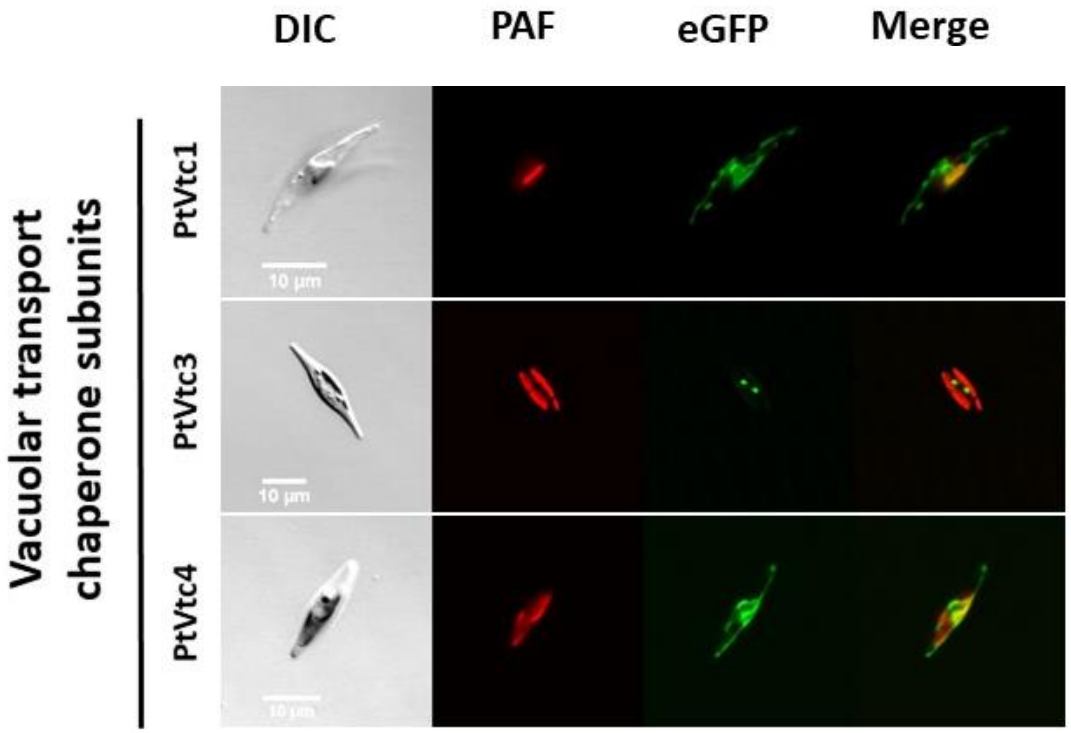

Figure 15. *In vivo* localization of eGFP-fusion subunits of putative vacuolar transporter chaperone complex. DIC: transmission light; PAF: plastid autofluorescence; eGFP: eGFP fluorescence. The expression of eGFP-fusion proteins was performed incubating cells in f/2 containing 0.9 nM $NaNO_3$ instead of 1.5 nM NH_4Cl for 24 h in

sterile reaction tubes in the conditions described in the material and methods section. Localization studies were performed using confocal laser scanning microscopy using a Leica TCS SP2 with an HCXPL APO40/1.25-0.75 Oil CS objective.

In Schreiber et al., (2017), PtVtc2 localization was unclear according to *in vivo* localization of the eGFP-fusion protein and only the immunolabeling approach gave more information on its precise localization. Thus, PtVtc3 localization was further studied via electron microscopy but unlikely PtVtc2, it did not result in a vacuolar localization but an unclear pattern of immunolabeled gold particles with no association with the vacuoles being positioned in non-compartmentalized areas of cytosol (Figure 16).

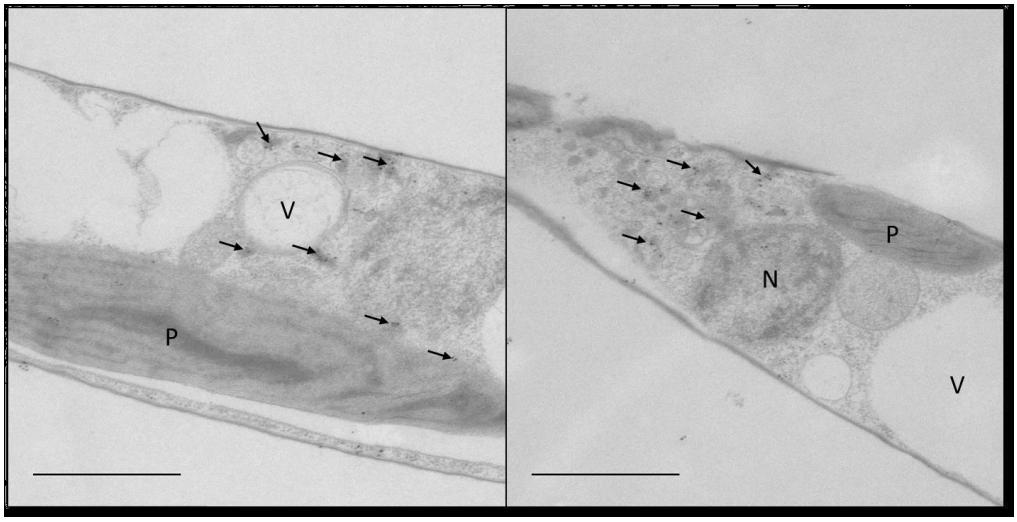

Figure 16. 50 nm ultrathin section showing PtVtc3-eGFP (black arrows). P: plastid; N: nucleus; V: vacuole. Scale bar 1 µm.

3.5.2. ***ΔVtc2* strains characterization.**

PtVtc2 was the only putative polyP-related protein that localized in the vacuolar membrane (Schreiber et al., 2017). This protein was further investigated using KO (knock out) strains lacking a functional gene encoding for this protein. The mutants were obtained with an optimized CRISPR/Cas9 system which was created in the hosting laboratory (Stukenberg et al., 2018). Two homobiallelic *Δvtc2* strains were selected for phenotype characterization: the first indicated as vtc2-158 cl-7iB (1bp deletion) and vtc_272 cl-5iA (1bp insertion) named here

*Δvtc2*_7_2 and 5_11 respectively. Since this protein was localized in vacuolar membranes accumulating especially were two vesicles in fusion collide (Schreiber et al., 2017), possible morphological effects of deletion of this gene were investigated. Cells were stained with the MDY-64 (Invitrogen), a dye for vacuolar membrane, and observed *via* confocal laser scanning microscopy. As shown in PtVpt1 localization studies (Figure 11), the eGFP signals showed two lobes, which are separated from each other in the middle of the cell vacuolar membrane as already reported for *P. tricornutum* (Huang et al., 2016; Schreiber et al., 2017; Huang et al., 2018). The vacuolar membrane structures showed no alterations when the cells of two *Δvtc2* strains were grown in P_i-deplete and high-P_i (108 µM PO_4^-) f/2 (Figure 17).

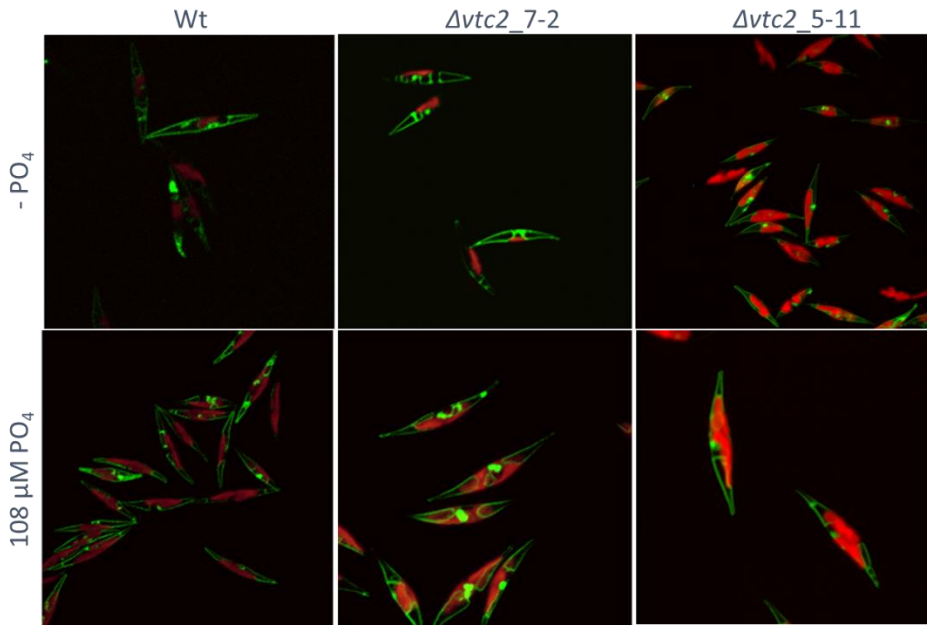

Figure 17. MDY-64 staining of *Δvtc2* and *wildtype P. tricornutum* cells observed in confocal laser scanning microscopy. Autofluorescence is indicated in red and MDY-64 fluorescence in green.

Next, these knockout lines were inspected for possible defects in growth. The cells were first cultivated in high-P_i (108 µM) medium to reset the P_i-stress response and eventually induce the cells to accumulate the excess of P_i. Cells were then moved both to P_i-free and high-P_i f/2 in order to compare the viability under two P_i-conditions (Figure 18). The strains in high-P_i f/2 reached the stationary phase at day 9. A slight difference in cell concentration was observed at day 10 where wildtype culture had a higher cell concentration. The *wildtype* strains grown in P_i-deplete entered in stationary phase at day 3 and individual *Δvtc2* strains one day earlier. From day 3, differences in cell concentration between wildtype and the *Δvtc2* strains were not entirely confirmed by statistical tests in the course of the stationary phase (Figure 18).

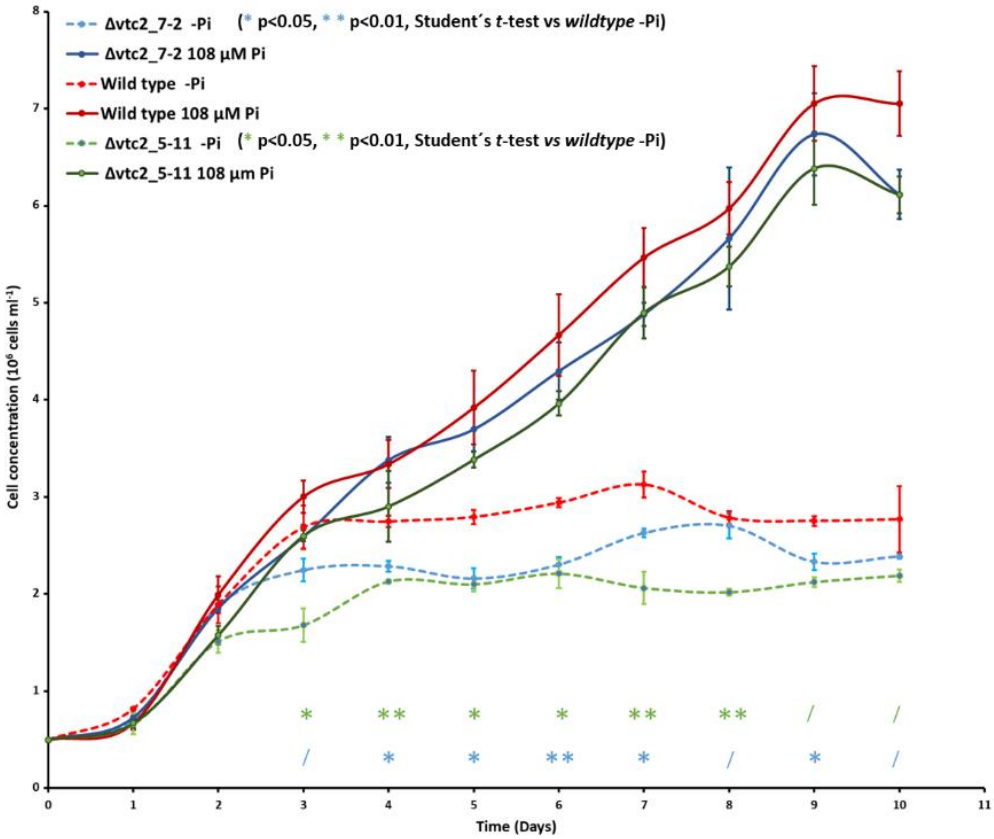

Figure 18. Growth curves of *wildtype* and *Δvtc2* strains under P_i-deplete and replete conditions. The curves are represented as 106 cells/ml over 10 days (x-axis). Error bars indicate standard deviation and the cell concentration values are means of three individual biological replicates measurements. Student´s *t*-tests were conducted to assess the significant differences between wildtype and individual *Δvtc2* strains in P_i-deplete conditions. (*) indicates p-values < 0.05. (**), p-values < 0.01. (/) indicates no statistically-verified differences.

3.6. PtPhos1 posttranslational control

PtPhos1 (Phatrdraft_49678) is one of the essential players in P_i-starvation being strongly upregulated among the different data sets in response to P_i-deprivation (Yang et al., 2014; Cruz de Carvalho et al., 2016; Alipanah et al., 2018). According to the data shown in figure 7, this phosphatase is secreted into the medium only in the case of P_i-deprivation. However, according to the transcriptional regulation results shown in figure 6, the *ptPhos1* gene displayed a low level of expression when cultivated in 36 µM P_i f/2. Thus, a further level of regulation might modulate the secretion of this protein. Screening the amino-acids sequence of PtPhos1, several putative phosphorylation sites after the signal peptide (Figure 19), a

pattern that was not present in the case of PtPhos2 in which the secretion followed the transcriptional regulation (Figure 5-6).

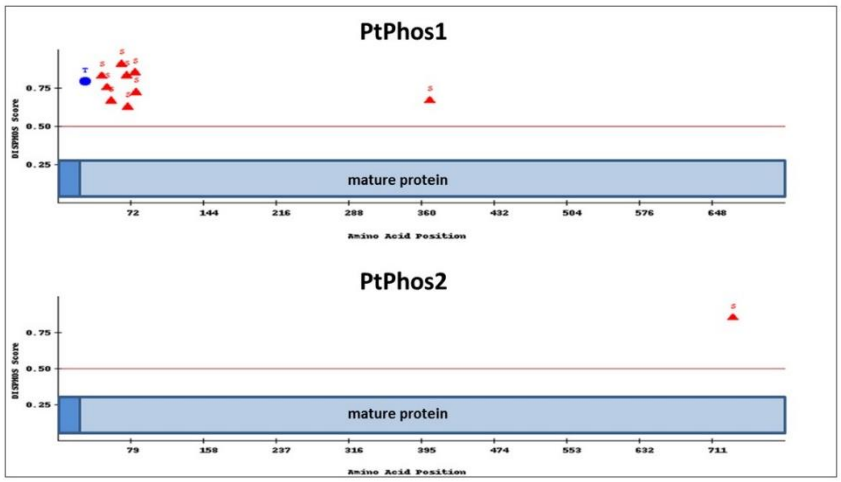

Figure 19. Putative phosphorylation sites prediction using DISPHOS2 (http://www.dabi.temple.edu/disphos/). Predicted phosphorylation sites are shown with red triangles (serine) or blue circle (threonine). The signal peptide is shown in darker blue.

The expression/secretion discrepancy and the cluster of putative phosphorylation sites suggested modulation of the PtPhos1 secretion via reversible phosphorylation. A working hypothesis for fine regulation of PtPhos1 can be assumed: when the P_i external concentration is not limiting, *ptPhos1* gene expression is repressed (Figure 20A) as confirmed by eGFP expression data (Figure 5). In P_i-deficient conditions, the *ptPhos1* gene is slightly expressed (Figure 20B), but the protein would be not secreted as long the N-terminus serines are phosphorylated. The phosphorylation state of PtPhos1 might be mediated by the availability of the internal P_i-stores or the cytosolic P_i-pool. When intracellular P_i-pools are not available subsequently prolonged starvation condition than PtPhos1 could be not phosphorylated and then it is secreted into the medium (Figure 20C).

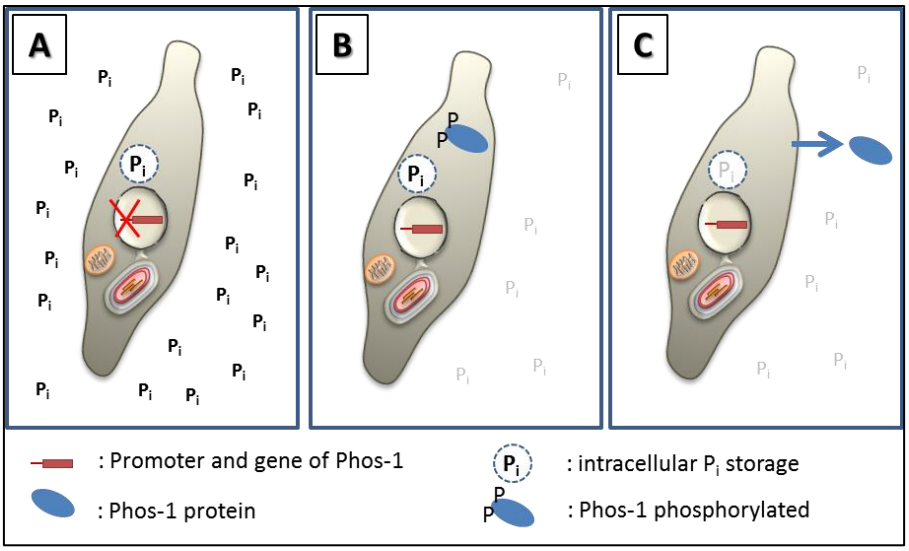

Figure 20. Working hypothesis in the fine regulation of PtPhos1. A: *ptPhos1* is not expressed under high phosphate concentrations. B: *ptPhos1* is expressed, N-terminally phosphorylated, and not secreted as long as intracellular phosphate pools are available. C: in the case of empty phosphate stores PtPhos-1 is not phosphorylated and next secreted.

To investigate wheater these phosphorylation sites are important to regulate the secretion of PtPhos1, the "phospho-mimicry" approach was applied: PtPhos1 overexpression was carried out exchanging serines either to glutamic acid (constitutive phospho-mimicry) or to alanine (non-phosphorylation mimic) and the expression/secretion of them was assessed via western blot analysis in medium and cellular fractions. If the potential phosphorylation sites would be important for secretion, alanine clones should show constitutive secretion in respect of the intra/extracellular P_i-conditions whereas glutamic acid exchange should abolish or attenuate secretion in P_i-replete conditions.

The first experiment was carried expressing all the PtPhos1-FLAG versions in P_i-deplete conditions after a preculturing them in high-P_i f/2 (108 µM). In these early starvation conditions, Phos1 strain (unmutated PtPhos1-FLAG) show attenuated secretion into the medium (Figure 21). Two glutamic acid strains (ΔGlu2 and 9), displayed different patterns: ΔGlu2 showed a stronger signal in the medium fraction compared to the cell pellet one, whereas ΔGlu9 showed no signals in both fractions (Figure 21). Strains expressing alanine-mutated PtPhos1 versions, showed an attenuated secretion as shown for Phos1 strain (Figure 21). After 4 days of P_i starvation, all the strains showed enhanced secretion. Interestingly, ΔGlu9 strain that was not expressing the phosphatase in early starvation conditions, showed expression and weak secretion as expected. However, ΔGlu2 showed a very efficient secretion

which is in contrast with the initial hypothesis. For that, the experiment was repeated including also overexpression in P_i-replete condition (Figure 22)

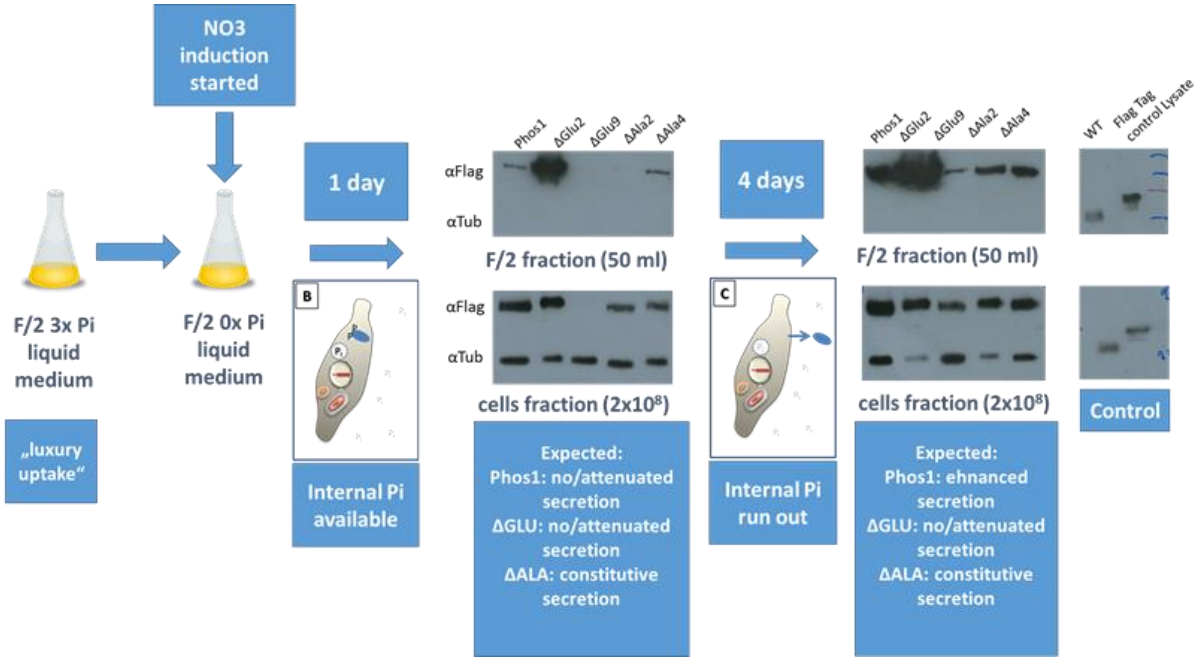

Figure 21. Expression and secretion of PtPhos1-FLAG endogenous and mutated versions. This experiment was carried out as described in paragraph 4.2.1.3 but without the overexpression in P_i-deplete conditions.

Overexpression in P_i-replete conditions showed contrasting results: the phos1 strain did not show weak secretion as expected. ΔGlu2 still strongly secreted the protein whereas ΔGlu9 showed weak secretion and no protein signals were present in the cell fraction (Figure 22). A similar pattern was found in ΔAla strains: ΔAla2 cells displayed expression of the protein in the cellular fraction but a weak secretion into the medium. ΔAla4 showed a weak signal in medium fraction but not in the cellular fraction. In early P_i-starvation, Phos1 and ΔGlu2 strains strongly secreted the phosphatase, while ΔGlu9 showed reduced cellular expression and completely abolished secretion. Again, ΔAla strains showed inversion of behavior in secretion when compared to the previous phase but both expressing the proteins at the cellular fraction level. In the late P_i-starvation, all the strains showed enhanced PtPhos1 proteins in the medium than cellular fraction with a low efficient secretion in the case of ΔGlu9 and ΔAla4 (Figure 22). The results of both experiments showed inconsistent results with the initial hypothesis and the behavior of some strains concerning the secretion and expression of PtPhos1 was additionally not homogeneous in the different phases of the experiments.

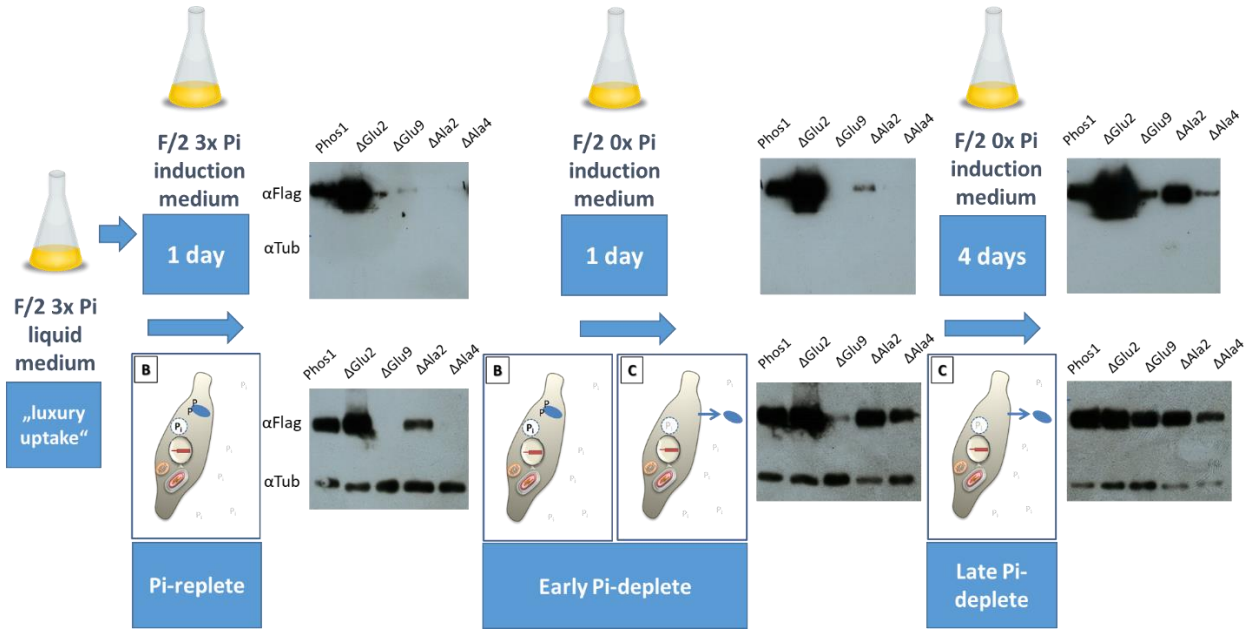

Figure 22. Expression and secretion of PtPhos1-FLAG endogenous and mutated versions (2nd experiment). This experiment included the overexpression in P_i-deplete conditions.

3.7. Genome editing of PtVtc4.

In order to reproduce the method described in Stukenberg et al., (2018), *vtc4* gene was additionally knocked out. One sgRNA was designed using Benchling (Benchling [Biology Software], 2017). After the procedure indicated in 1st level, sequences of 4 clones were obtained (Figure 23): the clone 1 and 2 showed a wildtype sequence with no ambiguities, while clones 3 and 5 chromatograms were characterized by mixed sequences close to the PAM region. Notably, in the case of clone 5, it was already possible to detect a 2 bp deletion. The clones 3 and 5 showed a mixed sequence possibly because they might be composed of a mosaic of cells harboring different mutations on the *vtc4* gene. Thus, either hetero-biallelic or monoallelic mutation is possible. To better characterize these mutations, clone 3 and 5 were analyzed in the 2nd screening level.

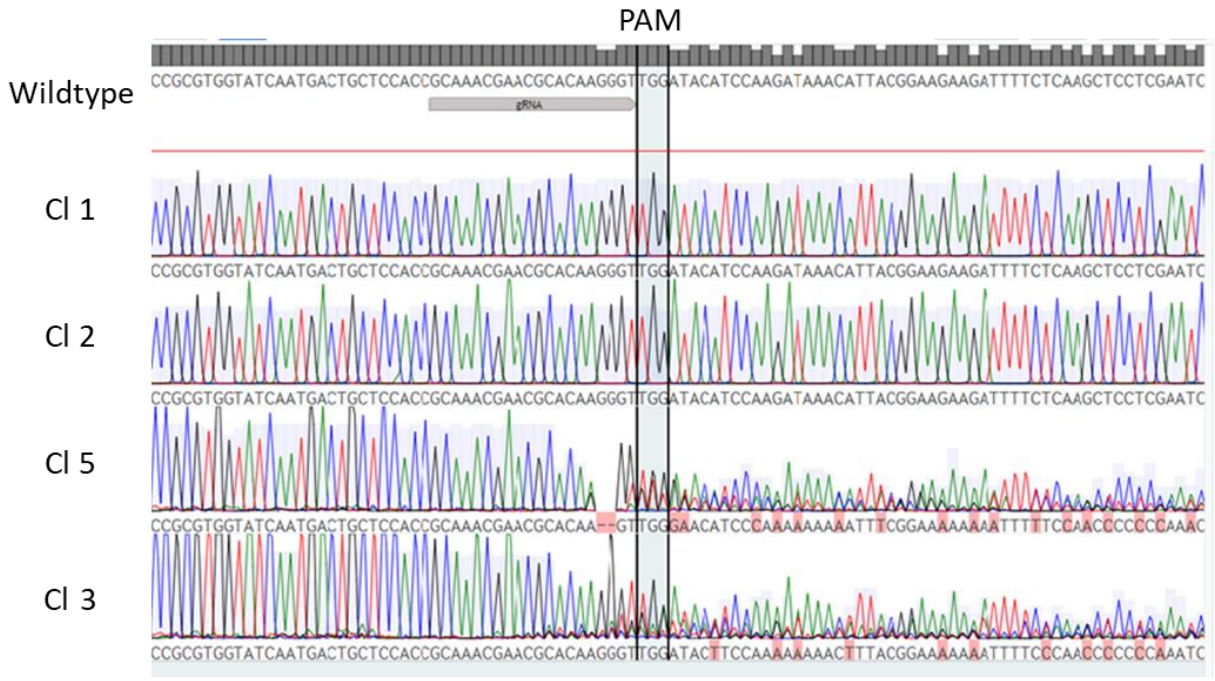

Figure 23. Wildtype and vtc4 1st screening level chromatogram analysis.

For the 2nd level of screening clones, 3 and 5 were cultivated in liquid cultures and then spread into plates containing f/2-agar to obtain single colonies. No colonies were obtained for the of clone 3, while one subclone of clone 5 was isolated and screened for the genotype. The latter showed a single bp deletion with mixed sequence after the expected double-strand break position (Figure 24). Thus, a further level of screening was necessary.

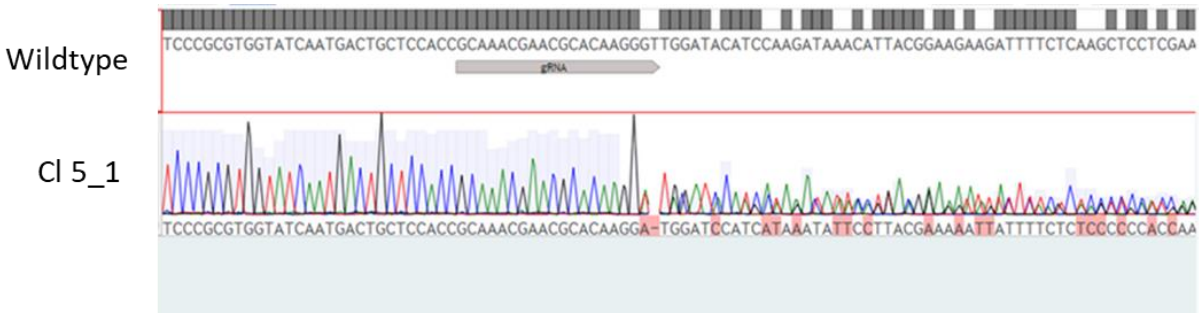

Figure 24. Wildtype and vtc4 sub-clone 2nd level chromatogram analysis. PAM sequence TGG.

The clone 5-1 was thus subjected to a 3rd screening level to obtain information on the allelic composition of *vtc4* after the Cas9 activity. The *vtc4* gene was amplified from this strain and cloned into pJet1.2 which was used to transform *E. coli* TOP10 cells.

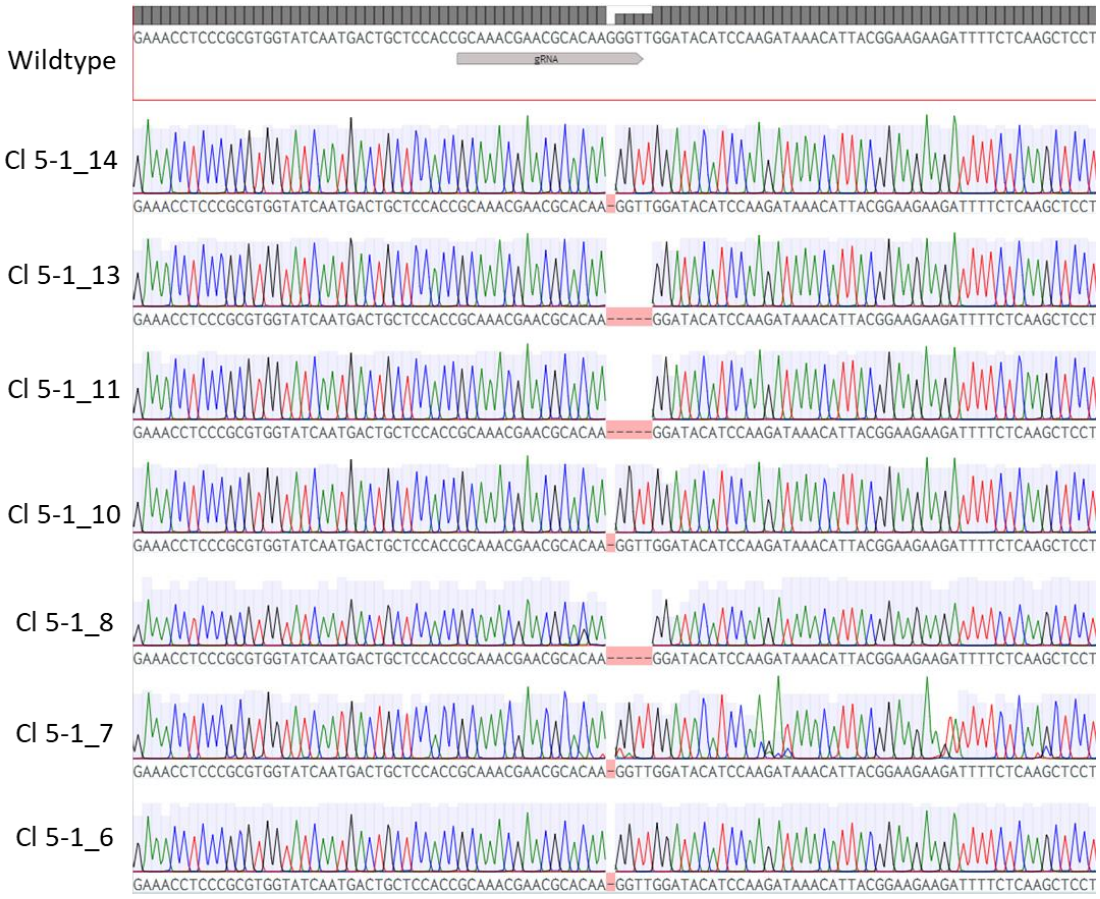

Figure 25. Wildtype and vtc4 3rd level chromatogram analysis of the 5_1 subclone. PAM sequence TGG.

In figure 25, are shown the results of the sequencing of the *vtc4*-PCR products cloned into *E. coli* TOP10: three clones out of seven displayed a 4 bp deletion, while the remaining clones showed a *vtc4* with a single nucleotide deletion. Two different mutations detected in the 3rd screening level, most likely mean that two alleles harbor different mutations after the double-strand break induced by the Cas9. Thus, an hetherobiallelic mutant cell line was isolated.

4. Discussion

4.1. Characterization of the P_i-starvation response

Phosphorus is an essential element of life. Its most common form, the phosphate, is a key molecule in the biology of living beings. It is an integral part of the structure of nucleic acids and phospholipids and plays an important role through the phosphorylation of proteins. However, the bio-availability of this element often influences the biological activity of primary producers, requiring these organisms to implement different strategies to overcome and survive under these limiting conditions.

This also applies to marine diatoms that are important primary producers whose biologic activity in the marine environment, is strongly modulated by the availability of essential nutrients such as Si, N, Fe, and P. For this reason, many studies have been aimed at understanding the mechanisms that allow these efficient microalgae to survive and perform under limiting conditions. This has a relevant importance in the field of basic research to understand how the responses at the cellular level then are extended to higher ecological levels, but also in biotechnology: very often microalgae redirect carbon metabolism in response to nutrient deprivation, producing and accumulating, for example, fatty acids of industrial interest. Although the cellular mechanisms involved in P_i mobilization and intracellular distribution in diatoms are not well understood, several studies have investigated whole-cell transcriptomic responses concerning P_i deprivation (Dyhrman et al., 2012; Yang et al., 2014; Shih et al., 2015; Cruz de Carvalho et al., 2016; Zhang et al., 2016; Alipanah et al., 2018). These studies have shown that some aspects are part of a general stress response and others are phosphate-specific, identifying several factors that can be essential to maintain cellular P-homeostasis. However, the study of the differential expression of these factors alone is not sufficient to fully characterize the adaptive mechanisms. First, transcriptional data do not indicate whether the expression of these candidates starts from a basal level or is activated only in case of phosphorus deprivation. In addition, the expression has only been studied by comparing deprivation and standard conditions. Furthermore, missing data on the localization of candidate proteins hinder more detailed analyses to sketch an atlas of cellular P-homeostasis.

In this work, I was interested in the P_i-stress response in *P. tricornutum* for which three transcriptomic studies are available (Yang et al., 2014; Cruz de Carvalho et al., 2016; Alipanah et al., 2018). Screening these datasets and *P. tricornutum* genome (Bowler et al., 2008; Rastogi et al., 2018), several candidates were identified as putative major players in P_i-starvation. These candidates were studied in respect of sub/extracellular localization and transcriptional regulation in different P_i-conditions. According to the obtained results, three levels of activity are important for P-homeostasis in *P. tricornutum*: (i) extra- and intracellular P_i mobilization, (ii) P_i-uptake, and (iii) transport/export of P_i into/out of organelles.

4.1.1. **Extracellular phosphate mobilization**

4.1.1.1. Secretion of alkaline phosphatases

When inorganic P_i concentration reaches limiting concentrations, the induction of alkaline phosphatases is a widespread strategy adopted by microalgae (Dyhrman and Palenik, 1999; Dyhrman and Ruttenberg, 2006; Lin et al., 2012b; Lin et al., 2016). The activity of these enzymes enables microalgae to scavenge P_i from alternative forms of phosphorus such as organic phosphorus (DOP), thereby increasing the inorganic P_i concentration in the surrounding environment.

In this work, four enzymes acting most likely extracellularly were identified (Figure 6-7): PtPhos1, 2, 3 and 8. The first two phosphatases, PtPhos1 and 2 were shown to be secreted under P_i-deprivation (Figure 5) as reported in other studies on the *P. tricornutum* secretome (Lin et al., 2013; Buhmann et al., 2016; Erdene-Ochir et al., 2019). According to the predicted domains, PtPhos1 is a PhoA phosphatase previously characterized in respect of its biochemistry and shown to be a homodimeric enzyme that requires Mn^{2+}, Mg^{2+}, or Ca^{2+} for its activity (Lin et al., 2013). Furthermore, knockout lines lacking the *ptPhos1* gene, loosed the 95% of extracellular and 75% of the total alkaline phosphatase (AP) activity (Zhang et al., 2020), underlining the role of this protein as the major contributor to extracellular P-scavenging during P_i deficiency. According to the same work, this enzyme was shown to efficiently hydrolyze glycerol-3-phosphate (G3P). PtPhos2 is predicted to be a phytase-like enzyme. Phytase enzymes catalyze the degradation of phytate [myo-inositol(1,2,3,4,5,6) hexakisphosphate] sequentially dephosphorylating it to myo-inositol pentakisphosphate and

inorganic P_i (Wyss et al., 1999; Konietzny and Greiner, 2002). Phytate is present in seawater (Suzumura and Kamatani, 1995a, 1995b), and it is considered as an indicative biomarker of terrestrial phosphorous input. Therefore, *P. tricornutum* might be able to use phytate molecules through the activity of PtPhos2 in addition to other DOP molecules. Furthermore, since this class of enzymes covers a great industrial interest because it has a wide range of applications in animal and human nutrition (Vats and Banerjee, 2004), many efforts were aimed to produce recombinant phytases in microalgae (Yoon et al., 2011; Georgianna et al., 2013). However, the PtPhos2 enzyme requires further characterization to add a new potential biotechnological application for this organism.

The two genes encoding for these proteins were amongst the most upregulated in P_i-deprivation (Yang et al., 2014; Cruz de Carvalho et al., 2016; Alipanah et al., 2018). I investigated the transcriptional regulation with respect to the external P_i concentration using the upstream/downstream region to drive eGFP reporter. According to the protein analysis both candidates are strongly induced under P_i-starvation (Figure 5), as reported in the available datasets (Yang et al., 2014; Cruz de Carvalho et al., 2016; Alipanah et al., 2018). However, the behavior in P_i replete conditions is different: *ptPhos2* expression is repressed under P_i replete conditions, while *ptPhos1* showed a basal level of expression when the cells were cultivated in the 36 µM P_i f/2 (Figure 5). In principle, a basal expression level in media having an initial non-limiting P_i concentration could have been induced by an early starvation response, caused by P_i consumption of the cells. Repression of the expression underlines the possibility to use of *ptPhos2* promoter/terminator modules for synthetic approaches that require fine transcriptional regulation. This was also recently proposed for the upstream region of *ptPhos2* where, P_i regulation was not observed, most likely because of the small size of the analyzed upstream region (499 bp) (Erdene-Ochir et al., 2019). Here the authors fused part of the *ptPhos2* upstream region with the PtPhos2 signal peptide coding sequence creating a synthetic module that can lead to high expression and efficient secretion of a putative transgene-encoded protein (Erdene-Ochir et al., 2019).

4.1.1.2. Fine regulation of PtPhos1 secretion.

An additional level of phosphatase control can take place posttranslationally. PtPhos1 and PtPhos2 secretion is strictly related to the external P_i-concentration as shown in figure 5. However, the transcriptional expression profile of *ptPhos1* displayed a basal level of

expression but secretion was not detected in the same culture conditions (cell concentration, P-concentration). Thus, a further form of control might be present and interestingly, by analyzing the amino acid sequence of PtPhos1 *in silico*, several predicted phosphorylation sites in the N-terminal region of the mature protein were identified (Figure 29). These putative targets for posttranslational modification were not identified in PtPhos2 (Figure 29) where the secretion was in line with the expression patterns (Figure 5-6). According to these findings, it is possible to propose a model for fine regulation of PtPhos1 that is shown in figure 20. To demonstrate that this hypothesis was valid, a phospho-mimicry approach was used. However, according to the used experimental setting, the results obtained do not provide clear indications on the role of these putative phosphorylation sites. Two experiments displayed different secretion patterns that are non-consistent to each other even within the same strain. Only in the first trial, partially promising results were obtained. The NR-overexpressed unmutated version of PtPhos1 (phos1 strain, figure 21), showed attenuated secretion in the first phase of the experiment. This pattern is in line with the suggested model because the protein was overexpressed in early P_i-starvation conditions and the internal phosphorus reserves were probably supposed to be not yet exhausted. In this phase, most of the overexpressed PtPhos1 proteins would have been phosphorylated and thus the secretion might have been blocked. Since the protein was overexpressed using an NR promoter, a significative signal in the cell fraction was detected via WB. Secretion efficiency increased after 4 days of starvation and this could be explained by a combined effect of longer overexpression and depletion of internal P_i. However, the secretion pattern of the same strain was not reproduced and confirmed in the second experiment, where the cells did not show attenuated secretion when the protein was overexpressed under both P_i-replete and deplete conditions (Figure 21). The strains carrying the glutamic acid mutation showed an odder behavior. ΔGlu2 strain showed high secretion levels throughout the duration of the experiments regardless of P-conditions which is in contrast to the proposed model. Glutamic acid can mimic the phosphoserine due to the negative charge of its side chain (Tateyama et al., 2003), thus the phosphomimetic strains must have shown attenuated or even blocked secretion. A second phosphomimetic strain, ΔGlu9 showed an interesting secretion pattern. In the first experiment, no signals in both cellular and medium fractions were detected under early P_i-starvation. After 4 days of overexpression under P_i-deplete conditions, the protein was expressed and scarcely secreted (Figure 21). According to these results, a possible scenario

can be deduced: in the early P_i-starvation phase, the protein was poorly expressed probably due to a low integration frequency of the module. Thus, the amounts of the not secreted phosphomimetic protein would have been adequate to the protein-degradation capacity of the cell at that moment and that would explain the absence of signal in the cell fraction. After 4 days, overexpression became stronger but still, the secretion might have been controlled by the phosphomimetic effect of the glutamic acid. Despite this strain behaves perfectly according to the model, its secretion patterns were not fully reproduced in the second experiment (figure 22). Still, the strains carrying the alanine-mutated version have varied their behavior during the experiments according to all P_i-conditions (Figure 21-22). The substitution of serine with alanine should prevent phosphorylation (Reiken et al., 2003) and thus a constitutive secretion of alanine-mutated PtPhos1 was expected. However, the secretion was attenuated or even not present.

Due to the results, colony-PCR products from the different strains were sequenced to verify the presence of the correct mutations. The strains used were correct, so in light of the obtained results, it is not possible to determine whether these putative phosphorylation sites are involved in the regulation of PtPhos1 secretion. However, other types of PMTs are not excluded. Such modifications might be the cause of the mass shift seen in the experiments in which PtPhos1 and 2 were involved.

4.1.1.3. Cell-surface alkaline phosphatases

The extracellular activity of alkaline phosphatase is not only supported by proteins that are secreted outside the cell. These enzymes can also perform their extracellular catalytic activity by remaining anchored to the cell surface, being integrated into the plasma membrane or cell walls (Dyhrman and Palenik, 1999; Lin et al., 2016). A study revealed that *P. tricornutum* possesses, besides extracellular, a cell-surface associated AP activity (Flynn et al., 1986). However, studying the AP activity in diverse cell fractions does not indicate that the catalytic domains are exposed to the extracellular environment. To identify such enzymes in *P. tricornutum*, the phosphatase activity of potential plasma membrane-localized enzymes was tested via ELF™97 assay. The assay is based on the hydrolysis of a specific substrate (2-(2'-phosphoryloxyphenyl)-4(3H)-quinazolinone) by AP activity that produces an alcohol precipitate at the site of the reaction. The resulting molecule is fluorescent when properly excited making it visible *via* microscopy. This method is commonly used to assess the P-state

of phytoplankton cells in field samples revealing the induction the alkaline phosphatases in response to P-stress (González-Gil et al., 1998; Dyhrman and Ruttenberg, 2006). The enzymatic assay was performed *in vivo* on cells cultivated under different P_i conditions revealing a constitutive AP activity (Figure 8). However, the ELF signals in this experiment do not indicate the exact localization of the activity since they might potentially be generated by intracellular enzymes. The possibility that cells can internalize and process the ELF substrate was indeed reported previously in diatoms and other microalgae (Dyhrman and Palenik, 1999; Dyhrman et al., 2012). The activity seen in the ELF test can be potentially attributed either to cell-surface or intracellular phosphatases. Indeed, the contribution of secreted phosphatases can be excluded since the cells underwent several washing steps that eliminated them before the incubation with the ELF97 substrate.

To better understand the source of the ELF-AP activity, putative membrane phosphatases were studied more in detail. According to *in vivo* the localization studies, PtPhos3 and PtPhos8 might be integrated into the plasma membrane and cER when expressed as eGFP-fusion proteins (Figure 8). PtPhos8 might be a membrane phosphatase that could expose its catalytic domain into the extracellular environment contributing to the activity seen in the ELF tests (Figure 8) and Flynn et al., (1986). According to the topology predictions, this protein might be a membrane protein possessing one single spanning region at C-terminus, and the presence of the signal peptide in the pre-protein sequence might direct its integration in the plasma membrane *via* secretory pathway, leading to expose the catalytic domain extracellularly. This protein possesses a predicted aty-PhoA domain which is conserved in many microalgae (Lin et al., 2015; Li et al., 2018). In the case of PtPhos3, a putative PhoD phosphatase is not possible to predict its orientation concerning the position of the catalytic domain according to the topology predictions.

Studying the transcriptional regulation of these two genes, as performed for *ptPhos1* and *2*, is revealed that PtPhos8 might important in extracellular P-scavenging, since it displayed an increase of expression under P_i-deplete conditions, maintaining a basal level of expression under P_i-replete conditions (Figure 5).

Differently, *ptPhos3* showed a slight increase in expression under P_i-replete conditions (Figure 6) in agreement with weak upregulation seen in the transcriptomic studies (Yang et al., 2014; Cruz de Carvalho et al., 2016; Alipanah et al., 2018). It is possible to hypothesize that PtPhos3

might act intracellularly but its activity would be not crucial or strictly related to the P_i-stress response.

P_i-constitutive phosphatase activity seen in the ELF experiment is in contrast to what is seen in a similar test conducted using *T. pseudonana* where ELF signals were observed only in P-starved cells (Dyhrman et al., 2012). However, *P. tricornutum* could possess such extracellular basal phosphatase activity in P-replete conditions, as previously shown in this species (Cañavate et al., 2017a). Since the concentration of DOP is significantly higher than DIP molecules in the euphotic zone (Figure 2), a basal level of extracellular AP activity might be advantageous to maintain P-balance also when DIP levels are not limiting. However, a posttranslational control on extracellular-acting phosphatases is not excluded also in this case. Thus, *P. tricornutum* scavenges P from extracellular DOP molecules, secreting two alkaline phosphatases and integrating a third one into the plasma membrane. This strategy might enable the diatom to exploit the P scavenging in a very efficient way, living in an aquatic environment where fluid physics potentially impacts on the nutrient acquisition dynamics. The immediate environment of a cell in a fluid medium, such as that of a diatom in the ocean, is not uniform. Instead, the cell is surrounded by a layer that has a higher viscosity than the surrounding fluid. Nutrients in this layer can be taken up by the cell, thereby creating a nutrient-depleted region (Pasciak and Gavis, 1974). Fine-scale turbulence can distort this layer, such that components of the surrounding medium can diffuse more easily to the cell surface (Karp-Boss et al., 1996) and diatoms can benefit from this boundary-layer distortion by increasing phosphate uptake from the medium (Peters et al., 2006; Dell'Aquila et al., 2017). However, microturbulence can also result in molecules drifting out of the layer, including secreted phosphatases. Therefore, it would be advantageous to express a second set of phosphatases that are anchored to the cell surface to provide additional activity within the boundary layer.

4.1.1.4. 5´Nucleotidase activity

The microbe-mediated 5´ nucleotidase activity is recognized to be an important player in P regeneration in aquatic environments (Ammerman and Azam, 1985). In addition to alkaline phosphatase, 5´nucleotidase is induced in response to P-deprivation (Alipanah et al., 2018). One of the most upregulated protein according to transcriptomic data, was investigated in this work, revealing that *P. tricornutum* possess a P_i-regulated 5´nucleotidase that is

integrated into the plasma membrane (Figure 12-13). Alipanah and coworkers (2018) hypothesized that this protein might be secreted in the extracellular environment according to their topology predictions. However, the secretion of FLAG-tagged PtNtase was investigated *via* WB, showing no signals in the medium fraction (Figure 14). Flynn and coworkers (1986) detected 5´ nucleotidase activity in the cell surface fraction and according to the topology predictions and the here shown *in vivo* localization studies, highlight that PtNtase protein can act extracellularly. Unlike the phosphatases, 5´-nucleotidase enzymes can recognize the carbon moiety of the nucleotides, acting more specifically than simple mono/diesterases (Ammerman and Azam, 1991; Benitez-Nelson, 2000). Thus, the presence of a P-inducible 5´nucleotidase expands the spectrum of alternative DOP compounds that can be used by the diatom when inorganic P_i concentrations are limiting. This finds confirmation in the identification of PtNtase, a putative 5´nucleotidase that is P-inducible and localized into the plasma membrane exposing the catalytic domain extracellularly.

4.1.2. **Intracellular phosphate mobilization**

The mobilization of P_i occurs most likely also within the cell. In this work, three phosphatases were identified to be localized intracellularly in the endomembrane system. PtPhos5, and PtPhos7 were found in the cER while PtPhos6 in both cER and ER when expressed as eGFP-fusion proteins (Figure 7). If for PtPhos5, localization of the catalytic domain in the cER lumen is possible due to the presence of the signal peptide (see the PtPhos8 case), for PtPhos6 and 7 it is not possible to speculate on the topology only according the predictions. For these two proteins, the catalytic activity could reside in the lumen or the cytosol if integrated via the GET pathway as C-tail anchor proteins. In order to have more indications about the possible integration pattern and topology of PtPhos6, localization was additionally studied cloning the *eGFP* at 5´ position of the *ptPhos6* gene. This strategy would have underlined possible mistargeting caused by positioning the eGFP at C-terminus where potential targeting motif might be essential for GET pathway-mediated integration (Moog, 2019). Expressing this second version of PtPhos6-eGFP resulted again in ER/cER localization (Figure 7), thus no precise conclusions can be drawn with respect to the topology of this protein.

PtPhos5 and 6 were investigated concerning transcriptional regulation under different P_i-condition. *PtPhos5* show a constitutive expression in all P_i-conditions confirming the non-significant differential expression reported at the transcriptomic level (Yang et al., 2014; Cruz

de Carvalho et al., 2016; Alipanah et al., 2018). In the case of *ptPhos6*, expression was higher under P_i-starvation (Figure 5). A basal level of expression was found under 36 µM P_i f/2 that might be triggered by an early weak P_i-starvation response cause by P_i cell consumption as explained for *ptPhos1*.

Thus, an intracellular ER/cER localized phosphatase, PtPhos6 might be essential in the starvation response. P_i-Inducible phosphatases were predicted to act intracellularly according to a computational study (Lin et al., 2012a), and PtPhos6 is the first P-regulated intracellular alkaline phosphatase to be reported in microalgae. Zhang et al., (2020), also predicted this protein to be intracellular as the knockout of its encoding gene did not produce significative variations in extracellular AP activity. As a predicted PhoD phosphatase, it has a plethora of different phosphometabolites potentially usable to scavenge P like hexose, pentose, gluconates, glycerates, and pyruvate phosphates of intermediary metabolism (Cembella et al., 1984). Even if more studies are needed to establish substrate specifications for different phosphatases a possible role for PtPhos6 can be speculated. The reported reduction in phospholipids and an increase in betaine lipid content has been reported for *P. tricornutum* (Abida et al., 2015; Cañavate et al., 2017a; Cañavate et al., 2017b; Huang et al., 2019) might suggest that endomembrane-localized phosphatases might function in the degradation of phospholipids, and especially in hydrolyzing P_i from lipase-catalyzed phospholipid degradation products under P_i-limited conditions. PtPhos6, which is strongly induced under P_i-limited conditions (Figure 5), is an ideal candidate to perform this potential P_i "recycling" activity.

4.1.3. **Phosphate uptake**

Induction of putative P_i-transporters is a specific trait of the P_i-starvation response in *P. tricornutum*. In this study, four putative Na^+/P_i cotransporters ($PtNap_i2$, 3, 4, and 5) were localized at the plasma membrane (Figure 11) thus potentially involved in phosphate uptake from the extracellular environment. Notably, $PtNap_i3$ showed an additional eGFP spot intracellularly that can be potentially caused by an overexpression artifact: one possible hypothesis is that the endosomal compartment might contain overexpressed eGFP-fusion proteins that are transported from the plasma membrane via endocytic vesicles to lysosomes to be furtherly degraded (Lodish et al., 2008). Two among of the most upregulated transporters, $PtNap_i2$ and -4 (Yang et al., 2014; Cruz de Carvalho et al., 2016; Alipanah et al., 2018) were selected for transcriptional regulation studies and found to be highly expressed in

response to starvation keeping a basal level of expression in P_i-replete conditions (Figure 10). Notably, the upstream region of *ptNapi4* was recently proposed as a novel strong promoter for the expression of lipogenesis-related genes for industrial applications (Zou et al., 2019). In response to starvation, cells increase the number of transporters at the plasma membrane to maximize uptake efficiency, and the P_i-inducible transporter system in yeasts and microalgae is reported to be usually characterized by a high affinity for P_i (Hürlimann et al., 2009; Lin et al., 2016) but so far, no studies where these transporters are characterized in relation their functionality and P_i-binding affinity have been published for *P. tricornutum*. Furthermore, extracellular DOP hydrolysis by the PtPhos1, 2 and potentially by PtPhos8 and PtNtase, generates inorganic P_i in the direct surrounding of the cell. Thus, expressing PtNap$_i$2 and -4 among the others, *P. tricornutum* tends to maximize the uptake from the surrounding environment. These two transporters might be responsible for the increase of maximum nutrient-uptake (V_{max}) under P_i-deplete conditions recently reported by (Cáceres et al., 2019). In the same work, the V_{max} decreased using a P_i pulse supplementation (15 µM). Both increase and decrease of V_{max} were consistently coupled with upregulation and downregulation respectively of the *ptNapi4* gene (Cáceres et al., 2019). Genes encoding for Na^+/P_i cotransporters analyzed in this work still kept a basal level of expression that might justify the decrease of the V_{max}. In any case, a post-transcriptional/translational control could not be excluded. Interestingly, PtNap$_i$2 mRNA was predicted to form a concordant P_i-regulated NAT (natural antisense transcript) pair (Cruz de Carvalho and Bowler, 2020) revealing a possible scenario in the P_i-dependent post transcription regulation of this protein. A phosphorylated version of PtNap$_i$4 was instead detected in a *P. tricornutum* phospho-proteome profiling (Chen et al., 2014), suggesting a possible control of its activity via phosphorylation as proposed for PtPhos1.

PtHp$_i$2-eGFP showed the same localization pattern of PtNap$_i$3, namely into the plasma membrane and possibly in the endosomal compartment. Concerning PtHp$_i$1, it was no possible to determine subcellular localization. However, the gene encoding for this protein was investigated for transcriptional regulation. Expressing eGFP using promoter/terminator regions of this gene, led to a constant level of expression (Figure 9), with a slight downregulation level under P_i-deplete conditions (Figure 10). Transcriptional regulation patterns showed here suggest that this protein might function as low-affinity transporter. P_i-transport system was intensely studied in *S. cerevisiae*, where downregulation of low-affinity

transporters was seen in response to P_i-deprivation both at gene and protein levels (Hürlimann et al., 2009). The putative downregulation of $PtHP_i1$ in *P. tricornutum* might suggest thus a similar mechanism that was also hypothesized by Cáceres and colleagues (2019) according to mathematical models feed by gene regulation, V_{max} measurements, and nutrient uptake assays data. However, it is not clear if and how this P_i-transport modulation mechanisms take place and which molecular players are involved. The finding of the PtPSR alone does not explain the dynamics that drive the up/downregulation of the P_i-responsive genes and no data are supporting a P_i-regulated protein degradation process. Concerning the latter, it is known that this process in *S. cerevisiae* involves the SPX (SYG1/Pho81/XPR1) domain present in the low-affinity P_i-transporters. Interaction of this domain with Spl2 protein (Hürlimann et al., 2009) mediates their targeting into the vacuole for degradation (Ghillebert et al., 2011; Secco et al., 2012b). However, none of the putative plasma membrane P_i-transporter possesses SPX domain suggesting that this type of mechanism might be different in *P. tricornutum*.

4.1.4. **Phosphate distribution**

When inorganic P_i is internalized in the cell by transporters at cell borders, it must be distributed to different compartments. Localization studies highlighted the presence of putative P_i-transporters in the endomembrane systems, two of which ($PtNap_i1$ and PtPho4) were likely localized to the ER/cER (Figure 11). Transcriptional regulation studies of PtPho4 revealed that the gene encoding for this protein is strongly regulated by the external P_i concentration, being expressed only under P_i starvation conditions (Figure 10). However, the localization of PtPho4 in the endomembrane system was unexpected. This protein is a close homolog of Pho89, a repressible plasma membrane high-affinity P_i-transporter described in *S. cerevisiae* (Andersson et al., 2012; Secco et al., 2012b; Secco et al., 2012a) involved in the acquisition of external P_i (Sengottaiyan et al., 2013). Data shown here do not support that PtPho4 is a plasma membrane-localized transporter. However, is not excludable that this protein undergoes P_i-regulated posttranslational modification which led to the elimination of it from the plasma membrane as described in yeast in P_i-replete conditions (Secco et al., 2012b). In the case of degradation, this protein would be targeted to the vacuolar compartment as described for another plasma membrane P_i-transporter (Pho84) in *S. cerevisiae* (Ghillebert et al., 2011; Andersson et al., 2012). In PtPho4 localization studies, no

additional eGFP signals were observed in the vacuole, thus the endomembrane localization might be correct.

The surprising localization of a strongly P_i-regulated transporter such as PtPho4 reveals a possibly important role for this transporter namely to exchange P_i between the plastid (intended as ancestral endosymbiont) and the host cell. Interestingly *P. tricornutum* expresses triosophosphate transporters located in different plastid-enveloping membranes: TPT1 in the cER membrane, TPT2 in the periplastidial membrane (PPM) and two TPT4 in the inner envelope membrane (IEM) (Moog et al., 2015). Triosophosphate translocators exchange P_i with triosephosphates (phosphorylated sugars) resulting in no net import of P_i into plastids. Thus, PtNap$_i$1 and PtPho4 might be thus essential to maintain P_i-homeostasis both in the cER or plastid where crucial cellular processes take place.

With PtVpt1 present at the vacuolar membrane (Figure 11), another putative intracellular P_i-transporter was identified. The gene encoding for this protein is highly expressed under P_i-starvation conditions (Figure 11) making it essential for P_i-homeostasis in *P. tricornutum*. The conserved domain analysis revealed that this PtVpt1 belongs to the major facilitator superfamily (MFS) and possess an SPX domain at N-terminus. In plants, SPX-MFS is designated as P_i-transporters (PHT5) family whose members were shown to facilitate the translocation of small solutes including P_i from and into the vacuole (Allen et al., 2008; Wang et al., 2012; Liu et al., 2016). In *S. cerevisiae* the PHO91 is an SPX-transporter that mediates the export of P_i out of the vacuole (Hürlimann et al., 2007). Interestingly PtVpt1 shares a close homology with the vacuolar phosphate transporter (VPT1) in *A. thaliana,* which mediates the P_i-influx into the vacuole (Liu et al., 2015; Liu et al., 2016). As mentioned above, PtVpt1 possesses an N-terminal SPX domain that is likely to be exposed to the cytosol according to the predictions. These domains are known to be involved in P_i homeostasis *via* interaction with inositol polyphosphate (InsP) signaling molecules (Wild et al., 2016). It is not possible to assign a complete functional description to this transporter based solely on a determined subcellular localization; however, is plausible to hypothesize that this protein has a role in P_i influx/efflux in the vacuole, and the functionality of this protein might be both directly and indirectly controlled by the intra-/extracellular P_i levels *via* the SPX domain (Azevedo and Saiardi, 2017).

4.1.5. **Phosphate storage**

Another possible strategy for the intracellular mobilization of phosphate is to draw on intracellular phosphorus storages. There is direct evidence that supports microalgae storing excess of P_i in form of polyP in the vacuoles (Sforza et al., 2018; Solovchenko et al., 2019a; Solovchenko et al., 2019b). The polyP topic in *P. tricornutum* has been addressed only concerning osmotic stress where pronounced dynamic changes in size and amount of polyphosphate molecules were highlighted according to the osmotic conditions (Leitão et al., 1995). To study weather also *P. tricornutum* adopts this strategy, this scenario was investigated using different approaches. A first hint that suggested that the vacuole may be a cellular compartment for P storage in *P. tricornutum* was given by morphology changes of the vacuoles in relation to external P_i-availability. In a preliminary study in the hosting lab, it was seen that the size and number of the vacuoles increased in response to P_i-deprivation (Dr. Thomas Heimerl). Notably, vacuole enlargement is not restricted to conditions of P_i-limitation, as previously shown in a *P. tricornutum NR* knockout strains propagated in NO_3^--containing medium (McCarthy et al., 2017). Thus, this phenomenon might be the result of the general stress response or accumulation of other ions/metabolites like nitrate (Cresswell and Syrett, 1982; McCarthy et al., 2017).

In many unicellular eukaryotes, vacuolar polyP formation involves the vacuolar transporter chaperone complex (Vtc). Homologs of the 4 components of the Vtc complex are present in the genome of the diatoms (Armbrust et al., 2004; Bowler et al., 2008) and differentially expressed according to P_i-availability (Dyhrman and Palenik, 1999; Yang et al., 2014; Cruz de Carvalho et al., 2016; Alipanah et al., 2018). One putative subunit, Vtc2 was characterized in the hosting laboratory concerning its subcellular localization being detected at the vacuolar membrane in correspondence of colliding points between two vesicles (Schreiber et al., 2017). This approach was extended to the remaining putative Vtc subunits, whose *in vivo* analysis resulted in a non-vacuolar localization (Figure 15). PtVtc1 and -4 localized indeed in the endomembrane system while PtVtc3 showed an undefined localization when expressed as eGFP-fusion proteins (Figure 15). Interestingly, in yeasts, the Vtc complex formed by Vtc4/Vtc2/Vtc1 subunits is known to relocate from the nuclear envelope/ER to the vacuole under conditions of P_i limitation (Gerasimaitė and Mayer, 2016; Yang et al., 2017). However, PtVtc1 and PtVtc4 localization did not change with varying P_i availability suggesting that differently composed Vtc complexes may have different functions in *P. tricornutum.* Besides

polyP polymerization, the *S. cerevisiae* Vtc complex is indeed involved in diverse processes like autophagy (Uttenweiler et al., 2007) and V-ATPase stability (Cohen et al., 1999). However, the *in vivo* localization of the single eGFP-fused Vtc subunits might be not indicative of the localization of the putative final complex. The presence of eGFP at C-terminus might potentially interfere with the assembly of the putative final complex, potentially causing an altered localization of the single eGFP-fused subunits.

As PtVtc2 was the only subunit that localizes at vacuole, functional studies on this protein were performed to investigate its role in a possible polyP metabolism. Two independent knock-out lines were generated using the optimized CRISPR/Cas9 system described in Stukenberg et al., (2018). Possible altered phenotypes of mutant lines were analyzed first with respect to vacuole morphology using the MDY-64 vacuolar membrane marker. As Vtc2 was previously found to localize in the colliding point of vacuolar vesicles (Schreiber et al., 2017), defects in vacuole morphology were expected. However, no remarkable differences were detected using this approach both in P_i-replete and deplete conditions (Figure 17). A second approach to characterize the phenotype of cell lines lacking the *vtc2* gene was to test the viability under P_i-deplete and replete conditions. Two mutant lines showed slightly decreased growth when cultivated under P_i-starvation when compared to the *wildtype* (Figure 18). Differently, the three strains displayed comparable levels of growth when incubated in the high-P_i medium (Figure 18). Thus, the defect of growth shown in this experiment depends on the P_i-conditions and lack of the functional *vtc2* gene and not on additional genomic modifications. Indeed, secondary effects on growth potentially caused by random integrations of the transgene or off-target cleavages by the Cas9 might be thus excluded. In addition, the two mutant lines were generated using two different sgRNA, and both cell lines generated using these two targets showed a slightly decreased viability. One can speculate that the difference in growth between the *Δvtc2* mutants and *wildtype* under starvation conditions might be potentially caused by an early depletion of P reservoirs. if this protein is involved in the phosphorus storage process, the eventual accumulation of P_i in the high-P_i preculture phase of the experiment could have been impaired in the mutants due to the loss of PtVtc2 function, decreasing the P-storage levels. However, the growth difference is not remarkable and even not entirely verified by statistic tests (Figure 18). Interestingly, PtVtc1-3 subunits possess the same functional domain of PtVtc2 (DUF202) that might play an important role. The presence of this domain in other subunits might “complement” the Vtc2 subunit function,

therefore justifying the not “markedly altered phenotype”. Nevertheless, the different and unclear subcellular localization of the DUF202-containing subunits (Figure 15) does not support this “complementation” hypothesis.

The putative subunit Vtc4, should play an important role in PolyP metabolism. In yeast, it has been shown that the destruction of the gene encoding for Vtc4 abolishes the production of PolyP in vacuoles (Yang et al., 2017). in *P. tricornutum*, PtVtc4 locates in the endomembrane system and not in the vacuole when expressed as eGFP fusion protein. However, it may be of interest to study the effects of the deletion of the *vtc4* gene. In the host laboratory, the CRISPR/Cas9 application has been optimized in this organism to generate cell lines lacking the *vtc2* gene (Stukenberg et al., 2018). In this thesis work, the method has been reproduced, generating a *vtc4* KO cell line, ready for phenotype study. The sequencing results showed in figure 25, display the possibility that this gene was mutated on the different alleles. The two different deletions (1 bp and 4 bp), indicate that this strain might possess a non-functional PtVtc4 protein. Thus, this cell line is suitable for future studies on mutant phenotype. The latter could be evaluated assessing a growth curve as was done for *Δvtc2* strains or measuring the intracellular polyP levels. For the latter, several approaches can be used like *in vivo* NMR spectroscopy or analytic methods like extraction and measurement.

However, if one of the functions of the *P. tricornutum* vacuole is to store P_i, a phosphate transporter would be expected to be present in the vacuolar membrane. This was indeed the case, as PtVpt1 was found in the vacuolar membrane and transcriptionally upregulated according to P_i availability. Nonetheless, putative P_i-storage functions for the vacuole of the diatom need to be investigated more in detail.

4.1.6. **The P_i-atlas in *P. tricornutum*.**

The data shown in this thesis add new knowledge to the P_i-starvation response in the diatom *P. tricornutum*. According to expression data (Yang et al., 2014; Cruz de Carvalho et al., 2016; Alipanah et al., 2018) and localization studies, we depict a possible model that summarizes some P-limitation acclimation strategies (Figure 26): the P concentration in the medium is sensed and in case of limitations an unknown signal activates, through an uncharacterized cascade (blue dotted line), the transcription factor *PtPSR* which leads to the PtPSR-catalyzed transcriptional regulation of several P_i-starvation (PSR) genes (Sharma et al., 2019). The

activity of PtPSR might be negatively regulated by an SPX protein (red dotted line, Phatrdraft_47434, Zhang et al., 2020). Alkaline phosphatases (blue circles, PtPhos1, 3, and 8) might act extracellularly (Lin et al., 2013; Buhmann et al., 2016; Erdene-Ochir et al., 2019) (blue arrows indicate secretion to the extracellular environment) and possibly hydrolyze phosphate mono and -diesters. PtPhos2 (blue box) might attack phytate molecules, whereas the putative 5´nucleotidase PtNtase (green circle) might hydrolyzes P_i from nucleotides (adenosine monophosphate, is shown as an example). Extracellular phosphorus mobilization generates phosphates readily accessible to plasma membrane-localized NaP_i cotransporters PtPhos6 (blue circles) has been localized in the ER and cER. Its activity might be correlated with P-starvation lipid recycling as well as a putative phosphate transporter found in the cER (PtPho4). The putative vacuolar P_i-transporter (PtVpt1) might mediate phosphate storage/reallocation possibly *via* an SPX domain. Notice that the respective protein roles and functions for each reaction are not experimentally demonstrated, likewise the functionality of P_i-transporters.

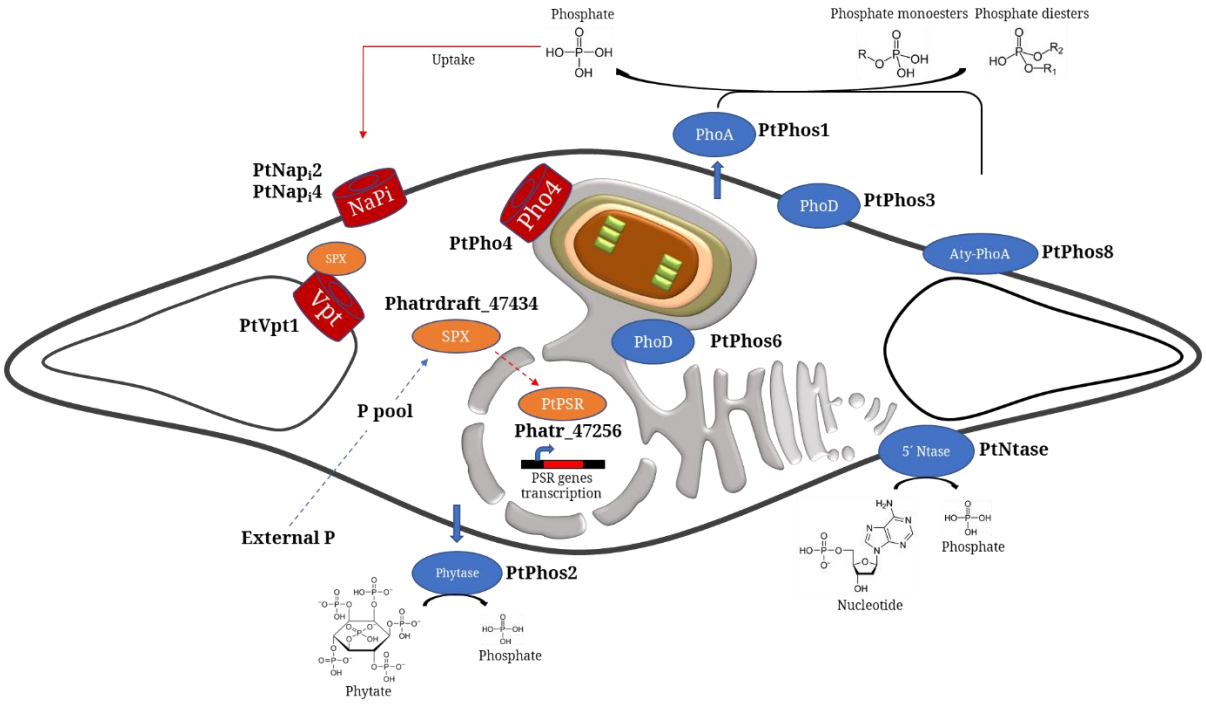

Figure 26. Model of a putative P_i-atlas in *P. tricornutum*.

5. Material and methods.

5.1. Material

5.1.1. Chemicals, buffer, and enzymes

All chemicals used in this work were procured from Roth GmbH, Sigma Aldrich, or Merck and stored and utilized according to the manufacturer's instructions. The compositions of buffers and solutions as well as enzymes were used are described in detail in the respective chapters.

5.1.2. Instruments

All the instruments and equipment used in this work are listed in table 4.

Table 4. List of the instruments and equipment utilized in this work.

Instrument	Supplier
Centrifuge 5810R	Eppendorf
Centrifuge 5417R	Eppendorf
Centrifuge 5415D	Eppendorf
Micro 22 R	Hettich
Eppendorf Research 1-5 mL	Eppendorf
Eppendorf Research 100-1000 µL	Eppendorf
Eppendorf Research 20-200 µL	Eppendorf
Eppendorf Research 2-20 µL	Eppendorf
Eppendorf Research 0.1-2 µL	Eppendorf
Mastercycler-Personal	Eppendorf
Mastercycler-Gradient	Eppendorf
Elektrophresis Power Supply EPS 200	Pharmacia Biotech
Pharmacia LKB GPS 200/400 Power Supply	Pharmacia Biotech
Transilluminator	PeqLab
Nitrocellulose membrane	Macherey-Nagel
Whatman-Filter paper 3mm	Schleicher&Schuell
FB30/ 0.2 CA – S Sterile filter	Schleicher&Schuell
Fuji Medical X-Ray Film 30x40 cm	Fuji
X-Ray Film developer	Kodak
X-Ray Film fixative	Kodak
Elektrophoresis Power Supply EPS 301/601	Amersham Biosciences
TE 77 Semy-Dry Transfer Unit	Amersham Biosciences
Bio-Rad Biolistic PDS-1000/He Particle Delivery System	Biorad Laboratories

Dryer	Nalgene
Climate chamber MLR 350	Sanyo
Climate chamber	Weiss
CLSM Leica TCS SP2	Leica Microsystems
CLSM Leica TCS SP5	Leica Microsystems
Zeiss Axioplan2	Carl Zeiss Microscopy GmbH
GeneQuant 1300	GE-Healthcare
Thermocycler 60	Bio-Med
Thermocycler comfort	Eppendorf
Vortexer REAX 1DR	Heidolph
Nanodrop Spectrophotometer ND-1000	PeqLab

5.1.3. **Software and internet applications**

MacBiophotonics ImageJ (Tony Collins, McMaster Biophotonics Facility)

LCS Lite 2.5 (Leica)

Sequencer 5.1 (GeneCodes)

BlastP, BlastN (https://blast.ncbi.nlm.nih.gov/Blast.cgi)

Phatr2 database (http://genome.jgi-psf.org/Phatr2/Phatr2.home.html)

Phatr3 database (http://protists.ensembl.org/Phaeodactylum_tricornutum)

SignalP3.0 (www.cbs.dtu.dk/services/SignalP-3.0)

SignalP4.1 (http://www.cbs.dtu.dk/services/SignalP-4.1/).

TOPCONS (http://topcons.cbr.su.se)

Phobius (http://phobius.sbc.su.se/)

TMHMM (http://www.cbs.dtu.dk/services/TMHMM)

TMpred (http://www.ch.embnet.org/software/TMPRED form.html)

NCBI Conserved Domain Database (http://www.ncbi.nlm.nih.gov/Structure/cdd/wrpsb.cgi)

PEPTIDEMASS (https://web.expasy.org/peptide_mass/)

DISPHOS 1.3 (http://www.dabi.temple.edu/disphos/).

Benchling (https://www.benchling.com/)

5.1.4. **DNA and protein ladders**

For gel electrophoresis, both 1Kb and 100bp ladder (GeneDire) were used to estimate the size of the DNA amplicons/fragments or to assess RNA quality. For the SDS-Page, a PageRuler™ Prestained protein ladder (Thermo Scientific) was used.

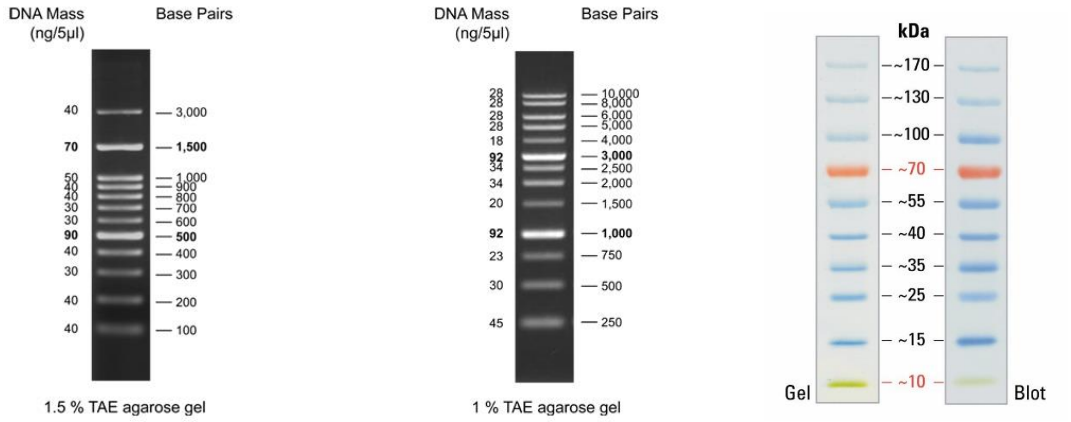

Figure 27. DNA and protein ladders used in this work.

5.1.5. **Oligonucleotides**

Oligonucleotides were synthesized by Sigma Aldrich. All the primer sequences utilized for the construction of the vectors are listed in the supplementary material.

5.1.6. **Plasmids**

All the plasmids used in this work for cloning or transgene expression, are listed in table 5.

Table 5. Plasmids used in this work.

Plasmid	Features	*Accession Number*
pJet 1.2	Rep (pMB1), ori, bla (ampR), eco471R, PlacUV5, T7-Prom, MCS	NCBI EF694056
pPha_NR	ampR, P*Nr*, MCS, T*Nr*, sh ble (Zeocin), ori	NCBI JN 180663
pPha_T1	ampR, P*fcp*, MCS, T*fcp*, sh ble (Zeocin), ori	NCBI AF219942
PtCC9	ampR, P*Nr*, *diaCas9*, T*Nr*, PU6, sgRNA, T*U6*, sh ble (Zeocin), ori	NCBI MH143578

5.1.7. **Antibodies**

All the antibodies used for immunodetection in this work, are listed in table 6.

Table 6. Antibodies used in this work.

Primary antibodies	**Company**
α-eGFP	Rockland
α-tubulin	Sigma-Aldrich
α-FLAG	Rockland
Secondary antibodies	
α-goat (HRP conjugated)	Sigma-Aldrich
α-mouse (HRP conjugated)	Sigma-Aldrich
α-rabbit (HRP conjugated)	Sigma-Aldrich

5.1.8. **Dyes**

The dyes used in this work are listed in table 7.

Table 7. Dyes and staining solutions used in this work.

Dye	Company
ELF™ 97 Endogenous phosphatase detection kit	Invitrogen
MDY-64	Invitrogen

5.1.9. **Organisms**

The diatom *Phaeodactylum tricornutum* was used for all the experiments carried out for this work. *Escherichia coli* was used for the cloning procedures. Specifics of these organisms are listed in table 8.

Table 8. Organisms used in this work

Organismus	Strain	Genotype features	Source
E. coli	TOP10	F-mcrA Δ(mrr-hsdRMS-mcrBC) φ80lacZΔM15 ΔlacX74 nupG recA1 araD139 Δ(ara-leu)7697 galE15 galK16 rpsL(StrR) endA1 λ	Invitrogen
P. tricornutum	CCAP1055/1, UTEX646, “Pt4”		Peter Kroth, Plant Ecophysiology, University of Konstanz

5.1.10. **Kits**

In table 9, all molecular biology kits used in this work are listed.

Table 9. Kits for molecular biology application used in this work.

Kit	Company
Q5 2x High Fidelity Master Mix	New England Biolabs Inc.
Zymoclean Gel DNA Recovery Kit	Zymo Research
NucleoBond® Xtra Midi	Macherey-Nagel GmbH & Co. KG
Site-Directed Mutagenesis kit	New England Biolabs Inc.
Clone Jet™ PCR cloning kit	Thermo Fisher Scientific
TriPure isolation reagent	Roche
DNase I	Thermo Fisher Scientific
RevertAid Reverse Transcriptase kit	Invitrogen

5.2. Methods

5.2.1. **Cell cultures of *P. tricornutum***

5.2.1.1. *P. tricornutum* cells maintenance

Phaeodactylum tricornutum (Bohlin, UTEX646, "Pt4") was cultivated in f/2 medium without silica (Table 10-11-12) (Guillard, 1975) containing 1.66% (w/v) Tropic Marin (Dr. Biener GmbH) and 2 mM Tris-HCl (pH 8.0) under constant light (8,000–10,000 lx) and shaking (100–150 rpm) or on plates with solid agar-containing (1.3% w/v) f/2 medium at 21 °C. To prevent bacterial growth, cells were periodically cultivated in liquid f/2 with Ampicillin (50 µg/µl) and Kanamycin (100 µg/µl). Cell cultures were then spread onto plates to obtain subsequently single colonies further selected for continuous cultures.

Table 10. Components of the f/2 medium used in this work. Concentration is related to end concentration in the medium.

Component	Molar concentration (M)
Tris-HCl (pH 8)	2×10^{-3} M
NaH_2PO_4	3.63×10^{-5} M
NH_4Cl	1.5×10^{-5} M
$NaNO_3$ *	8.83×10^{-4} M
Trace elements	/
Vitamins	/

*used instead of NH_4^+ in case of induction medium f/2 (see)

Table 11. Trace elements components in the f/2 medium. Concentration is related to end concentration in the final medium.

Component	Molar concentration (M)
$FeCl_3 \bullet 6H_2O$	1×10^{-5} M
$Na_2EDTA \bullet 2H_2O$	1×10^{-5} M
$CuSO_4 \bullet 5H_2O$	4×10^{-8} M
$Na_2MoO_4 \bullet 2H_2O$	3×10^{-8} M
$ZnSO_4 \bullet 7H_2O$	8×10^{-8} M
$CoCl_2 \bullet 6H_2O$	5×10^{-8} M
$MnCl_2 \bullet 4H_2O$	9×10^{-7} M

Table 12. Vitamin solution components in the f/2 medium. Concentration is related to end concentration in the final medium.

Component	Molar concentration (M)
Vitamin B12	3.69×10^{-10} M
Biotin	2.05×10^{-9} M
Thiamine HCl	2.96×10^{-7} M

5.2.1.2. Transcriptional regulation experiments

For transcriptional regulation experiments (promoter/eGFP/terminator cassettes), *P. tricornutum* cells of the different strains were maintained in the exponential growth phase for seven days in standard f/2 medium supplemented with 36 µM NaH_2PO_4. Before experimental treatment, approximately 1×10^8 cells were harvested (1,500 *g*, 21 °C, 10 min), washed twice with P_i-free f/2 medium, and transferred into 100-mL Erlenmeyer flasks containing 50 ml (initial cell concentration 2×10^6 cells/ml) of f/2 medium with 0, 36, 72, 90, 108 µM P_i in case of promoter/eGFP/terminator cassettes experiments. Cells were incubated for two days until protein and microscopy analysis. Cell concentration was determined by cell count using a Thoma chamber.

5.2.1.3. Phospho-mimicry experiments

To test whether PtPhos1 protein secretion is regulated by reversible phosphorylation, the so-called "phospho-mimicry" approach was used. pPhaNR-ptPhos1-FLAG, pPhaNRptPhos1-FLAG-Ala/Glu strains (see paragraph cloning strategies) were kept in exponential growth phase in f/2 with 108 µM P_i (NaH_2PO_4) (3-fold standard f/2 P_i-concentration). After six/seven days of growth, 10^8 cells were harvested and washed as described above and moved into a 100 ml flask with f/2 containing 50 ml of 0.9 nM $NaNO_3$ and 108 µM P_i with a starting cell concentration of 2×10^6 cells/ml. Cells were incubated for 24 h (overexpression in P_i-replete). After 24 h, the same procedure was repeated but harvesting a double number of cells in a way that 10^8 cells and the respective medium volume were taken for protein isolation and an equal number of cells were moved into a new 100 ml flask containing 50 ml of P_i-free f/2 with 0.9 nM $NaNO_3$ (overexpression in early P_i-deplete). After 24 h, this step was repeated and the last incubation lasted four days (overexpression in late P_i-deplete) (Figure 28).

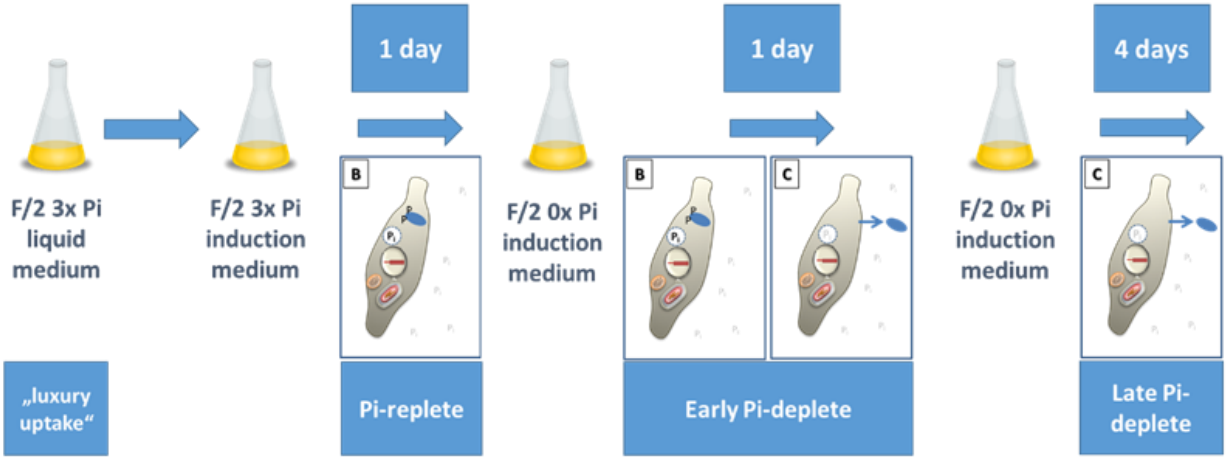

Figure 28. Phospho-mimicry experimental setting. The experimental setting is based on the model that hypothesizes that the secretion of PtPhos1 protein might be controlled by the reversible phosphorylation of serines present at N-terminus. The availability of extra/intracellular P_i pools would modulate the phosphorylation process and thus the secretion.

5.2.1.4. Growth experiments

Growth curves were assessed to evaluate the viability of different cell lines according to P_i availability. For the growth experiment, two *Δvtc2* and *wildtype* strains were grown individually in f/2 containing 108 µM P_i (3-fold standard P_i concentration for f/2) and kept in exponential phase in the above-mentioned conditions. Three 50 ml Erlenmeyer flasks containing f/2 with no P_i were inoculated with *Δvtc2* and wild type strains individually. Cells were washed twice with P_i-free f/2 and the inoculation was performed in a way to obtain an initial cell concentration of 5×10^5 cells/ml. The same was done using f/2 with 108 µM P_i. The growth curve of each culture was assessed measuring the cell concentration every 24 hours by direct cell counting using a Thoma chamber. Statistical analysis to verify differences in the growth curves was performed with Pairwise Student´s *t*-test between the independent *Δvtc2* lines and the *wildtype* in the respective P_i conditions.

5.2.2. Cell cultures of *Escherichia coli*.

E. coli TOP10 competent cells were long-term stored at -80˚C in LB (Table 13) with 50% of Glycerin. After transformation, cells were plated on 1.5% LB-agar plates containing 50 µg/ml Ampicillin or cultivated in liquid LB.

Table 13. Components of LB medium and relative concentration

Component	Final concentration
Tryptone	1% (w/v)
Yeast extract	0.5% (w/v)
NaCL	1% (w/v)

5.2.3. **Nucleic acid analytics.**

5.2.3.1. DNA and RNA isolation from *P. tricornutum*.

Cells from a 300 ml *P. tricornutum* culture in exponential growth phase were harvested by centrifugation (2000 *g*/ 10 min/ RT˚). The pellet was flash-frozen with liquid nitrogen and stored at -80˚C for further analysis. At the moment of the DNA extraction, the cell pellet was defrosted on ice and washed with PBS. After centrifugation (2000 *g*/ 10 min/ RT˚), the supernatant was discarded and resuspended in 800 µl of 2x CTAB containing buffer B. The suspension was incubated at 70˚ for 30 min and centrifuged (20000 *g*/ 5 min/ RT˚). The resulting upper phase was transferred to a new 1.5 ml Eppendorf tube and mixed gently with one volume of PCI. After centrifugation (20000 *g*/ 10 min/ RT˚), the supernatant was transferred to a new 1.5 ml Eppendorf tube and mixed gently with 2/3 volume of Isopropanol. The sample was centrifuged (20000 *g*/ 10 min/ 4˚), the supernatant discarded and the pellet washed with 500 µl of 70% Ethanol. After centrifugation (20000 *g*/ 10 min/ 4˚), the pellet was dried at RT˚ and resuspended in 40-50 µl of nucleic acids-free water. DNA concentration and quality were assessed using Nanodrop Spectrophotometer ND-1000 (PeqLab).

PBS	PCI	Buffer B
137 mM NaCl	Phenol/Chloroform/Isoamyl alcohol	0.1 M Tris pH 8
2.7 mM KCl	(25/24/1 v/v %)	1.4 M NaCl
10 mM Na_2HPO_4		20 mM Na_2EDTA pH8.6
1.8 mM KH_2PO_4		

RNA was isolated from cells incubated for 2 days in P_i-free f/2 to induce the expression of P_i-responsive genes and increase thus the possibility to obtain their transcripts for subsequent cDNA synthesis. After PBS washing step, the cell pellet was resuspended in 1 ml of TriPure isolation reagent (Roche) and flash-frozen in liquid nitrogen. At the moment of the RNA extraction, the pellet in TriPure was defrosted on thermo shaker at 60˚C for 15 seconds. The mixture was then further incubate using the same conditions and shaken at 1400 RPM for 10 minutes. 200 µl of Chloroform was added for 1 ml of TriPure and the sample agitated vigorously for 15 seconds followed by incubation at RT˚ for 15 minutes. Samples were centrifuged (10000 *g*/ 15 min/ 4˚C) to obtain three distinct phases. The upper phase containing RNA (500 µl circa) was transferred into a new tube and mixed with the same volume of Isopropanol and gently inverted. The mixture was incubated at RT˚ for 10 minutes and centrifuged (10000 *g*/ 15 min/ 4˚C). The supernatant was discarded and the pellet washed with 1 ml of 75% ethanol. After centrifugation (8500 *g*/ 15 min/ 4˚C) the pellet was dried for 20-30 minutes taking care to not over dry it. Pellet was then resuspended in 30 µl of RNAse-free water and incubated 5-10 minutes at 55-60 ^{0}C. RNA concentration and pureness were controlled using the Nanodrop Spectrophotometer ND-1000 (PeqLab). Samples were then stored at -80˚C.

5.2.3.2. DNase treatment and cDNA synthesis via reverse transcription (RT)

Before the cDNA synthesis, potential genomic DNA contamination was removed through a DNaseI (Thermo Fisher Scientific) treatment. 1 µg of total RNA was mixed with 1µl of 10× $MgCl_2$ buffer, 1 U of DNaseI, and RNase-free water up to 10 µl. The reaction was performed at 37˚C for 30 minutes and stopped adding 1 µl 50 mM EDTA (10 minutes at 65˚C). An aliquot of the DNase-digested RNA sample was run on 1× agarose-TBE gel to verify the presence of the two typical 16 and 32s ribosomal RNAs and the absence of residual genomic DNA contamination.

100 ng of DNase-digested samples were used to perform cDNA synthesis using the *RevertAid* Reverse Transcriptase kit (Invitrogen). The reaction and the settings are shown in tables 1 and 15

Table 14. cDNA synthesis reaction.

Total RNA	100 ng
Random Hexamer Primer (100 µM)	1 µL (0.2 µg)
5× Reaction buffer	4 µL
Thermo Fisher RiboLock RNAse Inhibitor (40 U/µL)	0.5 µL
dNTPs (10 mM)	2 µL
RevertAid Reverse Transcriptase (200 U/µL)	1 µL
ddH2O	x µL
Total volume	20 µL

Table 15. Thermocycling conditions for cDNA synthesis.

Temperature	Time	Cycles
25˚C	10 min	1×
42˚C	60 min	1×
70˚C	10 min	1×
4˚C	/	/

5.2.3.3. Polymerase chain reaction (PCR)

The polymerase chain reaction was largely used to amplify genes from *P. tricornutum* genomic or cDNA. Upstream and downstream regions of genes of interest were amplified from genomic DNA. For these purposes, a 2× Q5 *high fidelity* Master Mix (New England Biolabs Inc.) was used. Gene-specific primers were synthesized by Sigma–Aldrich. The reactions were performed according to the manufacturer´s instructions (Table 16 and 17).

Table 16. PCR reaction settings.

2× Q5 *high fidelity* Master Mix	12.5 µl
Forward Primer (10 mM)	1.25 µl
Reverse Primer (10 mM)	1.25 µl
Template	1 ng
ddH2O	x µl
Total volume	25 µL

Table 17. Thermocycling conditions for PCR using 2× Q5 high fidelity Master Mix

Phase	Temperature	Time	Cycles
Initial denaturation	98°C	2 min	1×
Denaturation	98°C	15 s	
Annealing	50 – 72°C	30 s	30-35×
Elongation	72°C	1 kb/20-30 s	
Final Elongation	72°C	2 min	1×
Hold	4°C	∞	

5.2.3.4. Agarose gel electrophoresis

For separation of DNA or RNA on an agarose gel, 10 µl of the sample was mixed with 6× DNA loading dye and loaded onto a 1-2% agarose gel according to the length of the fragment of interest. Roti®-Gel Stain (Roth) was added to the 1× TBE agarose gels. A voltage of about 150 V was used to run the gel in 1× TBE buffer. The bands were visualized exposing the gel to UV light using a transilluminator (PeqLab).

TBE Buffer		6x Loading dye	
Tris/HCl, pH 8.8	1 M	Urea	4 M
Boric acid	0.83 M	EDTA	50 nM
EDTA	10 nM	Saccharose	50% (w/v)
		Bromophenol blue	0.1% (w/v)
		Xylene Cyanole	0.1% (w/v)

5.2.3.5. Cloning strategies

For localization studies, all the genes were fused with the *eGFP* gene at 3´ ends. To build the constructs to express PtPhos3, 5, 6, PtPho4, PtNap$_i$1, 2, 4, 5, PtVpt1 PtVtc1, 3, 4-eGFP fusion proteins, traditional cloning was used. In this case, primers equipped with restriction sites were used. PtPhos6 (EGFP downstream of the gene), PtPhos7, 8, PtHp$_i$1, PtNap$_i$3, PtNtase EGFP-fusion protein, and PtNtase-FLAG constructs were generated via Gibson assembly (Gibson et al., 2009). All the inserts were cloned into pPha-NR (GenBank: JN180663). Gibson assembly was used to generate the constructs for transcriptional regulation studies. Different eGFP expression cassettes were built enclosing the latter between the putative promoter and terminator regions of the genes of interest. For each investigated gene, at least 900 bp upstream and 485 bp downstream of the coding sequence were used, including untranslated regions if annotated. Sequences and region lengths are included in the supplements. The expression cassettes were integrated into the pPha-T1 vector (GenBank: AF219942). To design constructs for the phospho-mimicry approach, *ptPhos1* cDNA was cloned at 3´ with 1× FLAG and integrated within the pPha-NR vector. Two additional versions of pPha-NR/PtPhos1-FLAG were subsequently generated and obtained as synthetic sequences provided by BioCat GmbH (Heidelberg,

Germany). These two versions were designed to modify the nucleotide sequences to mutate the serine codons, predicted to encode for putative phosphorylation sites, either in glutamic acid or alanine. More precisely, a cluster of 11 serines was exchanged after the predicted signal peptide. The synthetic sequences were inserted within pPha-NR/PtPhos1-FLAG using an *EcoRI* restriction inserted at 5´ of the start codon of the *ptPhos1* gene and a *Bpu1102i* already present within the gene sequence. Cloning strategies are summarized in figure 29.

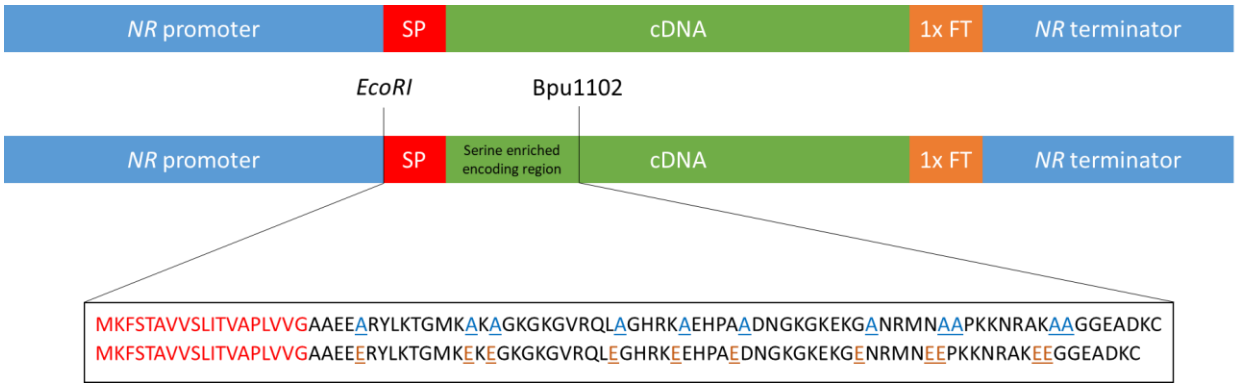

Figure 29. Scheme of phospho-mimicry cloning strategy. The resulting mutated amino-acid sequence is shown: the positions in which serine are exchanged are shown in blue (Alanine) or in brown (Glutamic acid). The predicted signal peptide is shown in red.

5.2.3.6. Plasmids isolation from E. coli

The mini-preparation is suitable for the isolation of small amounts of plasmid-DNA from a small culture. The isolation of recombinant plasmids from *E. coli* was performed by alkaline lysis from 1.5 ml out of a 3 ml overnight culture at 37 ˚C. Cells were pelleted at (20000 *g*/ 30 sec / 4˚C) and resuspended in 200 µl P1 buffer and then 200 µl P2 buffer was added. After several inverts, the mixture was incubated at RT for a maximum of 1 min. This was followed by the addition of 200 µl of P3 buffer and 20 µl of chloroform. After shaking vigorously, the mixture was incubated on ice for 5 minutes. Afterward, centrifugation (20000 *g*/ 30 sec / 4˚C) the supernatant was transferred to a new 1.5 mL reaction tube and the plasmid DNA was precipitated using 400 µl of isopropanol (20000 *g*, 20 min, 4°C). The supernatant was discarded and the pellet washed with 300 µl of 70% ethanol. After centrifugation (20000 *g*, 10 min, 4°C) ethanol was removed and the pellet dried on Thermo-block at 55˚C. Afterward, 40 µl of sterile water were used to resuspend the pellet. For plasmid preparations of highly pure DNA on a larger scale, suitable for transfection of *P. tricornutum* by particle bombardment, the NucleoBond® Xtra Midi (Macherey-Nagel) was used according to the manufacturer´s instructions. For each construct, the plasmid (verified by sequencing) was used to retransform *E. coli* TOP100 cells as described previously. One colony was used to inoculate 50 mL of LB medium and grown overnight culture grown at 37°C. A quota of culture (750 µl) was mixed with an equal volume of glycerin, flash-frozen, and stored at -80˚C. The principle here is also based on alkaline lysis and binding to a gravimetric column. Both Mini and Midi plasmid

preparations were further checked with restriction enzymes reaction and with NanoDrop for concentration estimation.

5.2.3.7. Sequencing

Mini- and Midi preparations samples that successfully passed the restriction control for correct insertion, were selected for sequencing. At least two clones were chosen for construct and Sanger sequencing was performed externally by Macrogen (Seul, South Korea) according to the company instructions.

5.2.3.8. Transformation of E. coli

Transformation of the generated vectors into *E. coli* TOP10 was performed on competent cells previously prepared with RbCl method. 50 µl of competent *E. coli* TOP10 cells were used for each transformation and mixed with the ligation mixture or Gibson assembly reaction. After 10 minutes of incubation on ice, the cells were undergone heat shock at 42˚C for 42 seconds. After a short recovery on ice (5 minutes), cells were plated on 1.5% agar-LB plates containing 50 µg/ml ampicillin for overnight culturing at 37˚C.

5.2.3.9. Biolistical transformation of *P. tricornutum*

Wildtype *P. tricornutum* cells were genetically transformed *via* particle bombardment using a modified protocol from Apt et al., (Apt et al., 1996). The first step was the preparation of DNA microcarriers. 60 mg of M10 Tungsten particles (Ø 0.7 µm) were resuspended in 1 ml of absolute ethanol (HPLC quality) and well mixed using a vortexer for 5 minutes. The mixture was centrifugated (14000 *g*/ 1 minute/ RT) and the pellet was washed twice with ddH_2O. The particles were finally resuspended again in 1 ml of ddH_2O and aliquoted in 1.5 sterile Eppendorf cups (50 µl each) and stored at -20˚C for further use. At the moment of the transfection, the tungsten particles were coated with the DNA. 5-7 µg of plasmid was added to the 50 µl of particles together with 50 µl of 2.5 M $CaCl_2$ and 20 µl of 0.1 M spermidine. The mixture was vortexed for 1 minute and incubated at RT for 10 minutes to facilitate sedimentation. The supernatant was removed and DNA-coated particles were mixed and washed with 250 ml of absolute ethanol (HPLC quality). After centrifugation (14000 *g*/ 5

minute/ RT), the supernatant was carefully discarded and the particles resuspended in 50 µl of absolute ethanol (HPLC quality). The 50 µl particle mixture was equally split onto three sterile macrocarriers e let them dry under sterile conditions where the Biolistic PDS-1000/He Particle Delivery System (Bio-Rad) was placed. Thus prepared, the DNA-coated particles were generally stable for 45 minutes.

For biolistic transformation, *P. tricornutum* cells were kept in the exponential growth phase until the cell number reach the desired value. For each construct, 100 µl of cell culture containing 10^8 cells were plated on three 1.3% agar-f/2 plates so that the cells mixture was positioned in the center of it. One day before transfection, a precise volume of cell culture was harvested (1500 *g*/ 5 minutes/ RT), plated, and let dry in a sterile bench.

Besides macrocarriers, all the components of the particle gun (rupture disks, metal ring) were cleaned with absolute ethanol and the metal grids flamed. To assemble the apparatus, the rupture disk was inserted in the upper part and screwed tight. The macrocarrier device, consisting of a holder, loaded microcarrier, and stopping screen was assembled and inserted into the particle gun. One position below the macrocarrier device was placed on the *P. tricornutum* cells-containing plate. After the device was closed and a vacuum (-25 psi) applied, helium gas was fed into the device until the pressure reached the rupture disk tolerance (1350 psi). The generated pressure was directed to the microcarrier in such a way that the particles were thrown on the grid causing the release of their content on the cells. The bombarded cells on f/2-agar plates were cultivated for 24 h under standard conditions. The cells were then washed off the agar plates with 1 ml f/2 medium and plated onto three f/2-agar plates supplements with 75 µg/ml Zeocin and also cultivated under standard conditions until the growth of colonies

5.2.3.10. Colony PCR

Colony PCR was used to verify the integration of the foreign expression cassette in Zeocin resistant colonies obtained after biolistic transfection. For this purpose, a 2× PCR Super Master Mix (BioTools). Colonies from raster plates were transferred into 1.5 sterile Eppendorf tubes containing 15 µl of ddH_2O. Cells were cooked on thermo-block at 96˚C until the green color derived from the release of chlorophyll from plastids, was visible. Samples were centrifuged

(14000 *g*/ 5 minute/ RT), and 2 µl of supernatant were used as a template for PCR whose reaction is described in tables 18 and 19.

Table 18. Colony-PCR reaction.

2× PCR Super Master Mix	10µl
Forward Primer (10 mM)	0.5 µl
Reverse Primer (10 mM)	0.5 µl
Template	2 µl
ddH2O	7 µl
Total volume	10 µL

Table 19. Thermocycling conditions for PCR using 2× PCR Super Master Mix

Phase	Temperature	Time	Cycles
Initial denaturation	94°C	5 min	1×
Denaturation	94°C	20 s	
Annealing	50 – 65°C	30 s	20-40×
Elongation	72°C	2 kb/1 min	
Final Elongation	72°C	5 min	1×
Hold	12°C	∞	1×

5.2.4. **Protein analytics**

5.2.4.1. Protein isolation from *P. tricornutum*

Protein isolation from *P. tricornutum* cells was performed with alkaline lysis. For protein analysis, a culture volume containing approximately 10^8 cells was harvested, flash-frozen, and

stored at -80˚C as described previously. Before cell lysis, cell pellets were defrosted and washed with PBS. The pellet was resuspended in 200 µl of lysis buffer, vortexed, and incubated on ice for 10 minutes. 1 ml of ddH_20 and trichloroacetic acid (TCA, 10% final concentration) were added, followed by incubation on ice for 15 minutes. Samples were centrifugated (20000 *g*/ 20 minutes/ 4˚C) and the pellet was then washed at least two times with 80% acetone until the supernatant after centrifugation (20000 *g*/ 15 minutes/ 4˚C) was clear. After acetone washes the pellet was dried in a desiccator and resuspended in 100-150 µl of 2× Urea buffer. Samples were incubated on thermo-block at 60˚C for 20 minutes at 1400 RPM to favor protein denaturation. The samples were centrifuged (20000 *g*/ 10 minutes/ RT) and the supernatant was transferred into a new Eppendorf tube.

Lysis buffer:		Urea Buffer:	
NaOH	1.85 M	Urea	10 % (v/v)
β-mercaptoethanol	7.5% (v/v)	Tris/HCl, pH 6.8	200 mM
		EDTA	0.1 mM
		SDS	5% (v/v)
		Bromophenol blue	0.03% (w/v)
		β-mercaptoethanol	1% (v/v)

5.2.4.2. Protein isolation from the culture medium

Protein isolation from the culture medium was carried out as described in (Hempel and Maier, 2012). A defined volume of culture was centrifuged to spin down the cells (1500 *g*/ 10 minutes/ RT). The supernatant was sterile-filtered (0.2-µm) to eliminate any eventual cells in suspension. Supernatant fractions were concentrated using Amicon Ultra Centrifugal Filters (10 kDa cut-off) (Merck) with centrifugations (3000 *g*/ 15 minutes/ 4˚C). The filter was additionally washed with 15 ml of sterile ddH_2O to remove the salts present the f/2 medium and again centrifuged. The proteins in the filters were resuspended in 1 ml od ddH_20 and precipitated with 10% of TCA. The samples were then processed as described in the previous paragraph.

5.2.4.3. Determination of protein concentrations

The concentration of the proteins in the samples was determined with the Amido-black method according to (Popov et al., 1975). 5 µl of denatured proteins were added to 95 µl of ddH_20 and mixed with 400 µl of the Amido-black staining solution. The mixture was vortexed and centrifuged (20000 *g*, 20 min, 4°C) and the supernatant discarded. The protein pellet was washed with 500 µl of washing solution and again centrifuged (20000 *g*, 20 min, 4°C). The supernatant was discarded and the pellet dried under vacuum and resuspended in 1 ml of 200 mM NaOH. The samples were subsequently read using a photometer to determine adsorption at 615 nm. For calculation of the protein concentration, a standard calibration line (y=0.0268x+0.0298) build on a dilution series of BSA was used. The formula is the next:

$$x\ (\mu g/\mu l) = \frac{OD615 - 0.0298}{0.0268}$$

Amino black staining solution:		Washing solution:	
Acetic acid	10 % (v/v)	Acetic acid	10 % (v/v)
Methanol	90 % (v/v)	Methanol	90 % (v/v)
Amido black	A pinch		

5.2.4.4. SDS-polyacrylamide gel electrophoresis (SDS-PAGE)

The separation of protein samples based on molecular mass was performed with an SDS-PAGE with SDS (Sodium Dodecyl Sulphate) serves as a detergent that gives a negative charge to all the proteins in a way that they could migrate into an electric field within a gel with a pore size given by the concentration of polyacrylamide. All the gels were prepared with 12.5% acrylamide/N,N`-methylene bisacrylamide (30:0,8) (Rothipherese Gel 30). The SDS-PAGE generally consists of two parts which are prepared in two different steps: I) a separation gel in which the linearized proteins are separated according to their size. II) a collecting gel that allows aligning all the proteins in the same position of the gel before the real separation. The composition of the two gels is shown in table 20.

Table 20. SDS-Page components. The volumes are valid for one single SDS-page cast in the gel chambers used in the hosting laboratory. Notice the last two components are added as the last step directly before the gel-polymerization.

	Separation gel (12.5%)	**Collecting gel (0.8%)**
30 % (v/v) Acrylamide	4.1 mL	0.9 mL
ddH2O	3.2 mL	2.9 mL
4x Separation buffer	2.5 mL	/
4x Collecting buffer	/	1.2 mL
TEMED	20 µL	15 µL
10 % (w/v) APS	150 µL	85 µL

Samples in Urea buffer were warmed at 60˚C and spun for 1 min at full speed to pellet residues of insoluble material. The supernatant was loaded onto gels together with the 5µl of protein standard PageRuler™ Prestained protein ladder (Thermo Fisher Scientific). Separation of the proteins was performed using Electrophoresis Power Supply EPS601 (Amersham Biosciences) set to 150 V, and 20 W. A single gel was initially run at 20 mA until the samples passed the collecting gel, then the density was adjusted to 25 mA.

5.2.4.5. Semi-dry Western Blot and immunodetection

After separation, proteins were immobilized on a nitrocellulose membrane to perform immunodetection. To transfer the proteins, the method of semi-dry Western Blot was used (Towbin et al., 1979). For the transfer, the SDS gel, the nitrocellulose membrane, and six Whatman papers were equilibrated in the WB transfer buffer. The TE 77 Semi-dry Transfer System (GE-Healthcare) was used as a blotting apparatus. Three Whatman papers were placed on the anode of the blotting chamber, followed by the nitrocellulose membrane, the SDS gel, and three other Whatman papers. The sandwich was composed in a way that the proteins migrated to the anode thanks to their negative charge, given previously by the SDS. The transfer of the proteins to the nitrocellulose membrane was performed for 70 min at a current of 0.8 mA/cm^2 and 50 V.

For the detection of proteins via antibodies, the nitrocellulose membrane was incubated for 1 h at RT in blocking solution by shaking to saturate non-specific binding sites. To detect two

different antibodies in the same gel, the membrane was cut after blocking. In the case of eGFP and tubulin detection, the membrane was separated at 40 kDa level to have the possibility to process the upper part to detect tubulin (55 kDa) and the lower part to detect eGFP (35 kDa). The membranes were then incubated with the corresponding primary antibody (in blocking solution) overnight at 4° C, on a rotor that allowed a gently shaking. After incubation, the membrane was washed 3 times with TBS-T for 10 min and then incubated with the HRP-coupled secondary antibody (in blocking solution) for 1 h at RT. The membrane was again washed 3 times with TBS-T, 1 time with TBS, and 1 time with ddH_2O for 10 min each. The blot was then incubated for 5 min in the Enhanced Chemiluminescence (ECL) solution. After removing the ECL solution, the resulting signals were visualized by impressing them on an X-ray film (Kodak). Developments were performed using three different exposure times (30 seconds, 1, 2, and 5 minutes) to confirm the eventual absence of a signal.

TBS:		TBS-T:	
Tris/HCl pH 7.5	100 mM	Tris/HCl pH 7.5	100 mM
NaCl	150 mM	NaCl	150 mM
		Tween-20	0.1% (v/v)

ECL solution:		Western blot buffer:	
Tris/HCl, pH 8.5	200 mM	Tris/HCl pH 8.3	25 mM
Luminol (in DMSO)	5 mM	Glycine	
Coomaric acid (in DMSO)	0.8 M	Isopropanol	10% (v/v)
H_2O_2 (30%)	1:1000		

5.2.4.6. Total proteins staining

To detect total proteins in SDS gels, a Coomassie staining was performed. After separation, the SDS gel was washed in ddH_2O and subsequently incubated overnight in the Instant Blue staining solution (Expedeon). After protein bands became visible, the staining solution was removed and the gel washed several times with ddH_2O.

5.2.5. In silico analyses

5.2.5.1. Identification of P_i-related proteins in *P. tricornutum*

Putative factors involved in P_i homeostasis were identified using available transcriptomic data (Yang et al., 2014; Cruz de Carvalho et al., 2016; Alipanah et al., 2018). Additionally, the "Phatr2_domaininfo_FilteredModels2.tab" file (https://genome.jgi.doe.gov/portal/Phatr2/Phatr2.download.html) was screened for protein domains known to be required for P_i homeostasis (e.g., PF02690 for the Na^+/P_i cotransporters, SPX domain, H^+-PPase). The identified proteins were then used as bait for local BLAST analyses in the Phatr2 and Phatr3 databases (http://genome.jgi-psf.org/Phatr2/Phatr2.home.html, (Bowler et al., 2008); https://protists.ensembl.org/Phaeodactylum_tricornutum, (Rastogi et al., 2018) using default settings.

5.2.5.2. Proteins topology predictions

N-terminal signal peptides of the analyzed proteins were predicted using SignalP3.0 (www.cbs.dtu.dk/services/SignalP-3.0) and SignalP4.1 (http://www.cbs.dtu.dk/services/SignalP-4.1/). For transmembrane helix prediction, several web-based tools were utilized, namely, TOPCONS (http://topcons.cbr.su.se), Phobius (http://phobius.sbc.su.se/), TMHMM (http://www.cbs.dtu.dk/services/TMHMM), and TMpred (http://www.ch.embnet.org/software/TMPRED). Conserved domains were determined using the NCBI Conserved Domain Database (http://www.ncbi.nlm.nih.gov/Structure/cdd/wrpsb.cgi). Protein mass and theoretical isoelectric point estimation were determined using PEPTIDEMASS (https://web.expasy.org/peptide_mass/, (Wilkins et al., 1997). Analysis of putative phosphorylation sites was performed using DISPHOS 1.3 (http://www.dabi.temple.edu/disphos/).

5.2.6. Microscopy

5.2.6.1. *In vivo* localization studies

To analyze the *in vivo* localization of each eGFP-fusion protein, gene expression was induced by incubating the cells in f/2 medium containing 0.9 nM $NaNO_3$ instead of 1.5 nM NH_4Cl for

24 hours in sterile reaction tubes under the conditions described in paragraph XXX. Localization of eGFP-fusion proteins was performed using a Leica TCS SP2 (Leica Microsystems) confocal laser scanning microscope with an HCXPL APO40/1.25-0.75 Oil CS objective. Excitation of eGFP and plastid autofluorescence was performed at 488 nm using a 65-mW Argon laser. For eGFP, emission was detected at a bandwidth of 500–520 nm and autofluorescence at 625–720 nm.

5.2.7. Cells staining

5.2.7.1. ELF97™ staining

With ELF97™ assay is possible to detect and localize phosphatase activity. The ELF97™ substrate is hydrolyzed by phosphatase activity generating an alcoholic precipitate at the site of the reaction. The resulting molecule can be visualized through a standard DAPI long-pass filter set, which provides the appropriate UV excitation and transmits wavelengths greater than 400 nm. The assays were performed using a modified protocol from Gonzalez-Gil et al., (González-Gil et al., 1998): a 1-mL sample of a P_i-depleted or P_i-replete (36, 72, and 108 µM P_i (NaH_2PO_4) wild-type culture (see paragraph XXX) was harvested (1500 × *g*, 21 °C, 10 min), resuspended in 95 µL of f/2 medium (with the respective P_i concentrations) containing 5 µL of ELF97™ solution (ELF97™ substrate and ELF97™ buffer, dilution 1:20) (Endogenous Phosphatase Detection Kit; Molecular Probes), and incubated in the dark at room temperature. As a control, cells were incubated with ELF97™ buffer only. After 30 min of incubation, the cells were washed with f/2 medium containing the respective P_i concentration. ELF97™ fluorescence was detected using a Zeiss Axioplan2 (Carl Zeiss Microscopy GmbH) equipped with a DAPI filter (Zeiss filter set 01, excitation BPP 365/12, beam splitter FT 395, emission LP 397).

5.2.7.2. MDY-64 staining

Tracking of the vacuolar membrane of *P. tricornutum wildtype* and *Δvtc2* strains was performed using the vacuole marker MDY-64 (Molecular Probes). 1 µl MDY-64 (1 mM) was added to 499 µl of a *P. tricornutum* suspension (containing approximately 1 x 10^6 cells in f/2 liquid medium) and incubated for 2 min at RT in the dark. Cells were examined with a confocal

laser scanning microscope where excitation of MDY-64 was performed with 65-mW Argon laser and emission detected in a bandwidth of 490-520 nm.

5.3. Genome editing

5.3.1. **Vtc4 sgRNA designing and cloning**

The target site for PtVtc4 was designed using the web-based software Benchling (Benchling, Biology Software, 2017). For the targeted gene, a 20 bp-gRNAs with an on-target score of 57.2, and an off-target score of 49.6 was designed (Table 21). Scores were calculated by the CRISPR-tool of Benching according to the algorithms described in (Doench et al., 2016) and (Hsu et al., 2013). A high on-target score means that the affinity of the gRNA to the target sequence is high while the off-target indicates at which positions and with which efficiency, off-target effects can be expected in the reference genome. Forward and reverse adapters were designed adding the *BsaI* overhangs to allow the exchange of the individual sgRNAs in the PtCC9 vector (Stukenberg et al., 2018).

Table 21. Spacers features for *vtc4*.The position of the target according to the cDNA sequence. The resulting adapters are integrated with *tcga* (forward) and *aaac* (reverse) which are the overhangs of the *BsaI* restriction sites.

Gene Position	**Spacer-Sequence 5`-3`**	**Score (On/Off)**	**Forward Adaptor 5`-3`**	**Reverse Adaptor 5`-3`**
ptVtc4 (162-181)	GCAAACGAACGCACAAGGGT	64.3/49.7	tcgaGCAAACGAACGCACAAGGGT	aaacACCCTTGTGCGTTCGTTTGC

Adapters were annealed incubating the mixture (described in table 22) for 10 minutes at 85 °C in a heating block. The heating block is then switched off and the preparation left in the heating block for about 1 hour until it was cooled down to room temperature.

Table 22. Settings for annealing of adapters to generate the spacer vector.

fwd Adaptor (100 pM)	1.5 µL
rev Adaptor (100 pM)	1.5 µL
10× T4-Ligase Puffer	5 µL
dH20	42 µL

The generated spacer was inserted in the PtCC9 vector via a golden gate reaction. The reaction mixture and setting are shown in tables 23 and 24.

Table 23. Golden Gate reaction settings.

Spacer mix	2 µL
PtCC9 plasmid	100 ng
T4-Ligase	5 Weiss U
BsaI	1000 U
T4-Ligase Buffer	2 µL
dH_20	to20 µL

Table 24. Golden Gate reaction thermocycler settings.

Step	**Time**	**Temperature**
1. Digestion	3 min	37 ˚C
2. Ligation	3 min	16 ˚C
3. Final Digestion	5 min	50 ˚C
4. Heat inactivation	5 min	80 ˚C

5.3.2. **Genotyping of the CRISPR/Cas9 mutant lines**

The genotyping of the *Δvtc4* cell lines was carried out as described in Stukenberg et al., (2018). *P. tricornutum* cells were transformed with individual PtCC9 loaded with specific one *vtc4* sgRNAs as described in the previous paragraph. For the screening of the mutants, a three-step screening procedure was designed: 1st level screening). After transfection Zeocin-resistant colonies were transferred in 1.3% agar-f/2 medium containing 0.9 nM $NaNO_3$ to induce the expression of the Cas9 and thus the formation of the module with the gRNA. After seven days, colonies were taken for colony PCR on the whole targeted gene to ascertain the occurrence of mutations caused by DNA-repair mechanisms. PCR products were run on a gel and the bands excised, extracted, and sent for Sanger sequencing using a nested primer. In case mixed sequences were observed at the expected position, the clone was used to inoculate 3 mL of f/2 liquid culture and after 3-4 days of growth, 100 µL of undiluted and 100 µL of 1:10 diluted culture was plated onto 1.3% agar-f/2 plates to obtain single colonies. 2nd level screening). The colony-PCR and sequencing process was repeated on isolated colonies. According to the obtained sequencing results (e.g. homozygous mutations or wildtype sequence), single colonies were further investigated, especially if they still showed overlapping sequences. The genes were again amplified and cloned into pJET1.2/ blunt Cloning Vector and transformed into *E. coli* TOP10. 3rd level screening). Purified plasmids from transformed *E. coli* from the 2nd level were sequenced. Each transformant represents one molecule of PCR product DNA and thus one allele. A sufficient number of transformants was sequenced to get reliable information about the allelic composition of the isolated clone.

6. References

Abida, H., Dolch, L.-J., Meï, C., Villanova, V., Conte, M., Block, M. A., et al. (2015). Membrane glycerolipid remodeling triggered by nitrogen and phosphorus starvation in Phaeodactylum tricornutum. *Plant physiology* 167, 118–136.

Alexander, H., Jenkins, B. D., Rynearson, T. A., and Dyhrman, S. T. (2015). Metatranscriptome analyses indicate resource partitioning between diatoms in the field. *Proceedings of the National Academy of Sciences* 112, E2182-E2190.

Alipanah, L., Rohloff, J., Winge, P., Bones, A. M., and Brembu, T. (2015). Whole-cell response to nitrogen deprivation in the diatom Phaeodactylum tricornutum. *Journal of experimental botany* 66, 6281–6296.

Alipanah, L., Winge, P., Rohloff, J., Najafi, J., Brembu, T., and Bones, A. M. (2018). Molecular adaptations to phosphorus deprivation and comparison with nitrogen deprivation responses in the diatom Phaeodactylum tricornutum. *PloS one* 13, e0193335.

Allen, A. E., LaRoche, J., Maheswari, U., Lommer, M., Schauer, N., Lopez, P. J., et al. (2008). Whole-cell response of the pennate diatom Phaeodactylum tricornutum to iron starvation. *Proceedings of the National Academy of Sciences* 105, 10438–10443.

Amato, A., Dell'Aquila, G., Musacchia, F., Annunziata, R., Ugarte, A., Maillet, N., et al. (2017). Marine diatoms change their gene expression profile when exposed to microscale turbulence under nutrient replete conditions. *Scientific reports* 7, 1–11.

Amato, A., Sabatino, V., Nylund, G. M., Bergkvist, J., Basu, S., Andersson, M. X., et al. (2018). Grazer-induced transcriptomic and metabolomic response of the chain-forming diatom Skeletonema marinoi. *The ISME journal* 12, 1594–1604.

Ammerman, J. W., and Azam, F. (1985). Bacterial 5-nucleotidase in aquatic ecosystems: a novel mechanism of phosphorus regeneration. *Science* 227, 1338–1340.

Ammerman, J. W., and Azam, F. (1991). Bacterial 5'-nucleotidase activity in estuarine and coastal marine waters: Role in phosphorus regeneration. *Limnology and Oceanography* 36, 1437–1446.

Anderson, L. D., Faul, K. L., and Paytan, A. (2010). Phosphorus associations in aerosols: what can they tell us about P bioavailability? *Marine Chemistry* 120, 44–56.

Andersson, M. R., Samyn, D. R., and Persson, B. L. (2012). Mutational analysis of conserved glutamic acids of Pho89, a Saccharomyces cerevisiae high-affinity inorganic phosphate: Na+ symporter. *Biologia* 67, 1056–1061.

Apt, K. E., Grossman, A. R., and Kroth-Pancic, P. G. (1996). Stable nuclear transformation of the diatom Phaeodactylum tricornutum. *Molecular and General Genetics MGG* 252, 572–579.

Armbrust, E. V. (2009). The life of diatoms in the world's oceans. *Nature* 459, 185.

Armbrust, E. V., Berges, J. A., Bowler, C., Green, B. R., Martinez, D., Putnam, N. H., et al. (2004). The genome of the diatom Thalassiosira pseudonana: ecology, evolution, and metabolism. *Science* 306, 79–86.

Azevedo, C., and Saiardi, A. (2017). Eukaryotic phosphate homeostasis: the inositol pyrophosphate perspective. *Trends in biochemical sciences* 42, 219–231.

Benitez-Nelson, C. R. (2000). The biogeochemical cycling of phosphorus in marine systems. *Earth-Science Reviews* 51, 109–135.

Bowler, C., Allen, A. E., Badger, J. H., Grimwood, J., Jabbari, K., Kuo, A., et al. (2008). The Phaeodactylum genome reveals the evolutionary history of diatom genomes. *Nature* 456, 239.

Bowler, C., and Falciatore, A. (2019). Phaeodactylum tricornutum. *Trends in Genetics* 35, 706–707.

Bowler, C., Vardi, A., and Allen, A. E. (2010). Oceanographic and biogeochemical insights from diatom genomes. *Annual review of marine science* 2, 333–365.

Brembu, T., Mühlroth, A., Alipanah, L., and Bones, A. M. (2017). The effects of phosphorus limitation on carbon metabolism in diatoms. *Philosophical Transactions of the Royal Society B: Biological Sciences* 372, 20160406.

Broecker, W. S., and Peng, T.-H. (1982). Tracers in the Sea.

Buhmann, M. T., Schulze, B., Förderer, A., Schleheck, D., and Kroth, P. G. (2016). Bacteria may induce the secretion of mucin-like proteins by the diatom Phaeodactylum tricornutum. *Journal of Phycology* 52, 463–474.

Butler, T., Kapoore, R. V., and Vaidyanathan, S. (2020). Phaeodactylum tricornutum: A Diatom Cell Factory. *Trends in Biotechnology*.

Cáceres, C., Spatharis, S., Kaiserli, E., Smeti, E., Flowers, H., and Bonachela, J. A. (2019). Temporal phosphate gradients reveal diverse acclimation responses in phytoplankton phosphate uptake. *The ISME journal* 13, 2834–2845.

Cañavate, J. P., Armada, I., and Hachero-Cruzado, I. (2017a). Aspects of phosphorus physiology associated with phosphate-induced polar lipid remodelling in marine microalgae. *Journal of plant physiology* 214, 28–38.

Cañavate, J. P., Armada, I., and Hachero-Cruzado, I. (2017b). Interspecific variability in phosphorus-induced lipid remodelling among marine eukaryotic phytoplankton. *New Phytologist* 213, 700–713.

Cavalier-Smith, T. (2000). Membrane heredity and early chloroplast evolution. *Trends in plant science* 5, 174–182.

Cavalier-Smith, T. O.M. (1999). Principles of protein and lipid targeting in secondary symbiogenesis: euglenoid, dinoflagellate, and sporozoan plastid origins and the eukaryote family tree 1, 2. *Journal of Eukaryotic Microbiology* 46, 347–366.

Cembella, A. D., Antia, N. J., Harrison, P. J., and Rhee, G.-Y. (1984). The utilization of inorganic and organic phosphorous compounds as nutrients by eukaryotic microalgae: a multidisciplinary perspective: part 2. *CRC Critical Reviews in Microbiology* 11, 13–81.

Chen, H.-Y., Fang, T.-H., Preston, M. R., and Lin, S. (2006). Characterization of phosphorus in the aerosol of a coastal atmosphere: Using a sequential extraction method. *Atmospheric Environment* 40, 279–289.

Chen, Z., Yang, M.-k., Li, C.-y., Wang, Y., Zhang, J., Wang, D.-b., et al. (2014). Phosphoproteomic analysis provides novel insights into stress responses in Phaeodactylum tricornutum, a model diatom. *Journal of Proteome Research* 13, 2511–2523.

Clark, L. L., Ingall, E. D., and Benner, R. (1998). Marine phosphorus is selectively remineralized. *Nature* 393, 426.

Cohen, A., Perzov, N., Nelson, H., and Nelson, N. (1999). A novel family of yeast chaperons involved in the distribution of V-ATPase and other membrane proteins. *J Biol Chem* 274, 26885–26893.

Cohen, P. (2002). The origins of protein phosphorylation. *Nature cell biology* 4, E127.

Cresswell, R. C., and Syrett, P. J. (1982). The uptake of nitrite by the diatom Phaeodactylum: Interactions between nitrite and nitrate. *Journal of experimental botany* 33, 1111–1121.

Cruz de Carvalho, M. H., and Bowler, C. (2020). Global identification of a marine diatom long noncoding natural antisense transcripts (NATs) and their response to phosphate fluctuations. *Scientific reports* 10, 14110.

Cruz de Carvalho, M. H., Sun, H.-X., Bowler, C., and Chua, N.-H. (2016). Noncoding and coding transcriptome responses of a marine diatom to phosphate fluctuations. *New Phytologist* 210, 497–510.

Cui, Y., Thomas-Hall, S. R., and Schenk, P. M. (2019). Phaeodactylum tricornutum microalgae as a rich source of omega-3 rich oil: Progress in lipid induction techniques towards industry adoption. *Food chemistry*.

Daboussi, F., Leduc, S., Maréchal, A., Dubois, G., Guyot, V., Perez-Michaut, C., et al. (2014). Genome engineering empowers the diatom Phaeodactylum tricornutum for biotechnology. *Nature communications* 5, ncomms4831.

Davis, B. D. (1958). On the importance of being ionized. *Archives of biochemistry and biophysics* 78, 497–509.

Dell'Aquila, G., Ferrante, M. I., Gherardi, M., Lagomarsino, M. C., D'alcalà, M. R., Iudicone, D., et al. (2017). Nutrient consumption and chain tuning in diatoms exposed to storm-like turbulence. *Scientific reports* 7, 1828.

Depauw, F. A., Rogato, A., Ribera d'Alcalá, M., and Falciatore, A. (2012). Exploring the molecular basis of responses to light in marine diatoms. *Journal of experimental botany* 63, 1575–1591.

Doench, J. G., Fusi, N., Sullender, M., Hegde, M., Vaimberg, E. W., Donovan, K. F., et al. (2016). Optimized sgRNA design to maximize activity and minimize off-target effects of CRISPR-Cas9. *Nature biotechnology* 34, 184.

Drum, R. W., and Gordon, R. (2003). Star Trek replicators and diatom nanotechnology. *Trends in Biotechnology* 21, 325–328.

Duce, R. A. (1986). "The impact of atmospheric nitrogen, phosphorus, and iron species on marine biological productivity," in *The role of air-sea exchange in geochemical cycling* (Springer), 497–529.

Dyhrman, S. T., Jenkins, B. D., Rynearson, T. A., Saito, M. A., Mercier, M. L., Alexander, H., et al. (2012). The transcriptome and proteome of the diatom Thalassiosira pseudonana reveal a diverse phosphorus stress response. *PloS one* 7, e33768.

Dyhrman, S. T., and Palenik, B. (1999). Phosphate stress in cultures and field populations of the dinoflagellate Prorocentrum minimum detected by a single-cell alkaline phosphatase assay. *Appl. Environ. Microbiol.* 65, 3205–3212.

Dyhrman, S. T., and Ruttenberg, K. C. (2006). Presence and regulation of alkaline phosphatase activity in eukaryotic phytoplankton from the coastal ocean: Implications for dissolved organic phosphorus remineralization. *Limnology and Oceanography* 51, 1381–1390.

Erdene-Ochir, E., Shin, B.-K., Kwon, B., Jung, C., and Pan, C.-H. (2019). Identification and characterisation of the novel endogenous promoter HASP1 and its signal peptide from Phaeodactylum tricornutum. *Scientific reports* 9, 9941.

Fabris, M., George, J., Kuzhiumparambil, U., Lawson, C. A., Jaramillo-Madrid, A. C., Abbriano, R. M., et al. (2020). Extrachromosomal genetic engineering of the marine diatom Phaeodactylum tricornutum enables the heterologous production of monoterpenoids. *ACS Synthetic Biology* 9, 598–612.

Falciatore, A., d'Alcalà, M. R., Croot, P., and Bowler, C. (2000). Perception of environmental signals by a marine diatom. *Science* 288, 2363–2366.

Falciatore, A., Jaubert, M., Bouly, J.-P., Bailleul, B., and Mock, T. (2020). Diatom molecular research comes of age: model species for studying phytoplankton biology and diversity. *The Plant Cell* 32, 547–572.

Falkowski, P. G., Barber, R. T., and Smetacek, V. (1998). Biogeochemical controls and feedbacks on ocean primary production. *Science* 281, 200–206.

Feng, T.-Y., Yang, Z.-K., Zheng, J.-W., Xie, Y., Li, D.-W., Murugan, S. B., et al. (2015). Examination of metabolic responses to phosphorus limitation via proteomic analyses in the marine diatom Phaeodactylum tricornutum. *Scientific reports* 5, 10373.

Field, C. B., Behrenfeld, M. J., Randerson, J. T., and Falkowski, P. (1998). Primary production of the biosphere: integrating terrestrial and oceanic components. *Science* 281, 237–240.

Flynn, K. J., Öpik, H., and Syrett, P. J. (1986). Localization of the alkaline phosphatase and 5'-nucleotidase activities of the diatom Phaeodactylum tricornutum. *Microbiology* 132, 289–298.

Georgianna, D. R., Hannon, M. J., Marcuschi, M., Wu, S., Botsch, K., Lewis, A. J., et al. (2013). Production of recombinant enzymes in the marine alga Dunaliella tertiolecta. *Algal Research* 2, 2–9.

Gerasimaitė, R., and Mayer, A. (2016). Enzymes of yeast polyphosphate metabolism: structure, enzymology and biological roles. *Biochemical Society Transactions* 44, 234–239.

Ghillebert, R., Swinnen, E., Snijder, P. de, Smets, B., and Winderickx, J. (2011). Differential roles for the low-affinity phosphate transporters Pho87 and Pho90 in Saccharomyces cerevisiae. *Biochemical Journal* 434, 243–251.

Gibson, D. G., Young, L., Chuang, R.-Y., Venter, J. C., Hutchison III, C. A., and Smith, H. O. (2009). Enzymatic assembly of DNA molecules up to several hundred kilobases. *Nature methods* 6, 343.

Gille, A., Stojnic, B., Derwenskus, F., Trautmann, A., Schmid-Staiger, U., Posten, C., et al. (2019). A Lipophilic Fucoxanthin-Rich Phaeodactylum tricornutum Extract Ameliorates Effects of Diet-Induced Obesity in C57BL/6J Mice. *Nutrients* 11, 796.

Gong, Y., Guo, X., Wan, X., Liang, Z., and Jiang, M. (2013). Triacylglycerol accumulation and change in fatty acid content of four marine oleaginous microalgae under nutrient limitation and at different culture ages. *Journal of Basic Microbiology* 53, 29–36.

González-Gil, S., Keafer, B. A., Jovine, R. V. M., Aguilera, A., Lu, S., and Anderson, D. M. (1998). Detection and quantification of alkaline phosphatase in single cells of phosphorus-starved marine phytoplankton. *Marine Ecology Progress Series* 164, 21–35.

Guillard, R. R. L. (1975). "Culture of phytoplankton for feeding marine invertebrates," in *Culture of marine invertebrate animals* (Springer), 29–60.

Guiry, M. D. (2012). How many species of algae are there? *Journal of Phycology* 48, 1057–1063.

Harke, M. J., Juhl, A. R., Haley, S. T., Alexander, H., and Dyhrman, S. T. (2017). Conserved transcriptional responses to nutrient stress in bloom-forming algae. *Frontiers in microbiology* 8, 1279.

Harold, F. M. (1966). Inorganic polyphosphates in biology: structure, metabolism, and function. *Bacteriological Reviews* 30, 772.

Helliwell, K. E., Harrison, E., Christie-Oleza, J., Rees, A., Downe, J., Aguilo-Ferretjans, M., et al. (2020). A novel Ca2+ signalling pathway co-ordinates environmental phosphorus sensing and nitrogen metabolism in marine diatoms. *bioRxiv*.

Hempel, F., Lau, J., Klingl, A., and Maier, U. G. (2011). Algae as protein factories: expression of a human antibody and the respective antigen in the diatom Phaeodactylum tricornutum. *PloS one* 6.

Hempel, F., and Maier, U. G. (2012). An engineered diatom acting like a plasma cell secreting human IgG antibodies with high efficiency. *Microbial cell factories* 11, 126.

Hsu, P. D., Scott, D. A., Weinstein, J. A., Ran, F. A., Konermann, S., Agarwala, V., et al. (2013). DNA targeting specificity of RNA-guided Cas9 nucleases. *Nature biotechnology* 31, 827.

Huang, B., Marchand, J., Blanckaert, V., Lukomska, E., Ulmann, L., Wielgosz-Collin, G., et al. (2019). Nitrogen and phosphorus limitations induce carbon partitioning and membrane lipid remodelling in the marine diatom Phaeodactylum tricornutum. *European Journal of Phycology*, 1–17.

Huang, W., Haferkamp, I., Lepetit, B., Molchanova, M., Hou, S., Jeblick, W., et al. (2018). Reduced vacuolar β-1, 3-glucan synthesis affects carbohydrate metabolism as well as plastid homeostasis and structure in Phaeodactylum tricornutum. *Proceedings of the National Academy of Sciences* 115, 4791–4796.

Huang, W., Río Bártulos, C., and Kroth, P. G. (2016). Diatom Vacuolar 1, 6-β-Transglycosylases can Functionally Complement the Respective Yeast Mutants. *Journal of Eukaryotic Microbiology* 63, 536–546.

Hunter, T. (2012). Why nature chose phosphate to modify proteins. *Philosophical Transactions of the Royal Society B: Biological Sciences* 367, 2513–2516.

Hürlimann, H. C., Pinson, B., Stadler-Waibel, M., Zeeman, S. C., and Freimoser, F. M. (2009). The SPX domain of the yeast low-affinity phosphate transporter Pho90 regulates transport activity. *EMBO reports* 10, 1003–1008.

Hürlimann, H. C., Stadler-Waibel, M., Werner, T. P., and Freimoser, F. M. (2007). Pho91 is a vacuolar phosphate transporter that regulates phosphate and polyphosphate metabolism in Saccharomyces cerevisiae. *Molecular biology of the cell* 18, 4438–4445.

Jackson, G. A., and Williams, P. M. (1985). Importance of dissolved organic nitrogen and phosphorus to biological nutrient cycling. *Deep Sea Research Part A. Oceanographic Research Papers* 32, 223–235.

Kamerlin, S. C. L., Sharma, P. K., Prasad, R. B., and Warshel, A. (2013). Why nature really chose phosphate. *Quarterly reviews of biophysics* 46, 1–132.

Karas, B. J., Diner, R. E., Lefebvre, S. C., McQuaid, J., Phillips, A. P. R., Noddings, C. M., et al. (2015). Designer diatom episomes delivered by bacterial conjugation. *Nature communications* 6, 1–10.

Karl, D. M., Björkman, K. M., Dore, J. E., Fujieki, L., Hebel, D. V., Houlihan, T., et al. (2001). Ecological nitrogen-to-phosphorus stoichiometry at station ALOHA. *Deep Sea Research Part II: Topical Studies in Oceanography* 48, 1529–1566.

Karp-Boss, L., Boss, E., and Jumars, P. A. (1996). Nutrient fluxes to planktonic osmotrophs in the presence of fluid motion. *Oceanography and Marine Biology* 34, 71–108.

Keeling, P. J. (2009). Chromalveolates and the Evolution of Plastids by Secondary Endosymbiosis 1. *Journal of Eukaryotic Microbiology* 56, 1–8.

Kolowith, L. C., Ingall, E. D., and Benner, R. (2001). Composition and cycling of marine organic phosphorus. *Limnology and Oceanography* 46, 309–320.

Konietzny, U., and Greiner, R. (2002). Molecular and catalytic properties of phytate-degrading enzymes (phytases). *International journal of food science & technology* 37, 791–812.

Leitão, J. M., Lorenz, B., Bachinski, N., Wilhelm, C., Müller, W. E. G., and Schröder, H. C. (1995). Osmotic-stress-induced synthesis and degradation of inorganic polyphosphates in the alga Phaeodactylum tricornutum. *Marine Ecology Progress Series* 121, 279–288.

Levitan, O., Dinamarca, J., Zelzion, E., Lun, D. S., Guerra, L. T., Kim, M. K., et al. (2015). Remodeling of intermediate metabolism in the diatom Phaeodactylum tricornutum under nitrogen stress. *Proceedings of the National Academy of Sciences* 112, 412–417.

Li, T., Guo, C., Zhang, Y., Wang, C., Lin, X., and Lin, S. (2018). Identification and expression analysis of an atypical alkaline phosphatase in Emiliania huxleyi. *Frontiers in microbiology* 9, 2156.

Li, W., Li, B., Tao, S., Ciais, P., Piao, S., Shen, G., et al. (2020). Missed atmospheric organic phosphorus emitted by terrestrial plants, part 2: Experiment of volatile phosphorus. *Environmental Pollution* 258, 113728.

Lin, H.-Y., Shih, C.-Y., Liu, H.-C., Chang, J., Chen, Y.-L., Chen, Y.-R., et al. (2013). Identification and characterization of an extracellular alkaline phosphatase in the marine diatom Phaeodactylum tricornutum. *Marine biotechnology* 15, 425–436.

Lin, S., Litaker, R. W., and Sunda, W. G. (2016). Phosphorus physiological ecology and molecular mechanisms in marine phytoplankton. *Journal of Phycology* 52, 10–36.

Lin, X., Wang, L., Shi, X., and Lin, S. (2015). Rapidly diverging evolution of an atypical alkaline phosphatase (PhoAaty) in marine phytoplankton: insights from dinoflagellate alkaline phosphatases. *Frontiers in microbiology* 6, 868.

Lin, X., Zhang, H., Cui, Y., and Lin, S. (2012a). High sequence variability, diverse subcellular localizations, and ecological implications of alkaline phosphatase in dinoflagellates and other eukaryotic phytoplankton. *Frontiers in microbiology* 3, 235.

Lin, X., Zhang, H., Huang, B., and Lin, S. (2012b). Alkaline phosphatase gene sequence characteristics and transcriptional regulation by phosphate limitation in Karenia brevis (Dinophyceae). *Harmful Algae* 17, 14–24.

Liu, J., Yang, L., Luan, M., Wang, Y., Zhang, C., Zhang, B., et al. (2015). A vacuolar phosphate transporter essential for phosphate homeostasis in Arabidopsis. *Proceedings of the National Academy of Sciences* 112, E6571-E6578.

Liu, T.-Y., Huang, T.-K., Yang, S.-Y., Hong, Y.-T., Huang, S.-M., Wang, F.-N., et al. (2016). Identification of plant vacuolar transporters mediating phosphate storage. *Nature communications* 7, 11095.

Lodish, H., Berk, A., Kaiser, C. A., Krieger, M., Scott, M. P., Bretscher, A., et al. (2008). *Molecular cell biology*. Macmillan.

Mackey, K. R. M., Labiosa, R. G., Calhoun, M., Street, J. H., Post, A. F., and Paytan, A. (2007). Phosphorus availability, phytoplankton community dynamics, and taxon-specific phosphorus status in the Gulf of Aqaba, Red Sea. *Limnology and Oceanography* 52, 873–885.

Mackey, K. R. M., van Mooy, B., Cade-Menun, B. J., and Paytan, A. (2019a). Phosphorus Dynamics in the Environment.

Mann, D. G. (1999). The species concept in diatoms. *Phycologia* 38, 437–495.

Martino, A. D., Meichenin, A., Shi, J., Pan, K., and Bowler, C. (2007). Genetic and phenotypic characterization of Phaeodactylum tricornutum (Bacillariophyceae) accessions 1. *Journal of Phycology* 43, 992–1009.

Martiny, A. C., Lomas, M. W., Fu, W., Boyd, P. W., Yuh-ling, L. C., Cutter, G. A., et al. (2019). Biogeochemical controls of surface ocean phosphate. *Science advances* 5, eaax0341.

Martiny, A. C., Vrugt, J. A., and Lomas, M. W. (2014). Concentrations and ratios of particulate organic carbon, nitrogen, and phosphorus in the global ocean. *Scientific data* 1, 1–7.

McCarthy, J. K., Smith, S. R., McCrow, J. P., Tan, M., Zheng, H., Beeri, K., et al. (2017). Nitrate reductase knockout uncouples nitrate transport from nitrate assimilation and drives repartitioning of carbon flux in a model pennate diatom. *The Plant Cell* 29, 2047–2070.

Migon, C., and Sandroni, V. (1999). Phosphorus in rainwater: Partitioning inputs and impact on the surface coastal ocean. *Limnology and Oceanography* 44, 1160–1165.

Mock, T., Otillar, R. P., Strauss, J., McMullan, M., Paajanen, P., Schmutz, J., et al. (2017). Evolutionary genomics of the cold-adapted diatom Fragilariopsis cylindrus. *Nature* 541, 536–540.

Moog, D. (2019). Higher complexity requires higher accuracy: tail-anchored protein targeting to the outer envelope membrane of plant plastids via a specific c-terminal motif. *Plant and Cell Physiology* 60, 489–491.

Moog, D., Rensing, S. A., Archibald, J. M., Maier, U. G., and Ullrich, K. K. (2015). Localization and evolution of putative triose phosphate translocators in the diatom Phaeodactylum tricornutum. *Genome biology and evolution* 7, 2955–2969.

Moog, D., Schmitt, J., Senger, J., Zarzycki, J., Rexer, K.-H., Linne, U., et al. (2019). Using a marine microalga as a chassis for polyethylene terephthalate (PET) degradation. *Microbial cell factories* 18, 171.

Moustafa, A., Beszteri, B., Maier, U. G., Bowler, C., Valentin, K., and Bhattacharya, D. (2009). Genomic footprints of a cryptic plastid endosymbiosis in diatoms. *Science* 324, 1724–1726.

Nenes, A., Krom, M. D., Mihalopoulos, N., van Cappellen, P., Shi, Z., Bougiatioti, A., et al. (2011). Atmospheric acidification of mineral aerosols: a source of bioavailable phosphorus for the oceans.

Norton, T. A., Melkonian, M., and Andersen, R. A. (1996). Algal biodiversity. *Phycologia* 35, 308–326.

Nymark, M., Sharma, A. K., Sparstad, T., Bones, A. M., and Winge, P. (2016). A CRISPR/Cas9 system adapted for gene editing in marine algae. *Scientific reports* 6.

Ogura, A., Akizuki, Y., Imoda, H., Mineta, K., Gojobori, T., and Nagai, S. (2018). Comparative genome and transcriptome analysis of diatom, Skeletonema costatum, reveals evolution of genes for harmful algal bloom. *BMC genomics* 19, 1–12.

Osmond, M. F. (1887). Sur une reaction pouvant servir on dosage coloimetrique du phospore dans le fontes, les aciers, etc. *Bull Soc Chim* 47, 745–749.

Osuna-Cruz, C. M., Bilcke, G., Vancaester, E., Decker, S. de, Poulsen, N., Bulankova, P., et al. (2020). The Seminavis robusta genome provides insights into the evolutionary adaptations of benthic diatoms. *bioRxiv*.

Pasciak, W. J., and Gavis, J. (1974). Transport limitation of nutrient uptake in phytoplankton 1. *Limnology and Oceanography* 19, 881–888.

Paytan, A., and McLaughlin, K. (2007). The oceanic phosphorus cycle. *Chemical reviews* 107, 563–576.

Peters, F., Arin, L., Marrasé, C., Berdalet, E., and Sala, M. M. (2006). Effects of small-scale turbulence on the growth of two diatoms of different size in a phosphorus-limited medium. *Journal of Marine Systems* 61, 134–148.

Popov, N., Schmitt, M., Schulzeck, S., and Matthies, H. (1975). Reliable micromethod for determination of the protein content in tissue homogenates. *Acta biologica et medica Germanica* 34, 1441–1446.

Rastogi, A., Maheswari, U., Dorrell, R. G., Vieira, F. R. J., Maumus, F., Kustka, A., et al. (2018). Integrative analysis of large scale transcriptome data draws a comprehensive landscape of Phaeodactylum tricornutum genome and evolutionary origin of diatoms. *Scientific reports* 8, 4834.

Rastogi, A., Vieira, F. R. J., Deton-Cabanillas, A.-F., Veluchamy, A., Cantrel, C., Wang, G., et al. (2020). A genomics approach reveals the global genetic polymorphism, structure, and functional diversity

of ten accessions of the marine model diatom Phaeodactylum tricornutum. *The ISME journal* 14, 347–363.

Redfield, A. C. (1934). On the proportions of organic derivatives in sea water and their relation to the composition of plankton. *James Johnstone memorial volume*, 176–192.

Reiken, S., Lacampagne, A., Zhou, H., Kherani, A., Lehnart, S. E., Ward, C., et al. (2003). PKA phosphorylation activates the calcium release channel (ryanodine receptor) in skeletal muscle defective regulation in heart failure. *Journal of Cell Biology* 160, 919–928.

Resing, J. A., and Sansone, F. J. (2002). The chemistry of lava-seawater interactions II: The elemental signature. *Geochimica et cosmochimica acta* 66, 1925–1941.

Riso, V. de, Raniello, R., Maumus, F., Rogato, A., Bowler, C., and Falciatore, A. (2009). Gene silencing in the marine diatom Phaeodactylum tricornutum. *Nucleic acids research* 37, e96-e96.

Rubio, V., Linhares, F., Solano, R., Martín, A. C., Iglesias, J., Leyva, A., et al. (2001). A conserved MYB transcription factor involved in phosphate starvation signaling both in vascular plants and in unicellular algae. *Genes & development* 15, 2122–2133.

Schreiber, V., Dersch, J., Puzik, K., Bäcker, O., Liu, X., Stork, S., et al. (2017). The central vacuole of the diatom Phaeodactylum tricornutum: identification of new vacuolar membrane proteins and of a functional di-leucine-based targeting motif. *Protist* 168, 271–282.

Secco, D., Wang, C., Arpat, B. A., Wang, Z., Poirier, Y., Tyerman, S. D., et al. (2012a). The emerging importance of the SPX domain-containing proteins in phosphate homeostasis. *New Phytologist* 193, 842–851.

Secco, D., Wang, C., Shou, H., and Whelan, J. (2012b). Phosphate homeostasis in the yeast Saccharomyces cerevisiae, the key role of the SPX domain-containing proteins. *FEBS letters* 586, 289–295.

Sengottaiyan, P., Petrlova, J., Lagerstedt, J. O., Ruiz-Pavon, L., Budamagunta, M. S., Voss, J. C., et al. (2013). Characterization of the biochemical and biophysical properties of the Saccharomyces cerevisiae phosphate transporter Pho89. *Biochemical and Biophysical Research Communications* 436, 551–556.

Serif, M., Lepetit, B., Weißert, K., Kroth, P. G., and Bartulos, C. R. (2017). A fast and reliable strategy to generate TALEN-mediated gene knockouts in the diatom Phaeodactylum tricornutum. *Algal Research* 23, 186–195.

Sforza, E., Calvaruso, C., La Rocca, N., and Bertucco, A. (2018). Luxury uptake of phosphorus in Nannochloropsis salina: effect of P concentration and light on P uptake in batch and continuous cultures. *Biochemical Engineering Journal* 134, 69–79.

Sharma, A. K., Mühlroth, A., Jouhet, J., Maréchal, E., Alipanah, L., Kissen, R., et al. (2019). The Myb-like transcription factor Phosphorus Starvation Response (PtPSR) controls conditional P acquisition and remodeling in marine microalgae. *New Phytologist*.

Shih, C.-Y., Kang, L.-K., and Chang, J. (2015). Transcriptional responses to phosphorus stress in the marine diatom, Chaetoceros affinis, reveal characteristic genes and expression patterns in phosphorus uptake and intracellular recycling. *Journal of experimental marine biology and ecology* 470, 43–54.

Shrestha, R. P., Tesson, B., Norden-Krichmar, T., Federowicz, S., Hildebrand, M., and Allen, A. E. (2012). Whole transcriptome analysis of the silicon response of the diatom Thalassiosira pseudonana. *BMC genomics* 13, 499.

Siaut, M., Heijde, M., Mangogna, M., Montsant, A., Coesel, S., Allen, A., et al. (2007). Molecular toolbox for studying diatom biology in Phaeodactylum tricornutum. *Gene* 406, 23–35.

Solovchenko, I. Khozin-Goldberg, I. Selyakh, L. Semenova, T. Ismagulova, A. Lukyanov, et al. (2019a). Phosphorus starvation and luxury uptake in green microalgae revisited. *Algal Research* 43, 101651.

Solovchenko, T. T. Ismagulova, A. A. Lukyanov, S. G. Vasilieva, I. V. Konyukhov, S. I. Pogosyan, et al. (2019b). Luxury phosphorus uptake in microalgae. *Journal of Applied Phycology*, 1–16.

Stukenberg, D. D. S., Zauner, S. S. Z., Dell'Aquila, G., and Maier, U. G. (2018). Optimizing CRISPR/Cas9 for the diatom Phaeodactylum tricornutum. *Frontiers in plant science* 9, 740.

Suzumura, M., and Kamatani, A. (1995a). Mineralization of inositol hexaphosphate in aerobic and anaerobic marine sediments: implications for the phosphorus cycle. *Geochimica et cosmochimica acta* 59, 1021–1026.

Suzumura, M., and Kamatani, A. (1995b). Origin and distribution of inositol hexaphosphate in estuarine and coastal sediments. *Limnology and Oceanography* 40, 1254–1261.

Tanaka, T., Maeda, Y., Veluchamy, A., Tanaka, M., Abida, H., Maréchal, E., et al. (2015). Oil accumulation by the oleaginous diatom Fistulifera solaris as revealed by the genome and transcriptome. *The Plant Cell* 27, 162–176.

Tateyama, M., Rivolta, I., Clancy, C. E., and Kass, R. S. (2003). Modulation of cardiac sodium channel gating by protein kinase A can be altered by disease-linked mutation. *J Biol Chem* 278, 46718–46726.

Todd, A. (1959). Some aspects of phosphate chemistry. *Proceedings of the National Academy of Sciences of the United States of America* 45, 1389.

Towbin, H., Staehelin, T., and Gordon, J. (1979). Electrophoretic transfer of proteins from polyacrylamide gels to nitrocellulose sheets: procedure and some applications. *Proceedings of the National Academy of Sciences* 76, 4350–4354.

Uttenweiler, A., Schwarz, H., Neumann, H., and Mayer, A. (2007). The vacuolar transporter chaperone (VTC) complex is required for microautophagy. *Molecular biology of the cell* 18, 166–175.

Vanier, G., Hempel, F., Chan, P., Rodamer, M., Vaudry, D., Maier, U. G., et al. (2015). Biochemical characterization of human anti-hepatitis B monoclonal antibody produced in the microalgae Phaeodactylum tricornutum. *PloS one* 10.

Vats, P., and Banerjee, U. C. (2004). Production studies and catalytic properties of phytases (myo-inositolhexakisphosphate phosphohydrolases): an overview. *Enzyme and Microbial Technology* 35, 3–14.

Wang, C., Huang, W., Ying, Y., Li, S., Secco, D., Tyerman, S., et al. (2012). Functional characterization of the rice SPX-MFS family reveals a key role of OsSPX-MFS1 in controlling phosphate homeostasis in leaves. *New Phytologist* 196, 139–148.

Westheimer, F. H. (1987). Why nature chose phosphates. *Science* 235, 1173–1178.

Whitmarsh, A. J., and Davis, R. J. (2000). Regulation of transcription factor function by phosphorylation. *Cellular and Molecular Life Sciences CMLS* 57, 1172–1183.

Wild, R., Gerasimaite, R., Jung, J.-Y., Truffault, V., Pavlovic, I., Schmidt, A., et al. (2016). Control of eukaryotic phosphate homeostasis by inositol polyphosphate sensor domains. *Science* 352, 986–990.

Wilkins, M. R., Lindskog, I., Gasteiger, E., Bairoch, A., Sanchez, J.-C., Hochstrasser, D. F., et al. (1997). Detailed peptide characterization using PEPTIDEMASS–a World-Wide-Web-accessible tool. *Electrophoresis* 18, 403–408.

Wolfe-Simon, F., Blum, J. S., Kulp, T. R., Gordon, G. W., Hoeft, S. E., Pett-Ridge, J., et al. (2011). A bacterium that can grow by using arsenic instead of phosphorus. *Science* 332, 1163–1166.

Wu, Y., Huang, X., Jiang, Z., Liu, S., and Cui, L. (2020). Composition and sources of aerosol organic matter in a highly anthropogenic influenced semi-enclosed bay: Insights from excitation-emission matrix spectroscopy and isotopic evidence. *Atmospheric Research*, 104958.

Wyss, M., Pasamontes, L., Friedlein, A., Rémy, R., Tessier, M., Kronenberger, A., et al. (1999). Biophysical characterization of fungal phytases (myo-inositol hexakisphosphate phosphohydrolases): molecular size, glycosylation pattern, and engineering of proteolytic resistance. *Appl. Environ. Microbiol.* 65, 359–366.

Yamagata, Y., Watanabe, H., Saitoh, M., and Namba, T. (1991). Volcanic production of polyphosphates and its relevance to prebiotic evolution. *Nature* 352, 516–519.

Yang, S.-Y., Huang, T.-K., Kuo, H.-F., and Chiou, T.-J. (2017). Role of vacuoles in phosphorus storage and remobilization. *Journal of experimental botany* 68, 3045–3055.

Yang, Z.-K., Zheng, J.-W., Niu, Y.-F., Yang, W.-D., Liu, J.-S., and Li, H.-Y. (2014). Systems-level analysis of the metabolic responses of the diatom P haeodactylum tricornutum to phosphorus stress. *Environmental microbiology* 16, 1793–1807.

Yoon, S.-M., Kim, S. Y., Li, K. F., Yoon, B. H., Choe, S., and Kuo, M. M.-C. (2011). Transgenic microalgae expressing Escherichia coli AppA phytase as feed additive to reduce phytate excretion in the manure of young broiler chicks. *Applied microbiology and biotechnology* 91, 553–563.

Young, C. L., and Ingall, E. D. (2010). Marine dissolved organic phosphorus composition: insights from samples recovered using combined electrodialysis/reverse osmosis. *Aquatic Geochemistry* 16, 563–574.

Zaslavskaia, L. A., Lippmeier, J. C., Kroth, P. G., Grossman, A. R., and Apt, K. E. (2000). Transformation of the diatom Phaeodactylum tricornutum (Bacillariophyceae) with a variety of selectable marker and reporter genes. *Journal of Phycology* 36, 379–386.

Zhang, C., and Hu, H. (2014). High-efficiency nuclear transformation of the diatom Phaeodactylum tricornutum by electroporation. *Marine genomics* 16, 63–66.

Zhang, K., Zhou, Z., Wang, J., Li, J., Lin, X., Li, L., et al. (2020). One enzyme many faces: alkaline phosphatase-based phosphorus-nutrient strategies and the regulatory cascade revealed by CRISPR/Cas9 gene knockout. *bioRxiv*.

Zhang, S.-F., Yuan, C.-J., Chen, Y., Chen, X.-H., Li, D.-X., Liu, J.-L., et al. (2016). Comparative transcriptomic analysis reveals novel insights into the adaptive response of Skeletonema costatum to changing ambient phosphorus. *Frontiers in microbiology* 7, 1476.

Zou, L.-G., Balamurugan, S., Zhou, T.-B., Chen, J.-W., Li, D.-W., Yang, W.-D., et al. (2019). Potentiation of concurrent expression of lipogenic genes by novel strong promoters in the oleaginous microalga Phaeodactylum tricornutum. *Biotechnology and bioengineering* 116, 3006–3015.

7. Supplements

7.1. Sequences of the upstream/downstream regions

Nucleotide sequences and length of the upstream and downstream regions used to design eGFP expression cassettes, obtained by Sanger sequencing of the fragments amplified from *P. tricornutum* (strain UTEX646). Untranslated regions (UTR) are underlined in blue.

>*PtPhos1* upstream region, 949 bp
CCGGTGTGTAAATATACGATACCCGGAGCCGCGTTGGAGATTCATTCACTGTCAACGCTCGGCCACGGCAATT
TGCCCTAATATCGTAACACATAAAATGGCGACGTTTCCCTGCACGACCATAATTTCGTTCACGGCAGGGATTTT
GGCGTCGAGATTCGTTCATGGGACCAAAACTAGCAGGAGGATTGGTTTTTCAGCATAATAGATTCGTGTCCCC
GTTTCGATTTTTCTCTGCGGCCGTCCCCACCGGACTCGAAAAAATTTCAAAGTTAGAGCATTTGGTGAAATCGT
ACGCCAAGTTTCCCGCTAGAAATAATGTGGACCGAGGGTTAAGTGTCGCGCATGTGCGAAGAATGCGCTGGG
AGCTGACTTCCCGGCCGACTGTAATTAGAGAAGAACATAGATTAAAAAAAGACTTGTCAATTCGGAAGACACA
CAAGTAGACACAGAATACTAAACAAGAAGAGAGAAGCATGACTCATCTTTTTAAGCATCATAATAGATGATTT
GCAGGGCGTTTGTATGAGTCAGCCAAGTGCAAATATGTTTTACGTGTCAACGAATCTTAAAGATCCATGACAA
AAACGCCATACACCAGAACCATGAAATGGACGCTTCGTTAATGTAAAGTGTCGAATCTTCAGTTCACATTTTTC
AAGATTCGCTAGATTCGACAGTGATAAATCATCTTTGTCAAAACAATCTTCATGGTTGTTGAACGATATACGGT
CTATACGTCCTAAATCAGAGAACCGTTCACAAATTACAATTAGATTCTTTAGAGAAACCATGACCAGGCTCACG
TGTACTTTCTTACAATTGATGGGATCGGATGCAAGACCGAGGAAAAGATCTCATCTCTTGGGCGCACTGATAA
AGCTCATAATTTTGTGAGTTGCCACCAAGGATTTTTCTATCGGCATCCTAACATTATCGGACCTGCAAA

>*PtPhos1* downstream region, 523 bp
TCGGATTCTTGCAAGCTTGAGCACAGGAATTTGAGACTTATATATGTTGCGTCCGAAATTTACAGTTAGGCTTT
CGTCCGATTTTGCTATGTAGGCGGAAATAGCATAGAATCATGTTACACAGTTAAGGCACTCATAGTTGTACATA
GTGTGGTGCATTTTAGAGCTGTTTGGAACAAGCAAACATTTTGAGTGCAGATTCCCCCACCCATGGAATGTGA
GCGTTGCTCGCGCAGAATGTCGATTTTACAGTTAGTTGGAACGGTGCGCCCGCTGGAGCCGACTTTTGATTGG
AAGTACTGTTCTGAACTGGTACACGTCGAGTCATACCCTGCCCTTCTTACATCTTATTGAGAGACGATGGCACTT
TGCGAACAAAGTGGTTGTGATGTTCTAACAGTAAATATAAAAGGCTGTAGGTAGTTTACCTAGCTCTACACGC
AAACGGAGGACCGCATCAATTCCGTCGGAGGCCGTTACCGTGTTCGCTTAGGCTACCGGACCGGCCCGTCTTT
AGGCACTC

>*PtPhos2* upstream region, 1042 bp
GACCTGCAATACACCTAAGCGGGCCTAGGGACTGTAAAACTCAACTCGCTTACGACGCTCCCCACGGGTTAGA
CAGCGGATACGAGGACCTATGCTAACGCAATATTTGGATCAATATCTTTCTAAAACAATGAGAAGAAGATTGTT
CTACTACTAGTCCATCGGGCTTGAGAGGTCCAGTTCACTGGACTACCGTTACCATGTTCCAGATAATCTTACTCA
CATATATGAGTCTTGTTCTTTTAAGTATAAATCCCTAAAAAACTATAGAAATCCTAGAAGCAGTCAGTAAATGTA
AATCCATCACTAATGTAACTCTAAGTTCCCTCTACTAGTCAATTGTACAACATAAATTCTTCACTGATTGTGACTT
TGAATTTTAGGACACACTCTCTAGAGAGGATTGATAGTGAAAACCTTATTCATTGTCAGAGCTTAAGCCGGTCT
GGTCTATCTTTCCACTGTCAAACAGCTCTTGATTGTCGCCCGCGCGAAAATAGTAGCACTAACTGTAACTTCAA
AATACAAAATGTTCTCTGTTACCATACAGTGAATGTAACTTTCGAATTGACAGTATTAGTAGTCGTATTGACAGT
GAGGCACGCCCCTCAATGTGCGAGGTGGAAAATATACCAGCATGACAATGAATCTTGGAGATTCTTTTGCTGT
CATCAAGATTCACCGCCAAATCTTCAGGAACCTATCACGTCCACAGGCGATGTTAATTCTTGAGTCGTCAAAAC

AAAGTCCTGTCCTACCTGTAGAAGTTGACAGCGAGCAATTGTATGCAAACTTCTGACTTTGTTATAATAACATT
AAAGGTAATTAAGTATCTTCAATTAGGCATTTTGTCACTGTCAGTCCGTTCCGACAATATAGGTAGATTTGGAA
TGAATCTTTTCTATGCTGCTGCGAATCTTGTACACCTTTGAGGCCGTAGATTCTGTCCGACGAAGCGATAATTAT
TGCAAAATACATGGACTCATTATTTTGATTCGATTTTCTTTTTGGTATCCGACTCGAAAAGATCCATCACGGCGAG
C

>*PtPhos2* downstream region, 500 bp
GTATAGAAGGTCACGTAGCTAGAGAAAGAAAGAGTTAATCTCAAAAAGAGTCAAGTCCACGAACTTCAAATA
AACCATAAGTCTTCTTTCGTTTACCCATTGGCCTTCATCCTTCCAATCAACACTCGATTCTGAACAGAAAATTGG
ACCGGGAATGATTCCTGCGATACTGTAAGCGATTTCCCTACCTGATTCCTCGATGCCATTAAATCTTCGGCAGCT
GCGCGGCGCATTGCGTTCAGTGCTCTAATCGCCCTATGCTGTCCACCAGATGAAGCTCCGGTTGAAAGAACCG
AAACACGCCTAATATCGTCACGAAATTTTTCTAATGACTTTTGGTTGGCATCGCTGCGAAACATGAAATCAGCA
CGACGGGTCAAACACGCCAGAATCTGGTTTGACCTGAAGCAGCAAGTAGATATACAGAACGAAGTCTGTGCTC
GAACAGCAATTTCTACAGCAGCTTCTGCAAGGCCTCCGCAGCAATGGAGACCTCCGGA

>*PtPhos3* upstream region, 1000 bp
CGCATTCGCAACCCGCTGGGTCGAATAAAGCGTTCGTATTTGGGAGCTTTCCGGGTAAAAGAGTCTCCTACAA
AGGTGCATTTGGTAACCACACGCTTCCACGCCTTGTTCTGTTTCTTACCGGTCCGCATGACTTTGAACATTTCGT
CATCGGCTACCGGCTTGACCTTGGGAATGGGCACTTCCCATTTTCCGGCCTTTTCTTTCCGCTTTTGCTTAATCGT
ATTCGACAAAACCTTGGCACGGGAGACACCTTGACGGTCTAACAAATAGGCCGGTACGGCCCCATCGGCGAC
GGCATCGTCGTCCGCGTGTTTGTTGTTGCGTTCGTTGTGCATCGCGATCGTTTTGCGCATGGTGGCCTTTTCCTT
GAACCGCTTCTTTTGGTAGAGTTTCGCCCGAATACCGTGTACTTTTTGGGCAAATTCGGAGCGCTTGTGCACCA
TACGCGCTTCCTTTTTGCGCTCACGCTCCTCGGCGTCGAACCGACGGCCGTGAAGCTTGGCGTGGCGTTCCATA
TGTTCGTGCTGCGGCATGGTGGAACGAAGGACCTGTTGTTTATTGCGCAACTACGATTGTCGGAGAATATGAA
TGAATAAATGAATGAATAAATTGGTTGTACCGTCTCTCTTGTGCACAGACGCTATTGTCTAGCGATGCGAACAA
ATCTGCCGAGATACGCCGGTGTACCAGCTTGGTTACTGGACGACGCGTCTATCCGGACGAGAAAGCCCAGCGC
GGAAAAACGGGAGATGCGCAAGTTTGGTCGGCATTATTTCCTTGGTTGGCGAGTTGCCCACGGGACCGGATG
ACGTCCAAACCTAACGACACCGGAAAATGTCTGACATCTGTCCCAAAGCCGTGGACCTTATGTGAATTGTAAG
ACACACGCGCCCGAGAAGCAAAACCGCACTCCGGCACGCGATTCGTCCTCCGGTGGGGGCGAATCTCAACGA
ACGGAGAATTTGACCGTACGCGTTCCGTCGTTCAATATTCTCATCGGTACACC

>*PtPhos3* downstream region, 538 bp
CACAATTCACATTTTTAAGTTTTCGAATGTGCTACAATAAACACCGTTTTTCTGGAGCTGTTCCAGTTTTGTTCCT
GTTGTTGGGATGCTCGGGCTGTAAGAGCTGCTTGATAGACGTTGAATATATACTGGTCGTCTAGTCCATTGGC
CAGTACCTTGCTATAGAAGAATATCGGGTTATTGCTTTCCAGAACCGCGGACACGTCGATTTGCATCATTGGAG
GCTCCAAGCGCTTCCGATGGTCCAAATTGCATTCGGATTGAAAGTGCCCGACCAAACCACAGTTCCAACAAGG
TGTCGCCGCTGCGGCAGCCTGTAAGAGGCAACTTTGAGCTTGCTTGTCGGGAGGAAGTGTGGGGCACTGTCG
GAGCCAGTGGTCCTTCGAGTCACAAAGGAAGCAGACTCCGATTGATCGGTTCTTCCTTCGCTTTGCTTCGTAGC
GTTCATTGTTTTGCCTGCGTTGCCTACGCTTTTCGTCGTTTTCGTAGCAGCAGACATACAAACAACGATCGGTAG
GGGCAATATTCTTGGCCGTTA

>*PtPhos5* upstream region, 1073 bp
AGAAATCGCGTGGTTGGAAATTGATGCCCCCCGAGTTATCGTAGTACATTGTGTTGATGGTACCGACGGCATG
ATCAAGTAGGGCGGCGTTGGCGGTGAGTCTTTCGTCCGGAGTCCCTTCCCGCATAATGTTCCAGTAGCGCTCTT
TAGAAGAAGGCAAACTGACCATTTCGCCTGCCAATACCGGTGCTATCATCACGGAACTAATTTGCAGTGCGAC
CAAAGCGCTGATGAGGCACTTGGACGCGTATTGGGCAAACGTGGACCGGGAGTACGCGGGGGACGGCGGAG
TGACCGCATCAGTGTTGGGAGCAAAGTCATCCGCATTGCACAAACGTTTCCGCGCCGTCAATGCCGTGGTAGG
ACAAAGGCCTAGAAGTACCTTACTTGAACGTGAATCCAACGACGATCGTGTAGGTGGTAAAATCCAAGCGTGC
ACGTCGCCTTGTGCAATAAAACCAATAGTGACGAGCAGCAGTGGCGTGAGAAGCCGACGACCGGAGAAGTTC
CGAATGTTCCGCAGGCTTTGGATCATCTCATTTCGAATCTCTCCTTGGGTGTACGGATACTCTGGGGGATTGTT
ACGGACTGGCAGTGGTGCAATGTTTGATGGGTTTGACAGTGAATCGTCCCACAACCTTTCTGTTAGTATGCGAC

GATTGCACTCTATAGGAGTAACGGAAGGAAAGGGCGAGAGGGCAAATTCGGTAAACAGCTCTTCGGTCCATG
TAGGAATTCGGCAGAGAGCATGTCAGCCAACGTGTGCTGGTGGTTTTGCTGACATCACGATTATACCAATGGT
CCTATGGTATTCCACGGATTCCAAAGGATACTTTCCTTCTTTATTCTCATTGGCCATAAATGTCGGACTTTGAAC
CTTCGCACCGTGCGATGCTCCTAGCTAGTAGGACATATAGACTGGACACGTAGAGTAGTAGCACAGTATATCG
GAAAGGAATACAAAGTGCATTGACCTGAATGGTCCTCTCACACAGTCAGTCTCTTGTATACGTACAAAGCACAC
ACTCGGTTTCTAGTACCAGTGTATATGTGTGTATCGAACAAGAATACCA

>*PtPhos5* downstream region, 500 bp
GCTCCCGAATGTTTGTTTTCGTCTCCTAGAGAACAGGACAAGCTAGGCCTCCAGCACTCTCCTTGGCACTGATT
GGAGCGGAAACGATCACCGTATACAAACTGTAAATATGTGTTTGCTAATTGACAGAGTACACGTCTTGCCAAT
GCAAATTAAGCCAGCACTGAACACTTATTACCTTAAAACATGGAACGCGTATTCGACTAGCCCGGAGTCGATTG
AATTCAACCAACACGGAACATTTCTTACGTCTACAGCGTGTTCGACTAGCCCGAAGTTGTTCGGTTTCCGTACTT
TTCAATCACCTTTGCCAGCTCTTCCTTGGCCGAGTCCTGAGAAGAGAAAGAAGTCAGGTTTGTCAAATTTACCA
ATACAAGGTTTAAGGATTTTTTTAATCACATACCTTGCAACTGTGACCCAGAGTGCACTGTCCCAGAAGATTGT
CTCGGGCAATGTCGATAATGTGGGATGTCAGATATTCGTTCATCCACCGCACTTGC

>*PtPhos6* upstream region, 1000 bp
TGTGAAAGTTTCTGCTCAAGTAGCAAATTGTAGGACAATAGAAAGGCAAAAAGGGAAAACGAAAAGGATTTA
AGAATAATGTGAGTAACGACTGAAAGGAAGCTGAGCTATTGTGCAACCTGTCGAATGAGTAATTGGTTGGCA
AAAATGTCTTGCCATAGCTTTTAATCTAAAAAGGTTTTGTGGCAACAAGTTCAAATTGTCCGCGGCTTCGAAAT
TGGTATCGAAAGTATCTGTCTTTCGTATTTAGCAGTAAGCAGAGAAACATTCACCCAGAGCGAAGCACTCGAA
CAAAGTATACCTATGGATATAAATGCTACACTTGGAATACACTGCGTGCTCTCATACCTGAGGAATGGAATGG
CGATGTAGCTGCAAAAAAGTTGGTTCCGCCAACAGACTTTCGGAGAGCAATTGTTTGTTTGCCTTCCTAACACA
CTCTTACAGTTAATCGACTGAGAAATAGAGATAATTTCCATTTTGCCGCGTTTAATTCGGGTCGTGCCCTTATTT
TCCAAAGTCAAGATTCATCTCATTCTCAAGATTCTTCGCAACATGACGTTTCTTGCTTCGTCGAGAATCTCTACAT
CGCATGAAAATGTCTCTTTGTGAAGTCTTCCGTAGGAACTGGAACAAGCAATGCTGCCTTGGTGTAGGGCTCC
GTAAGGCTAGTAGTGGTAGTAGATTTGTTTGAACGAATTTGAAGTTTAGGTTGGCTGAGGTCGCGAATCTCGG
AGATGGATTGACAACTGCCACTGAGAACTCCCACGCCGCACGCACAACGATTTTTTCACAATACAGGCCTTGTT
GCAACTGGCTAGAAAAGAAATAGACTCAGGCGTACTTGATGCACTGTATTCCATTTCGAATCCTCAAAAAAGA
GATTTGGATTATCTGGTCCCTTTTGTTGATTTCATTTTCCGATTATCCCTGTCTCGCTTTGCCAGACCCATTGAAA
CATATTCGGGAAATCCACCCCCGCTTTTTCTTACAGTGAAC

>*PtPhos6* downstream region, 500 bp
AAAGTTTTTGTTTTTGTCCCTTTATAAAAATCATCGTTGGGACAAACGTTCTTCCCAATTATGAACCGGCTTGTA
GTTTACAGTCGTAACATAGGCAGCGACGACGCGCCAGGTCCGTACCATGAAATCTAGAAGGCGCATTACGTAT
TCTTAACGTTAAAAAATGCTATTGACCGTAAGAACCCCTTGCCAGAATCTAAGACACGGCAGCAGCCTTGGCGT
AGGTTACTTCGGGATTGGCTCCGTCGATAGTCTTGGTCGACTGGGCGGGCGTTGGAGCACTCGCAGGCTCACC
GTTTTCCTTGACGAGTCCCAAGGGCTTGAGGACCGTCAAAAACAACGGTTTGAAAATCTCTTCCGTTTTACCGA
CCGCCCCCATGACGGTCTGAACCACGGCCTTGATGGCAGGATTCAAAACGTTATCGTCCAAGCCGTGCAAGTT
GTGCCTAAACGGAGGGGAATCGAGAGAACAGAAAGATACTTAGTATCATACGGTGTCG

>*PtPhos8* upstream region, 910 bp
ACAGGTTTGTTGCTTGGGAACAGCCGTCGCAACTGTCGTTGTGCTATAGTCTTCCGATGCCTTTCTAGGCGTCA
AAGGAGACTTTTAATTCTCGTGTAACAAGCAAGAATTGTTTCAAAAGCCAACAGTACTTTTTCTTCTAATTTCAC
GTCTTGTACCGTTTCCCATCTTCATCGACAGTAAGGTTGTTCGTCCCGTTGGCCTACGTAGTTTAGCTGTGAGCG
CTGTCAGTTGCAGCTATCACAAGAAAAGACATTTGCACAGTGGCATTCATCATGCAAAAGACTGGTGGTGAAT
CAACACTTAATGTGCATTTGCTGTTCAAAACTCCTGGAGTCCTGGCGACAGTTTGTGCTCTGTATGCTTGGGGT
AAAGTGTTCACAGTCAACTGCTGTGAAGCAGATTGATCGAAGCTTGACGGGTTGGAGGCAGCTCATCCATGCC
AATGCGATACCTCCGCTATATCATACACAGAGCATACACCAAGCATTGGATTATTTTCTAATTGCTAATTTTACT

TAAAAGCCGTTTCGCGTCGAAATAGCGATTTTTTCATGTCGCAGAGACCGAAATAGCGGTTTTCCTCAAGGTAT
TTCTATCCTTCTAATTGACGTTATGTATGACACATTTGCTGTAACACTGGGAGAGGTTAATTGAAAGTTCCCTGC
CAACTTATCTTACCAGATTCAAACTCTGAAAGGAGATTCATTCCTCCCACTCGCATTCCAAACAAGATTCTTCTG
CAAATCTTTTCGATTTGGAAAACAGATTCTTTTGATTCTTTCTGTACCATCTAGTATGCCTCATTTGTACCGACGC
TCAAGTTCCTGCAGACCACAAAAAAGATCTTTGCACATTTTCGTTTACAGTTTACTGTTACGCTGATTTCCCTGG
TGAAAAGAATTCTTCG

>*PtPhos8* downstream region, 500 bp
TTTTGTGGAGTTCTTTTTCTTTATCAATCCGGATTGTGATTGTTTGAAGTTTCCCTGATCAATACCTGACATCGCT
TGTCTACAACTACTGGACCGAAACGGATTCACAGTCACTGTCAGTACCTTTTGCATCTATATTTAACTACTCTTG
ATCGTTGGCTACGCCTGCAGAATTCAACTCTTCATACAAGTCTTTTACGCCGAATCTACATACGCACAAAATTGA
TCTGTATTAACAGAAAGGCGGTCTACGGAACAACTATGTATGATACAAAAAGCATATTCTTCTCCCATAGAAGA
ACACTAAAATACGACTGCAAACCTTCTCATCATCAACTTATTCGACATCGTTGCGTTCGTCATCTTCGAAGATGA
TCCGCTGTAGCTCACGCAAAATGGCATTCCCCAGGACTCGGTGTCCCTCCACCGAAAGATGAACATAGTCCGG
CATAAGATCCGAAACAATCTGTTGCGACTTTGCCGTATAGTGGTCGTTGCCC

>*PtPho4* upstream region, 996 bp
GAAACACTGGTATTTAAGTCAAAGTCGTATCCACCGAGAACGCTACTAACTTGGACCTAGTGCCAAACAATAG
CTCTTTGGACGGGACGGGTGGCAATGCGGATACCAAGACTGCGTCCACAATCCAATACATCGCTGTGATCTTG
TCGCCCTTGGTATCCTCCATGCCGTTACTGTCTCCATCGGACCCTCCAGTGTCCCCTCGCTAATACCTTCCCGACT
GCCTTCCACTCAAAAGTCCTCATCACCTCCAGGTAGTTCCAGTGCCTTGTCATCGGGAGTGCCTTCGAGCGCAA
AGTCGGCTACGCTGTCGTCAAATCCTTCGATTGCACCGTTGTTGAGTGCGTTGGGTATTCCATTGGCTTCACCG
TCCTTGCAACCTTTGTCATTGCCGTCGGAAAGGCCGCCCAGTACGCCTTTGGAAGCCCCGTCGGTATTTCCATA
TCCCTTTACGCTGACCCGAACCCTAATCTTCTGATGCCACATTAAAAGAAAATTACACCGTTAAAAGTTTTGTGC
GTAGGATACCAGTACTCGGAATCCGCTTCGACGTCTTCGTATGCCATTGCGTAAAAATTGCACACTTCGAAGAG
ACCTCACGACAGAGAGAAGGCAAACAAATCGACTTATGTTCGTTTTCTTTGCATCTTCGAGATTCATGCCGAGG
AGTCGCTTTTCTAGCGCTTCACTGTCATGCAACAGGTAAACTCGATTGATGGCTGCCTGAGTCTTCCTCGAATTC
TCTTTTCCAGCATGAAATCTTTGGCCGGAAATCGATTTTACCGGTCTATTTGACTCCCATTACAATGATAGCCCT
GAGTGAATTTTAAAGATCCGATACCGCAGAGAGCTCTTGGATACAATGCGAACTGTTCCAGACATTGCGATGA
TTGAAAAGTGGAAAAGTCGTCACCTGAAGGGGAGCTTATAAAACGACAGCCACTCTTCAACGATCTTCCCGAA
AAGCTAGCTTTCCATTTTGAGACCGATATCATC

>*PtPho4* downstream region, 500 bp
GACAGCTTGCGCATGCCCATGCACTGGATCCGTTTAAACAATGGGTAGAATATCCCAATTTGAGTAGCACTTAA
AATAATTCCATGAATTTATATGCATTCATAAATTGGAATAGTGCTTGCTGTTAATTTCATGAATGACATATATGA
AAAATAACTTGTATAACAGTGAATTCATAAATCAAAGAAAGAGAGGAAACTGTAAACTATTGGAAGGAGAAA
GAGAATGCTGTTATAGCGAAAGAGTTTGAAAGTAACAACAGGCTTATACCATCATTACTTTTGGTTTTCGTTTG
TCGTCGACGTTTGTATCCTCCCTATCGTCATCATGATTGCCACTCTCGCGTCCGTCTTCTTGCCCTTCTTCTGCAG
CACCCGTCTCGGCATCATCATAAATTGCACAGCTCGTGTCTTCTTCGTTTTGACTCGTCGCGAGCTCCAGATGCG
CTTCACCAGCTTCTTCCGGAAATCCTTCCCCTACCACATACCCAGACTCGGTGT

>*PtHp$_i$1* upstream region, 996 bp
TCAGACCTCGGGCAGCAAGCCTATAAGCCCTACTGGGGTTCAACGGTGGTTGATTATTTGTTGAATCAGTCCAA
TGAATCTTCGTTGAGCATTATGGACGTTTCGAAAAGGACATCAATCATGGCCGAAGACATCGTTTTTACGTTGA
ATCAACTAGGGATTTTGAAGATCATCAACGGTATATACTTTATCGCAGCCGAAAAGAGCCTGCTTCAGCGATTG
GCAGAAAAATACCCCGTAAAGGAACCTCGAGTGGATCCATCCAAGCTTCATTGGACTCCCTTTTTGACTGACAT
CAAGCGAGACAAGTTCAGTATACATAGCAAGAAGCCTAATGTTGAAACGGACGAAGTCCGAGGTACGGGAGG
CTTTTAAATGGTGGCTTTCCTCAACCAAATTGACGAAGCCAATATTACTTTGAAAGGAGGTTTTCTACTGGCAC
ACATTCGTTGGCTTGATGAGCCTTGTCTACACCTGGCTAGGCAAGTTTGGTGCCACGCGTGTGTTCGTTTTTTG
CCGCGTTGTTTCGCCTCTCATGAGAAAGCTTACGATTGGGTAGAAAGTTGACTAATTGTATCACCAACAGTAAG
GAATTCTGGCTGTTGCGCTTGCCTTCACAAATACTTTCAAATCTTCTAGCAGACAATCATCTTTAACAGTTAGTG
CAACGTTGAGGCTACGCTGCTGCCTCTAGAGGATTCAAATACTGCGCAGAACCGTGGGGCGGAAACAAAGTA

GACTTTGATGGTTCAGGCAAAAACAGAGAATGCTCTCATCAGTGAAAACATAACTCACCTTCGAGCTCCAAATA
GTTGGCTGTCAAATTTCCGCCGGTTGACAATAGGTGTTCTCATTTTTTACGGACGCTCCTGTAATCATGATCGG
ACGGGAAAGCGAACTGTCTCACTTTCATCAACTCACTATCAGTTCTGCGCCCACAAGTATTGGAAAAGCACCAA
CAATTCAGCAACTTACACTTGCATTAGCGTCGGTAAA

>*PtHp$_i$1* downstream region, 500 bp
GAAGGCAACACAGTTATTAACTTTAAGGAAGAAAGAACTAGGTAGTTGATCACGAATCTGTGGGTAAACAAA
GAGCTTTACCGCGTACATTCACTTCAGTCTTCGCGGGCATATGTATAGGAAACAAATAAGATTGTCTCCAATGC
GGCAAAAATGAAGCTTGATTTGCACACACAGCTAGAGCCTCTCTGATCCATCCACTCCAATTGATTGTAAAATA
TCACAGATGTACCATTTTATCTCGTTAGAAATACTCCTTTCCTTAAATACTCCATTACATGGTTCTTTCTATTTTTC
GAATTTTCTCGAGGAAAACCGCTATCCCGGTCTGCAAAACTTAAAAAATCGCTATTTCGATCAGATCTGAAAAT
CGCTAAGTATTTTTGAGTGAGCGCGAATCGGCTTTTAAGTAAAATTAACAATTATAATCCAATGCTCGGTGAAT
ACTCTGCATATGATATAGCGGAGGTATGGCGCTGGCAGGGATGAGCTGCTTCCAA

>*PtNap$_i$2* upstream region, 991 bp
GGTACGATTTCGGGTGGACGCCAAAACGGACAAAATTTTGGGAGCCAGTATTGTGGGAGTTGGCGCGGGAAA
TATGATTTCGGAAGTTACGCTTGCCATGCAGTCGGCAACTGGACTAGGATCACTGGCCAATGTAATTCATCCGT
ACCCAACTACCGCTGAAGTCCTTCGCCAGTCTGGCGATCTCTACAACCAAGACCAAATTGACAATGACGGCGA
AAAAGATTCTCCGTGGTGTCGTCAAGCTGCAACGTTAAAGGGACTTCTGTTACATGCATATTTCTTCGGGGAAA
GTCGGACAAAGTGACTTTCTACATTTAAAGTCTGTGGGAATCAAGTTTTGGAGGTCAAAAGATCTCATAAATGT
CAAAGATACTATCATGTTTGTTAGCAGAGACCACAAATATGAATCGCATACTTCCAGAATTGCGAGCTGGATGA
CCATGATTCACCGTCAGGGGGGTATAGTGGTCAGTAGCATATTTCTGACCGTGAAGCAGTACCTGTACAATGT
TTCTGGTGCAAACGTGATACTTACTCGCATGGAGAGATAATGACGTAGAAGTTTCTTCTTTTTAGACAAGACCA
GTACGCAGAGGGTTGTTGACATCCCTCCTCAATGAAATTTCGTATATGTGGGCTCGTGGGGCACTGTCGATTG
AAGATACACTGACGTAAAAGTTTCATGACGTCGAAAGCGAAAATGAACTTTGACTTTGAAGCTCCATGAATCT
GGAAGATTCATGTTGACTTCTGTAGAATTGGTATATTTCTTACGTAGAGATCTTTTGTCGATTATACCTTTGCGA
TGAGCGGAGGTGGCCTGGCTATGTTCCTTCATAGTATCAATAGTGATGTCTCATTCCTTGCGAGCTCGAAATTT
AAGAGATTTTTGGAGCTTGTTTTGAAGGTCTGCTCACAATTTGCAGTGGCAGCGACCGTGAAACATTCTGACAT
ACTGCGAGCTCGAGCAATCGTTTGAAAATCAACC

>*PtNap$_i$2* downstream region, 500 bp
GCATTCAATCACGAGAGGTCGATATCACCGTTGATCGGTTTGAGGTCCCCTCTATTTTCCCATATTTCTGTTTAG
CCAAATAAATACTGTGCCGAGAGCTTTCTCGTTGTGTGTGGTTTTGCGCACACTGCTGGAGAATATAACATCTT
GGATTAAAGTGTCTTTTACTTCCCCTTTCTGTGCTCCAACTTTAAATGGCTTGGTTGACTTCCTTGATCTCCAGCA
GGATTAGTCCTTTTGAAAAAATGGTGTTTGTTCAACCGGCGGCAACTACTACCTCTTTCTCCGGTTCACCGGATT
GCCATCAAGTGTCTCGTTTTTCACAGCACATCATTCTGACGATCGCTTCCAAAGCCGACGTGAAAAACGAGGAA
TATTGGTGAGTTGCTTCACTCTAGGCTGGAGAAACACGTTGGCCGGCGTCGTCAAATCTTTCTTCCTATACACG
ATTGCAAAGTTCCATCTCACAATGCGGTATTCTTACTGTAAATGCAATTTAT

>*PtNap$_i$4* upstream region, 1000 bp
AATTTGGTTGTTTTATTTGAATATTGTGCCAAGTCTGTTCTCGCTTGTTAAAGCTAGAGTTACTATAAACCTTTG
GAATATACCACGCTTTTTGTTTGATTCCGTTGTACGTAGGTATTCTAAGGTTCTGTGAAGCCCTCTTAAAACTAG
GACTTTTGACCAGGGGGGAAATGGTCTACAATTAGAAACTCTATTCCAATTGGAAGAATCGCTCTCGCAAGAA
TCCTTCAATGAAACAAAAATGTTCACTGTCATTCTGGGAGGAGAGGAGGATGTGACCGTGTGCTACAAACTCA
GTAGAAGTAGGTTTTCACATTAAGACAAATATTCCATTTTTGATGTCCAAAGTCTCGGAGAATGGGTCTTTTAA
ATCAGGGCCTGGAGCGGATTGATTGATACCACAGATTTGATCATTGCGAAACAGAAAATTTCTCAAGTTTTCAC
TTCTCTAGTTTCTGATGCTTGTTCCTCACAGTCAGTATTAGGCGAAACTTTATATTCTGGCAGTGAATTCCTTTCA
TTGTTGGCACGCTTGATCTATAGAGATTCGGACTAGAGTAAGAGAGTTTAGACTTGGGACGGATCATCTCGCT
ATCCTAAAAAATGTACCTGAAAAATCAAAGTTTTTGGGACGATGTTGATTCACCCTAATGTAACATATGGATAA
ATTTGAGTTGACGTTTATCGGAGACTTCACGCAGCTCATGTCAACAGTTCTGGACATGTTTCTCTTTCTAAGAAA
GAGATCGAACCGCGACTAAACGACGGAATTTTATATCGAAAGGATGACGTCAATCGGCGCTCCATTGCTTTTA
CAAAGAAAAAGATTTTCCGCGATGTGAATCTGCGAGATTCGTGATCGATTCTGTAGAAACGGTATACTTCGTAC

GTAGATCTTGAAATTATCTCGTGGATTTGTGTAGGAGGCCGTACATACGTGGCTCAGTCAGCTTGATGTGAGTT
GTCACTTTCGCCTTTGGTCTGACTTTGAGGAGTCTCC

>*PtNap4* downstream region, 500 bp
GCACCAAACAAGAGGTCGATATCGCCGAATATTGGTTGGAGGTCCCCTTTTGATTATCCGTTTAGTATATATAG
TATATACAACCTGTGCCAAGACCATAGTTCTCGCAGATTCTGCTTGAGAATAAAATAACTTGGGAATGTTTATC
TTATTCTGACTGCATGTAGAAACATTATAGTATCAGGATGCTGCACACAGCTCTTTTCATTTCAACTGCGGTTCA
AACTAACTGTAAACCTTAATCGTTGTGCTGTCAATGGTCGGCGTCCCTAGCCGTAAAAAGGTTAACGCCACATT
CATGAATCAATTGTTTCTTAACTTTGCTTCTGAATCTATCGGCGTGTACGTTTCTCCCTATTAAGGTCTAAAGAG
AGAATGTGACTTCGAGTAGAAATAGGATATCTATTCATATACGAACGATTTTCACTCACCTCGCCGTGAACTTC
AACAATTATATCGACCCTGACAGCACGAGCAGTCGTGTTGCACAGTGCACCCGA

>*PtVpt1* upstream region, 1025 bp
TTGGAAACCGAATTTTCAGCTGTGTGCGTACCCGCGATACTCTGATGTGCTGGAATAGCAGCCGGGCTGCGTT
GACTGGATTGGGCGTGGTATTCATCGTTCGTCATCGCTTGGCGTTCACTGTAGGCATTCTGCGAGTCAGGTTTT
TTATCAGCGAGACCACCGCGGCACTCTACAACGGTCTCTGAATTGTGTGGCTTATGCACAATGTCGACCAAAG
AAGAAGTAGGGAAGGGGACAGCCAACGAATCATTGGCTTTGACGCGAGTATTCACAACAGAGATTTTCGCGC
CAACGTCGACTTTTTCCTTGTTTGAGGAGGAGCCAATACCGAGATTTCGCTGGTTCGTTGCCCGGGGAGACTGT
ACATTCATCCTCCGCTGCGAATGGGAAGGGCGCAACGACCCTTGGATGCTGTGGTCGGTATTCATATGGTGAC
GGAAGTACTCAGTGCGTTGCCGAAACAAGCCAACGAAAATATTGTTGTATTCCAAATGGCGATTTTTGCTGTTT
GTGCAGTCGCGTTGCTTACAGTGAAATACGAAATTAACAGTACCATAAAAAAGGAGGCAATGTGAGTTTTTCG
TTCAAATTACCAAATTCTTCCCAGTTCGACAGGATTTCCTGCGTTGGCAACAACATTCCTGATTCCATAGATTAA
ATTTCGAATCAAAGTATGGTAGGTATTGATAGACCAAAGCGAGATTCCATTTTGAATCTTACAGAAAAGTCTGT
ATCTCTGTCCACGCAAGGTTGTCTTTTTTGTTCGTGCTTTCGAAAGCATCGTTTCTGATATTGCGTGAAAAGCAT
AGGTATACCCATTTCATCGGCAAAACCGACTTTTTTGCATCTATGGATTGTTGCAAAACACACTCGAATATATTG
ACTTACTGTTAGAATCTCGTAGTGCAACTTTACGCATACGCAGAGGCGCTGCCGAGACGACGCGACGTAAACT
CTAGTCGCGTTCTTGAATTGTGAATGACGCCGTTACCGTTCCTTGGCGAAAGCTCAATTTTACAAAC

>*PtVpt1* downstream region, 503 bp
AGGTAGTAACATTGCCTCTTGGTGCTACTACACGATTTGATATCGATATCCTTCAGTACATGTTGACATGTGAGT
AGAATGTGCAAATAAAAACGAAAACAATTTGCGGAGACTCTTCAAAATATCATCCCCTTTAAAAATTTCCTTATT
TTTATGGACACATAGTAAACTATATAGAAGTTTGTGTTCTTATACATATACCTGCGGACTGGTGACTCACTTGTT
CACTTTAGATCTGCTCCGTTCATTGTTCCCTTCAACCCTTGAGCCTCCTTGTTTTGTAGCATAAATTCGTAGCCCC
GCTTTTTAATGTACGGGCGTAGAGATTTAGTATTGATTGGATTCCACCAACAGTGGGTGCAGCGAATTATGGT
ATCCAAATTTTCTGGATCACAATGCATGCTGTGCTTGGATCGGTTGTCCCGAATCGTGGATCTAATTTCGTCCTT
GAGCTCCGTCGAAATGGTATGCTCTGACGCGTACAT GTGAGTCACCTTGGTATC

>*PtNtase* upstream region, bp 1000
TCTTTCTCTTCCGTCGGTTTGATACCATTTCGTTTCCGCAGTTAACACCACAGATACTTGTTGTCCAAGAAACAGT
GGGAAGTCTTCGCACGAGGTTTCTTCGTTGATGATTGACTGTGACGAAGGAAATTTGGTGCGTTATGAGAAAT
GTCGCGGAGACAAGCAAGGAATCCCCACGATCAGAAATTGACAATGAGAGATCGACATTTCACAGCGAGCGG
TTCAAGTCATGAACGTAGTCCCGAGACTACCGTTCATCCCGGAGATGGACGTCACGAAGATCTGTTTTCGATTG
CATTAAGAATGAGAGTTGTTTCATCACATTTAGAGCTAATGAAAATCGTCTACTAGTTAGCTATTATTTGTCACA
CAAGACTGCGAGCTATCATAAGAGCAAAGGGGACCACTTTACTCATACTTCCACCTTTTTATACATAAGTGTAG
ACCGAAATATCCATTGTCAAAAATATTTTTTTCTGTCTCATGTTAAATATAGCCATCGTTTTTACAGTATATAGAT
TGTTGTGACTAATTGTTCCTGATTCGGCCAGTAAAGCTTCCCACTTGCCAAATTGGACGGAGTAATACTGGTAC
CGGATCGCAAGCGAACCAACCAAGAAGTGCTTTCGTTCGCAGTGGCACAATTCATTAAAATTATGGCAATGGA
TGTTCAAGATTCACCAGCATCATACCTTTTTAGGTTTACATTAGGTCATTCACACCACCTAGTCTCCCGCCCCATT
GCGATCGTTATTACAGTTAGTCAACTCGGAAGAAAAAGATTCACCGTAATGTATGTAATTTTGAGTCAAAACTG
AAGTTGAATCTTGTCAATCAACTCTTACGCATGAATTGCTGCAAAAACAAAACAAAAGATTCATGCTCATGCAA
TCTTACTTTCATTGGTTTTTTTACACGATACCTCACTTTTCCCAAGTTGGCATTTTGAAGATTGCAACGACCGTGT
GAAGTCTACAGAACTGAGATACAGGCTGCGAAG

>*PtNtase* downstream region, bp 499
ATTTTTCTATTTTAGTATAAAAGGCCATAACTATCGTTTTGCTTCGAGTCATCACTTTTAGTATCTTGATTTCATT
GCGGAAAGTCGTTCTTCTACGGATCGTAGGGAAGCTTCAATCGAACTACCACGATTCCGGCCGTCAATACGAT
GCGCCAAAACATCCGCCTCAACCAAAGCAAGTTCGGCCAAATGACCAAGCAATGGATGCGGGTGCCCGCGGA
CGCCGAGCGCCGAAAAGACGTTGACGAGATAGTTCAAGTCAGTATTCAAATGCTCACATCCTTTCGGAGTCAA
GGAAGGAATTCGCATGATCCGCTCTAACAGACGACCAGTGACAGCCGTTGATACAACATCCAACCAAACGTTA
CAAAACTTGTTGGCCTCGCTTTCTTCCTCTTCGGTTCCTTCTTCCTCTCCAAGCGCAGCCGATGCTACAACGAAG
TTGTCGAGGTTTTTCCCGTTCATCAGGCTCTTGATGACATCTTCTGAACCCATGGAG

7.2. Sequences of the oligonucleotides used in this work

7.2.1. Primers used to amplify the genes for localization studies

Restriction sites sequences are underlined and sequences marked in yellow indicate the overlap generated to use the Gibson assembly reaction to generate the constructs. The red marked sequence indicates oligo region encoding for the FLAG-tag

Running name	Forward	Reverse
PtPhos3	GAATTCATGGAGAGTCAGGGGAAGGAATGTCC	TCTAGAAAAGCTGTGAACTTGTGATGATA AAATTGTTCCCG
PtPhos5	GAATTCATGGCGGGTCCATCGAAACGGCCTTG	TCTAGACTTTTTGTTCTGCTCATTCC
PtPhos6	GAATTCATGAACGATGACCGGATAAGTGACCG	TCTAGACATCAATAATTTGGTGGACGGAA CCG
PtPhos6-Nterm GFP	CAGGTCTAGAATGAACGATGACCGGATAAG	CTAGTCTTAAAGTAAATTGAAGCTTTTACA TCAATAATTTGGTGGAC
PtPhos7	GTCACCACTTGTGCGAACGGAATTCATGAGCCG TGCGCCAACG	CCTCGCCCTTGCTCACCATTCTAGAGTCGA TTTTGAGTTGACGCTTGTTGG
PtPhos8	GTCACCACTTGTGCGAACGGAATTCATGACGCA AATCTTGATCTTG	CCTCGCCCTTGCTCACCATTCTAGAAGCTA GACCATCTACGGTC
PtPho4	GAATTCATGAGCGTTGACATGAG	TCTAGAGGCAGAGGGGGAAAAAG
PtHpi1	GTCACCACTTGTGCGAACGGAATTCATGGAACC ATCGGACAAATTG	CCTCGCCCTTGCTCACCATTCTAGAAACAG TATCTGCGAGAAC
PtNapi1	GAATTCATGGTAAGTTGCCGTCTTCATATTGAGT GTG	TCTAGACGCCTCGACTTCGTTGTCGTC
PtNapi2	GAATTCATGTCTGCAGAAAATCCTGAGG	GGATCCAGCTGCAACCTCATCTGAGTCCG
PtNapi3	GTCACCACTTGTGCGAACGGAATTCATGGAGAT CAACAACGCC	CCTCGCCCTTGCTCACCATTCTAGATGTTA TTCTCAAACAGTATCTGC
PtNapi4	GAATTCATGTCCAACGCACAATTCTTCTGTG	TCTAGAGGCATCAACCTCAGCATCCGAAG TATC
PtNapi5	GAATTCATGAATGTCATCCACGAGACCG	TCTAGAGGATTTTCAACGGTAT
PtVpt1	GAATTCATGGTGAACTTTGGCAATAAG	TCTAGAGTCATCATTGTCTAAAGGCTC
PtVtc1	GAATTCATGAGCCATTCTGAAACGACGCCG	TCTAGACGCTTCAATCATCGAATAC
PtVtc3	GAATTCATGCCGCCGCAACAGTCCCGAG	TCTAGATACAGTCGCCGCAGCGCATTCG
PtVtc4	GAGCTCATGAAGTACGGTGAACACC	TCTAGACATTAGGTCCATTTTCGAAATGG
PtNtase	GTCACCACTTGTGCGAACGGAATTCATGGTGCA GCTTTATTCTTC	CCTCGCCCTTGCTCACCATTCTAGAGATAG CAGCAAGCACAGC
PtNtase-FLAG	GTCACCACTTGTGCGAACGGAATTCATGGTGCA GCTTTATTCTTC	AAAGTAAATTGAAAGCTTTTATTTATCATC ATCGTCTTTGTAATCGATAGCAGCAAGCAC

7.2.2. **Primers used to generate promoter/eGFP/terminator**

Running name	**Sequence**
Phos1_Pro_nde	CATATGCCGGTGTGTAAATATACGATACCC
Phos1_Pro_eco	GAATTCTTTGCAGGTCCGATAATGTTAGG
Phos1_Ter_HindIII	AAGCTTGAGCACAGGAATTTGAGACTTATATATG
Phos1_Ter_AccIII	TCCGGACCTAAAGACGGGCCGGTCCGGTAGCC
Phos2_ Pro_nde	CATATGGTCAAACAGCTCTTGATTGTCGCCCGCG
Phos2_ Pro_eco	GAATTCGCTCGCCGTGATGGATCTTTTCGAGTCGG
Phos2_ Ter_HindIII	AAGCTTGTATAGAAGGTCACGTAGCTAGAG
pPhaP3 GIB fw	ATTGTACTGAGAGTGCACCATATGCGCATTCGCAACCCGCTG
egfp3 GIB rv	CCATGAATTCGGTGTACCGATGAGAATATTGAACGAC
pro3_GIB fw	TCGGTACACCGAATTCATGGTGAGCAAG
ter3 GIB rv	GTGAATTGTGAAGCTTTTACCTGTACAG
eGFP3 GIB fw	GTAAAAGCTTCACAATTCACATTTTTAAGTTTTC
pPhaP3 GIB rv	AGATTGAATTTTGAATCTCTCCGGATAACGGCCAAGAATATTG
pPhaP5 GIB fw	ATTGTACTGAGAGTGCACCATATGAGAAATCGCGTGGTTGGAAATTG
Egfp5 GIB rv	CCATGATATCTGGTATTCTTGTTCGATACACAC
Pro5_GIB fw	AAGAATACCAGATATCATGGTGAGCAAG
Ter5 GIB rv	ATTCGGGAGCAAGCTTTTACCTGTACAG
eGFP5 GIB fw	GTAAAAGCTTGCTCCCGAATGTTTGTTTTCG
pPhaP5 GIB rv	AGATTGAATTTTGAATCTCTCCGGAGCAAGTGCGGTGGATGAAC
Phos6_pro_NdeI	CATATGGCTACACTTGGAATACACTGCG
Phos6_pro_EcoRI	GAATTCGTTCACTGTAAGAAAAAGCGGGGG
Phos6_ter_HindIII	AAGCTTAAAGTTTTTGTTTTTGTCCC
Phos6_ter_AccIII	TCCGGAGTATCAGGGTGCCAAGGGCG
Phos8_1	ATTGTACTGAGAGTGCACCATATGACAGGTTTGTTGCTTGGG
Phos8_2	TGCTCACCATCGAAGAATTCTTTTCACCAG
Phos8_3	GAATTCTTCGATGGTGAGCAAGGGCGAG
Phos8_4	CTCCACAAAATTACCTGTACAGCTCGTCC
Phos8_5	GTACAGGTAATTTTGTGGAGTTCTTTTTCTTTATC
Phos8_6	AGATTGAATTTTGAATCTCTCCGGAGGGCAACGACCACTATAC
PtNtase_1	ATTGTACTGAGAGTGCACCACATATGTCTTTCTCTTCCGTCGGTTTG
PtNtase_2	TGCTCACCATCTTCGCAGCCTGTATCTC
PtNtase_3	GGCTGCGAAGATGGTGAGCAAGGGCGAG
PtNtase_4	ATAGAAAAATTTACCTGTACAGCTCGTCC
PtNtase_5	GTACAGGTAAATTTTTCTATTTTAGTATAAAAGGCC
PtNtase_6	AGATTGAATTTTGAATCTTCCGGACTCCATGGGTTCAGAAGATG
Pho4_1	ATTGTACTGAGAGTGCACCATATGAAACACTGGTATTTAAGTCAAAG
Pho4_2	TGCTCACCATGATGATATCGGTCTCAAAATG
Pho4_3	CGATATCATCATGGTGAGCAAGGGCGAG
Pho4_4	GCAAGCTGTCTTACCTGTACAGCTCGTCC
Pho4_5	GTACAGGTAAGACAGCTTGCGCATGCCC
Pho4_6	AGATTGAATTTTGAATCTCTCCGGACACCGAGTCTGGGTATGTG
HPi1_1	ATTGTACTGAGAGTGCACCATATGTCAGACCTCGGGCAG
HPi1_2	TGCTCACCATTTTACCGACGCTAATGCAAG
HPi1_3	CGTCGGTAAAATGGTGAGCAAGGGCGAG
HPi1_4	TGTTGCCTTCTTACCTGTACAGCTCGTCC
HPi1_5	GTACAGGTAAGAAGGCAACACAGTTATTAACTTTAAG
HPi1_6	AGATTGAATTTTGAATCTCTTTGGAAGCAGCTCATCCC
NaPi2_1	ATTGTACTGAGAGTGCACCATATGATGGATGGGTACGATTTC

NaPi2_2	TGCTCACCATGGTTGATTTTCAAACGATTG
NaPi2_3	AAAATCAACCATGGTGAGCAAGGGCGAG
NaPi2_4	GATTGAATGCTTACCTGTACAGCTCGTCC
NaPi2_5	GTACAGGTAAGCATTCAATCACGAGAGG
NaPi2_6	AGATTGAATTTTGAATCTCTCCGGATAAATTGCATTTACAGTAAGAATAC
NaPi4_1	ATTGTACTGAGAGTGCACCATATGAATTTGGTTGTTTTATTTGAATATTGTG
NaPi4_2	TGCTCACCATGGAGACTCCTCAAAGTCAG
NaPi4_3	AGGAGTCTCCATGGTGAGCAAGGGCGAG
NaPi4_4	TGTTTGGTGCTTACCTGTACAGCTCGTCC
NaPi4_5	GTACAGGTAAGCACCAAACAAGAGGTCGATATC
NaPi4_6	AGATTGAATTTTGAATCTCTCCGGATCGGGTGCACTGTGCAAC
Vpt1_1	ATTGTACTGAGAGTGCACCATTGGAAACCGAATTTTCAG
Vpt1_2	TGCTCACCATGTTTGTAAAATTGAGCTTTCG
Vpt1_3	TTTTACAAACATGGTGAGCAAGGGCGAG
Vpt1_4	GTTACTACCTTTACCTGTACAGCTCGTCC
Vpt1_5	GTACAGGTAAAGGTAGTAACATTGCCTC
Vpt1_6	AGATTGAATTTTGAATCTCTGATACCAAGGTGACTCAC

7.2.3. **Primers for sequencing.**

pJet1.2 fw	GCACAAGTGTTAAAGCAGTT
pJet1.2 rv	CTCTCAAGATTTTCAGGCTGTAT
pPhaT1 fw	GGCGTATCACGAGGCCCTTTCG
pPhaT1 rv	CGAAGTCGTCCTCCACGAAGTCCC
pPhaNR fw	GGTCGGGTTTCGGATCCTTCC
pPhaNR rv	GATGAACATAAAACGACGATGAG
eGFP 5´ raus	GGCAGCTTGCCGGTGGTGCAGATG
Vtc4KO seq primer	GGCTGGAACGGTAGGAGGACACCGT

Acknowledgments

First, I would like to deeply thank Professor Uwe Maier for believing in me by offering me the position of PhD student in his laboratory. Thanks for giving me time, space to my ideas, trust, guidance, continuous encouragement and support especially in the “not easy” moments of my research. If I ever have to continue working in science, besides all the teachings I will always have an answer to many dilemmas: "it´s science".

I would like to thank the members of the committee Professors Alfred Batschauer, Andreas Brune and Lars Voll. Thank also to Prof. Dr. Gert Bange and Alfred Batschauer for taking part in thesis advisors committee for the Marburg School of Microbiology graduate school.

I want to thank Dr. Stefan Zauner for his teachings and introductions, always ready to answer my constant questions, requests and explanations. Thanks to our "scientific big brother" Dr. Daniel Moog with whom I have had myriad scientific discussions and received endless and always useful advices on my project and beyond.

Thanks to all the people that somehow were involved in my project: Dr. Franziska Hempel, Dr. Thomas Heimerl, Dr. Uwe Linne, Marion Schon, Daniel Stukenberg, Simon Runge, Sara Chaban, Vera Samel-Gondesen, and Elmar Utesch.

A great “thanks” to all my lab mates: PhD students Vicky, Johnny, Stephie, Jana with whom I shared successes, failures, doubts, and all the aspects of the “PhD student life”. Thanks to the my “compagno di merenda” Neri, for all the dumb mathematic/chemistry calculations, advices, chats and scientific discussions. Thanks to all the students and technicians, Angela, Sebastiano, Vasilij, and all the others. Thanks for the soccer, BBQs, beer, lab pranks and all the good time spent in the lab and outside.

Last but not the least, a big thank to my wife Laura always encouraging and supporting me and to our families that even from afar have made us feel the support and help.

Erklärung

Hiermit versichere ich, dass ich meine Dissertation

„Diatoms and their response to phosphate limitation “

Selbstständig, ohne unerlaubte Hilfe angefertigt und mich dabei keiner anderen als den von mir ausdrücklich bezeichneten Quellen bedient habe.

Die Dissertation wurde in der jetzigen oder einer ähnlichen Form noch bei keiner anderen Hochschule eingereicht und hat noch keinen sonstigen Prüfungszwecken gedient.

Marburg, den Gianluca Dell´Aquila